Technische Universität München

Physik-Department E17

Conformational Changes in Hemoglobin triggered by changing

the Iron Charge,

High and Low Affinity Hemoglobin

Simonetta Croci

Vollständinger Abdruck der von der Facultät für Physik der Technischen Universität München zur Erlangung des akademischen Grades eines

Doktors der Naturwissenschaften

genehmigten Dissertation.

Vorsitzender: Univ. Prof. Dr. Sighart Fischer

Prüfer der Dissertation:
1. Univ. -Prof. Dr. F.G. Parak, i.R.
2. Univ. -Prof. Dr. F. E. Wagner, i.R.

Die Dissertation wurde am 04.05.2006 bei der Technischen Universität München eingereicht und durch die Facultät für Physik am 30.05.2006 angenommen.

Life is what happens while you are making other plans

To my husband Marco
and my parents.

Index

Zusammenfassung

Diese Arbeit beschäftigt sich mit Konformationsänderungen des Hämoglobin, die durch eine Ladungsänderung des Eisens induziert werden. Die Ergebnisse werden mit Myoglobin verglichen. Die Konformationsänderung des Eisens wurde mit Mössbauerspektroskopie untersucht.

Um die Konformationsrelaxation von Hämoglobin und Myoglobin zu charakterisieren und einen möglichen Einfluß der Quartärstruktur zu erkennen, wurde ein intermediärer metastabiler Zustand durch Bestrahlung von Methemyoglobin mit Röntgenstrahlung bei tiefer Temperatur erzeugt. Die Bestrahlung reduziert das Fe(III) der Hämgruppe zu Fe(II) „Low Spin", wobei ein Wassermolekül als sechster Koordinationspartner erhalten bleibt. Ein zyklisches Erwärmen von 140K bis 200K ermöglicht es den Molekülen, eine Aktivierungsenergiebarriere zu überwinden und in die stabile Konformation, wie Deoxy-Hämoglobin oder Carboxy-Hämoglobin, falls CO anwesend ist, zu relaxieren. Leicht unterschiedliche Strukturen (Konformationssubzustände) bewirken eine Verteilung von Energiebarrieren ($\Delta G^{\#}$). Die Verteilung der Aktivierungsenergie für den Zerfall des Fe(II) „Low Spin" Intermediates wurde mit einer Gausskurve angepasst. Zum Vergleich wurden publizierte Ergebnisse von Myoglobin in derselben Weise neu analysiert. Unterhalb einer charakteristischen Temperatur können die Daten für Hämoglobin und Myoglobin mit jeweils einer Anfangsenergieverteilung angepasst werden. Mit zunehmender Temperatur verliert die Verteilung ihre Gaußform, da Moleküle mit einer kleinen Energiebarriere zuerst über die Barriere springen. Oberhalb der charakteristischen Temperatur ist es notwendig eine eigene Gaussfunktion für jede Temperatur zu wählen. Unterhalb dieser Temperatur sind die Moleküle in Konformationssubzuständen eingefroren, daher ist eine Wiederbesetzung der depopulierten Zustände sehr unwahrscheinlich. Oberhalb der charakteristischen Temperatur können die Moleküle jedoch einen flexiblen Zustand einnehmen, der eine Wiederbesetzung erlaubt. Die durchschnittliche Aktivierungsenergie bei der charakteristischen Temperatur ist für Myoglobin und Hämoglobin sehr ähnlich. Die freie Energie der Aktivierung hat zwei Beträge, die Aktivierungsenergie um den flexiblen Zustand zu erreichen und das Brechen der Wasserbindung. Die größere Energieverteilung bei Myoglobin verglichen mit Hämoglobin zeigt, dass in Myoglobin mehr Konformationssubzustände verfügbar sind. Ein Grund dafür könnte sein, dass eine größere Proteinoberfläche wasserzugänglich ist. Im Hämoglobin sind aufgrund der Quartärstruktur Teile der Ketten nicht mit Wasser in Kontakt. Die Bildung von HbCO während des Erwärmens von bestrahlten Hbmet-Proben wirft die Frage nach dem Ursprung des CO auf.

Daher wurde Deoxy-Myoglobin in Pufferlösung mit und ohne Glycerol bestrahlt und erwärmt. Dabei wurde das Protokoll der vorherigen Experimente wiederholt. Nach dem Erwärmen befand sich in den Proben ohne Glycerin praktisch kein Carboxy-Myoglobin, in den Proben mit Glycerin jedoch sehr wohl. Diese Experimente zeigen, dass CO durch Glycerin-Radiolyse und nicht durch Proteinzerstörung erzeugt wird. Neben der Möglichkeit den Zerfall des Intermediärzustandes zu untersuchen, erlaubten die Temperaturzyklen nach der Bestrahlung die Bildung von HbCO und MbCO aus der Deoxy-Konformation zu untersuchen. Wegen der bezogen auf das Deoxy-Hämoglobin niedrigen CO Konzentration gab es keinen T nach R Übergang der Quartärstruktur des Hämoglobins. Der Vergleich zwischen bestrahlten Mbdeoxy und Hbdeoxy Proben zeigte eine höhere freie Energie für die CO Bindung am Hämoglobin. Das kann wahrscheinlich durch die höhere Affinität des Mb für Liganden im Vergleich zu einem Hb Monomer erklärt werden, wenn alle vier Untereinheiten in der Deoxy-Konformation sind (T Zustand). Die Rolle der Quartärstruktur ist der Schlüssel zum Verständnis der allosterischen Eigenschaften des Hämoglobins. Es ist wohlbekannt, dass Hämoglobin wenigstens zwei Quartärstrukturen hat: R wenn, das Protein sauerstoffbeladen ist und T wenn es vollständig deoxygeniert ist. Der Einschluss von Hämoglobin in nasses Silicagel, das eine Änderung der Quartärstruktur verhindert, erlaubte es die Existenz zweier T Zustände zu beweisen. Um mögliche Unterschiede in der Eisenumgebung der zwei Quartärstrukturen zu untersuchen wurde High Affinity (HA) und Low Affinity (LA) Deoxy-Hämoglobin, das in nasses Silicagel eingeschlossen war, mit Hilfe der Mössbauer-Spektroskopie untersucht. Die Temperaturabhängigkeit der Quadrupolaufspaltung von Deoxy-Hämoglobin in Lösung wurde mit der des in Silicagel eingeschlossenen Deoxy-Hämoglobins im HA und LA Zustand verglichen. Die Berechnung der Vielelektronen-Energiezustände des Eisens liefert eine Information über die Bindungsstärke des Eisens an das proximale Histidin bzw. die Stickstoffe der Pyrolringe. Kleine Unterschiede in der Quadrupolaufspaltung des HA und LA konnten bei niedrigen Temperaturen aufgelöst werden. Diese Unterschiede deuten darauf hin, dass im Falle der HA Probe die Bindung zwischen dem Eisen und den Stickstoffen der Pyrolringe stärker ist als in der LA Probe, während die Bindung ans proximale Histidin in der LA Probe stärker ist, als die der HA Probe. Die Qualität der Daten ist jedoch nicht ausreichend, um daraus einen signifikanten Unterschied der Eisenumgebung in den HA und LA Hbdeoxy Zuständen zu beweisen. Diese Schlussfolgerung unterstützt die These, dass die unterschiedliche Affinität durch die Bindung der Liganden (induced fit model) und nicht durch verschiedene Tertiärstruktur-Konformationen der ligandenfreien Untereinheiten des T Zustandes hervorgerufen wird.

Summary

In this work the hemoglobin conformational changes induced by changing the iron charge have been studied and compared with Myoglobin. Mössbauer spectroscopy was used to follow the change of the iron conformation. In order to compare the conformational relaxation of hemoglobin and myoglobin, and to study a possible influence of the quaternary structure, an intermediate metastable state of hemoglobin has been created by low temperature X-ray irradiation of methemoglobin. The irradiation reduces the Fe(III) of the heme groups to Fe(II) Low Spin, where the water is still bound on the sixth coordination.   Heating cycles performed at temperatures from 140K to 200K allow the molecules to overcome an activation energy barrier and to relax into a stable conformation such as deoxy-hemoglobin or carboxy-hemoglobin, if CO is present. Slightly different structures (conformational substates) reveal themselves as a distribution of energy barriers ($\Delta G^{\#}$). The distribution of the activation energy, for the decay of the Fe(II) Low Spin intermediate, has been fitted with a Gaussian. For comparison, published myoglobin data were re-analysed in the same way. Below a characteristic temperature, the data can be fitted with one starting energy distribution for hemoglobin and myoglobin respectively. With increasing temperature the distribution looses the Gaussian shape, since the molecules with low energy barrier decay first. Above the characteristic temperature, it is necessary to use a single Gaussian for each temperature. Below this temperature, the molecules are frozen in conformational substates: hence a repopulation of the depopulated states is very unlikely. However, above the characteristic temperature the molecules can reach a flexible state which allows repopulation. The average energy value at characteristic temperature is very similar in case of myoglobin and hemoglobin. The free energy of the activation has two contributions, the activation energy to reach the flexible state and the breaking of the water binding. The larger Gaussian energy distribution for myoglobin with respect to hemoglobin shows that more conformational substates are available. This may be caused by a larger area exposed to water. In hemoglobin, part of the surface of the chains is not water accessible due to the quaternary structure. The formation of HbCO during the heating cycles of irradiated Hbmet samples raised the question where the CO was coming from. Therefore deoxy-myoglobin in buffer solution, with and without glycerol, has been irradiated and heated, following the same procedure used in case of the previous samples. After the thermal cycle, in the sample prepared without glycerol there was practically no formation of carboxy-myoglobin, in contrast to the samples prepared in presence of glycerol. These experiments show that CO is produced by glycerol radiolysis and not by damaged proteins.

Besides the study of the decay of the intermediate state the temperature cycles after irradiation allowed to follow the formation of HbCO and MbCO starting from the deoxy conformation. Because of the low CO concentration produced with respect to the deoxy-hemoglobin concentration there was no T to R transition of the quaternary hemoglobin structure. Nevertheless, the comparison between irradiated Mbdeoxy and irradiated Hbdeoxy samples showed a higher free energy for CO binding to hemoglobin then to myoglobin. This is probably due to the higher affinity that the Mb has for the ligand in comparison with the affinity of the Hb monomer when all the four subunits are in the deoxy conformation (T state).

The role of quaternary structure is a key point to understand the hemoglobin allosteric properties. It is well known that hemoglobin has at least two quaternary structures: R when the protein is fully oxygenated and T when it is fully deoxygenated. The encapsulation of hemoglobin in wet silica gel, preventing a change in the quaternary structure, gave the opportunity to show the existence of two T states. To detect possible differences in the iron surrounding of the two quaternary states, High Affinity (HA) and Low Affinity (LA), deoxy-hemoglobin encapsulated in wet silica gel have been studied by Mössbauer spectroscopy. The temperature dependence of the quadrupole splitting deoxy-hemoglobin in solution has been compared to that of encapsulated deoxy-hemoglobin in the HA and LA state. The calculation of multi electron energy levels of the iron gives information on the bond strength of the iron with proximal histidine and with nitrogens of the pyrrolic rings. Small differences between the quadrupole splitting of HA and LA have been seen at low temperatures. These differences indicate that in the case of HA sample the binding between the iron and the nitrogens of the pyrrolic rings is stronger with respect to the LA sample, while the binding with the proximal histidine is stronger in the LA sample with respect to the HA sample. However, due to the quality of the data these differences are too small to deduce that the HA and LA Hbdeoxy states differ at the iron surrounding. This conclusion supports the thesis that the different affinity is due to the effect of the ligand binding (induced fit model) and not to a different tertiary conformation of the unbound subunits of the T state.

1 Introduction

Proteins are biologically important macromolecules. They have a complex three dimensional structure which is important for the function of the protein itself. The nature of this structure is usually explained in terms of a structural hierarchy, from primary to quaternary. The primary structure of a polypeptide or protein is the sequence of amino acids in the protein. The secondary structure refers to the folding of the chain of amino acids into a helix or a β pleated sheet. Many proteins have β sheets and helices. The secondary structure arises from the geometry of the bond angle between amino acids as well as hydrogen bonds between nearby amino acids. The tertiary structure refers to a higher level of folding in which the helices and sheets of the secondary structure fold upon themselves. To know the tertiary structure of a protein it means to know the x,y,z coordinates of at least all non hydrogen atoms. This higher level folding arises for several reasons. First, different regions of the amino acid chain are hydrophilic or hydrophobic and arrange themselves accordingly with water molecules. Second, different regions of the chain bind with each other via hydrogen bonding or disulfide linkages. The quaternary structure arises when polypeptide chains are bound together usually by hydrogen bonds and hydrophobic interactions
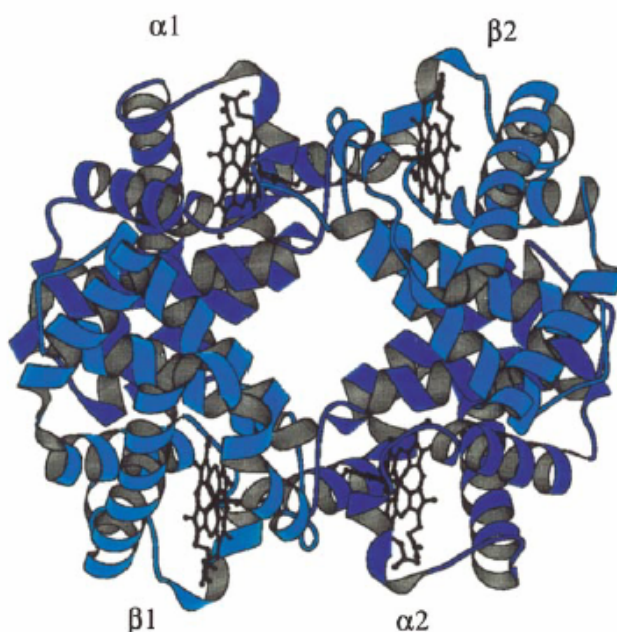

Figure 1.1: Quaternary structure of Hbdeoxy T state: two α and two β chains. The α subunits are in light blue while the β subunits are in dark blue. Each subunit has a heme group shown in black ball and stick model (Paoli et al., 2001).

For example hemoglobin has four subunits hydrogen bonded together. Hemoglobin (Hb) shows the complexity and the typical behaviour of many proteins. Hemoglobin gives the chance to study the tertiary and quaternary structures, and how these are related to allostery. Although hemoglobin has been studied since 1900, there are still many open questions, mainly linked to its functions and dynamics. It is extremely fascinating to find out how the nature developed tuning mechanisms to perform many functions maintaining one sequence, the primary structure. As already mentioned Hb is a tetramer (Fig.1.1) with two chemical identical heterodimers each with an α and β subunit. Each subunit is conjugated with a heme group that binds oxygen to ferrous ion – Fe(II). In this way each Hb molecule is able to carry four oxygen molecules. Apart from the differences in the amino acids sequence, the α and β chains have nearly the same fold structure that is made by α-helices, and nearly the same globin structure as myoglobin (Mb). The overall Hb structure is quite compact with a diameter of 50-55Å, where each subunit contains a heme. A representation of the basic structure of the individual subunits is shown in Fig 1.2. The helices have been traditionally named from A through to H from the N- to the C- terminus and the intervening non-helical segments are called AB, EF, FG and so on. The α-subunit has not the D helix in contrast with the β subunit.
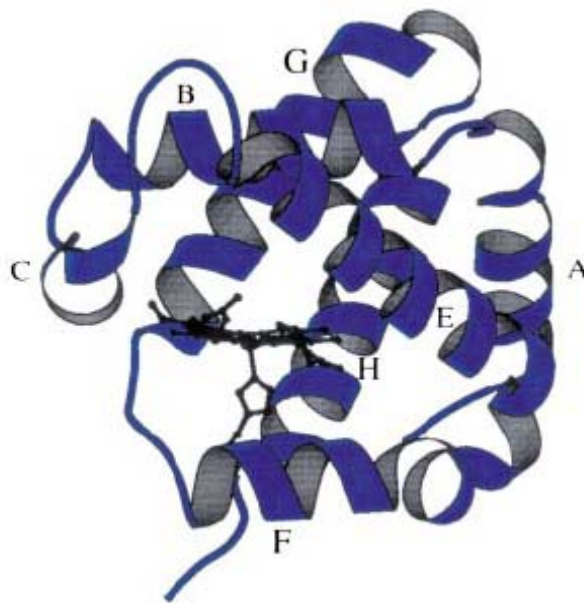
Figure 1.2: Schematic diagram showing the secondary and the tertiary structure of the globin fold as seen in the α-subunits of human hemoglobin. The heme is shown in a black ball and stick representation covalently linked to the proximal histidine F8, from the end of the F helix. The nomenclature of the helices is reported from A to H. In the α-subunit the D helix is absent in contrast with the β-subunit (Paoli et al., 2001).

Hemoglobin can be found with a ferrous five coordinated high spin configuration of the iron with a domed heme shape and with the iron out of the plane or in a six coordinated ferrous low spin ligated e.g. with CO_2. It is also possible to find hemoglobin with the ferric iron as in the

methemoglobin (Hbmet) case. In this state, a water molecule binds iron in the sixth position showing a high spin configuration at room temperature, whereas a mixture of high and low spin configuration appears at lower temperature. The ratio between high and low spin state depends on the freezing velocity. The hemoglobin is a very efficient carrier of oxygen from lungs to tissues and of carbon dioxide from tissues to lungs. The job of hemoglobin is to bind oxygen efficiently in the lungs, where the partial pressure of oxygen is about 13.3 kPa, and to release the oxygen in the tissues, where the partial pressure is about 5 kPa. During oxygenation Hb has a sigmoidal binding curve instead of hyperbolic, as would occur for a simple $Hb + O_2 \leftrightarrow HbO_2$ equilibrium (Fig. 1.3), as it is in the case of myoglobin binding curve of O_2. The myoglobin is almost fully saturated at 5 kPa pO_2. In the capillaries of the tissues the pO_2 is low (2.6 kPa-5.3 kPa) and therefore the hemoglobin releases the O_2 molecules. In the muscles then the Mb binds O_2. At tissue pressure in fact the affinity for the O_2 molecules is much higher for Mb than for Hb. In this way the oxygen molecules from lungs can be efficiently delivered to tissues.
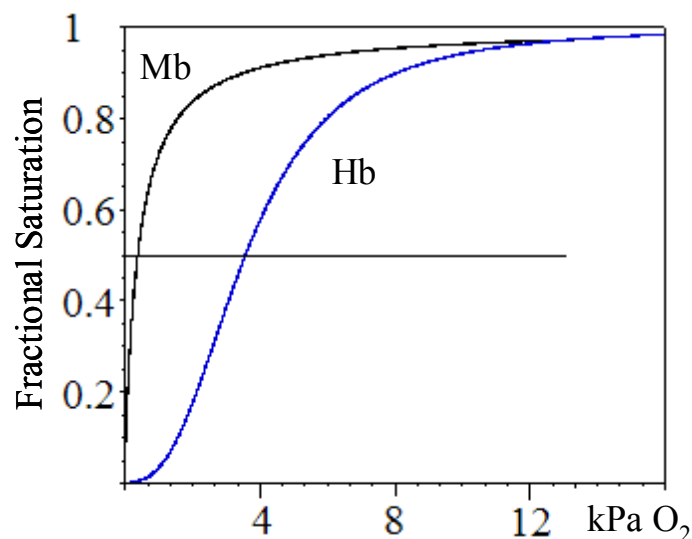
Figure 1.3: Black line - Mb fractional saturation curve as a function of O_2 partial pressure. This curve has a hyperbolic form. Blue line - Hb fractional saturation curves as a function of O_2 partial pressure. This curve has a sigmoidal form.

From looking at the sigmoidal curve, it can be seen that hemoglobin binds oxygen relatively less strongly at low oxygen concentrations, than at high oxygen concentrations. This behaviour is referred to as *allostery*. Hemoglobin is an allosteric protein. An allosteric protein is one in which the binding of a ligand to one site affects the binding properties of a ligand to another site on the same protein. If the same ligand modulates further binding of itself to the protein, this is called *homotropic allostery*. If a ligand modulates binding of a molecule that is different from itself, this is called *heterotropic allostery*. When the hemoglobin is completely unligated it is a in quaternary

structure called T (tense) structure, while when it is in full ligated structure, it has a different quaternary structure called R (relaxed) structure. Six intersubunit salt bridges can be seen as "cross-links" between the αβ dimers: they stabilize the T quaternary structure relative to R. The T structure is a low oxygen affinity state while the R structure is an high affinity state. The binding of O_2 causes a conformational change in the Hb to the high affinity R-state. The quaternary conformational changes consist of a rotation of symmetrically related αβ dimers by about 15° relative to each other, and a translation of about 0.1 nm along the rotation axis. The X-ray crystal structure of Hbdeoxy as well as HbCO has been resolved firstly by Perutz (Perutz et al., 1960). This essential contribution together with the knowledge of the dynamic parameters, like binding constants, gives much of the information to understand the hemoglobin functions.
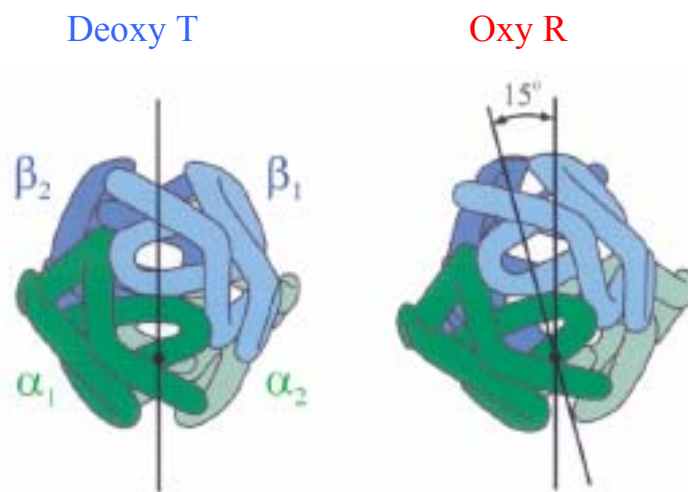
Figure 1.4: Schematic representation of the hemoglobin quaternary change: Hb in the T structure and in R structure. The quaternary conformational change from T to R structure consists of the rotation of $\alpha_1\beta_1$ and $\alpha_2\beta_2$ dimers respect to each other of about 15° and a translation along the rotation axis of about 0.1 nm (Henry et al., 2002).

The sigmoidal binding curve can be changed by the so called *allosteric effectors*. Particularly relevant in this respect is the action of the pH of the 2,3-disphosphoglycerate (2,3-DPG), as well as of the other compounds like inositol hexaphosphate (IHP). The pH lowering, as it happens in the tissues, decreases the O_2 Hb affinity. This is the so called "Bohr effect". The 2,3-disphosphoglycerate (2,3-DPG), derived from the glycolytic intermediate 1,3-disphosphoglycerate, stabilizes the tense (T) structure, hence an increased 2,3-DPG concentration favours the T state. Several experiments have been performed to better analyse the cooperative behaviour with heterotropic and homotropic effectors. These experiments gave rise to several models developed to explain the cooperative Hb behaviour. Among them, two are the most famous. One was proposed by Monod, Wyman, and Changeux (MWC), and it is designated as the "concerted" model. It

assumes that each subunit is identical and can exist in two different conformations or states. The two states have different affinities for the ligand; however, all the subunits within one protein can exist in only one of the two states. The binding of ligand to a subunit in the low affinity state could result in a conformational change that places the state itself in a high affinity conformation. All the other subunits, even though they do not have a bound ligand, must follow suit. In the other model, the Koshland one – called the "sequential" model – ligand binding can induce a conformational change in just one subunit. This will then make a similar change in an adjacent subunit, making the binding of a second ligand more likely. However, many other formulations have been proposed to explain the cooperative behaviour. A deeper explanation of the models is given in Chapter 2.

To avoid the additional complexity of the quaternary structure, myoglobin was often used as a model protein. During the last 30 years many experiments were performed to study the protein kinetics and dynamics using myoglobin. Myoglobin became a paradigm in the study of protein dynamic (Parak et al., 2002). The aim of these studies was to find the connection between protein structure, dynamic and functions. Even simple proteins like myoglobin can adopt different conformations correlated with their functions. Moreover, within a well defined conformation, molecules can assume a large number of slightly different structures called Conformational Substates (CS) (Frauenfelder et al., 1988; Austin et al., 1975; Young et al., 1984). At very low temperatures, protein molecules are frozen in a particular substate. Their dynamics is mainly described by vibrations in analogy to phonons in simple solids. However, the kinetics of CO or O_2 rebinding after flash photolysis in Mb or other heme proteins has elucidated the complexity of the energy landscape (Ansari et al., 1985; Ansari et al., 1987; Doster et al., 1982; Kriegl et al., 2002; Steinbach et al., 1991). These experiments show that the rebinding kinetics can not be described by an exponential law but rather by a power low. Above a characteristic temperature, T_c, structural fluctuations become observable by Mössbauer spectroscopy (Parak et al., 1971; Parak et al., 1982) and incoherent neutron scattering (Doster et al., 1989; Ferrand et al., 1993), indicating that the molecules can go into a flexible state (Parak, 2003). While well below T_c, the rebinding of CO or O_2 can be explained by a barrier height distribution which is independent of temperature: this distribution becomes temperature dependent in the region around T_c. Moreover, the rebinding has then to be described as the motion of the ligand over a number of energy barriers (Doster et al., 1982), where the last one is connected with the ligand passage from the protein matrix into the solvent. Conformational changes are strongly connected with the structural fluctuations above T_c. As demonstrated by X–ray structure analysis on carboxy myoglobin (MbCO) crystals of the L29W mutant, a measurable conformational relaxation takes place only above T_c (Ostermann et al., 2000).

For an investigation of conformational changes, one has to produce a metastable intermediate state which then relaxes into the equilibrium conformation. In the experiments mentioned above, the photolysis of the CO molecule creates as intermediate state an unligated Mb molecule with the structure of a ligated one. Another way to obtain an intermediate state which is metastable at low temperatures is the irradiation of metmyoglobin (Mbmet) with X–rays. Mbmet, which is mainly Fe(III) high spin (Bizzarri et al., 1995) with a water coordinated at the 6th position, becomes Fe(II)LS low spin without loosing the water and without changing the structure significantly. The relaxation into the 5 coordinated Fe(II)HS high spin structure of deoxy-myoglobin, Mbdeoxy, has been investigated as a function of temperature and time (Prusakov et al., 1995). For relaxation an energy barrier has to be surmounted, which has also an energy distribution as the barrier in the CO rebinding experiments.

This thesis extends a previous investigation on myoglobin (Prusakov et al., 1995) to the more complex hemoglobin system. An intermediate state is created changing the valence of the heme iron from Fe(III) to Fe(II) by X–ray irradiation at low temperature. We start with Hbmet where the protein is in the R quaternary state (Chevion et al., 1979). In comparison with myoglobin, we want to study the influence of the quaternary structure. Moreover, we study the way CO is produced by X-ray irradiation in the glycerol water matrix. In particular, we follow the CO binding to irradiated Mbdeoxy that has been prepared in solution with and without glycerol to evidence its role. In addition, a deoxy-hemoglobin (Hbdeoxy) sample in glycerol solution has been irradiated with X-ray. With this procedure it is possible to follow the binding of the CO in comparison with the Mb data. Again, this yields information about the effect of the quaternary structure.

 The importance of the quaternary structure is also shown in the attempt to better understand the allosteric heterotropic behaviour of the Hb. In fact there are still some open questions concerning the T to R transition in presence of allosteric effectors (Monod et al., 1965; Koshland et al., 1966; Pauling et al., 1935; Henry et al., 2002; Viappiani et al., 2004). The separation of tertiary from quaternary conformational changes seems the way to understand this allosteric behaviour. The encapsulation of Hemoglobin in wet silica gels gave the opportunity to study the tertiary dynamics slowing down dramatically the quaternary ones, which can be considered as blocked. The encapsulation does not alter the Hb optical spectral and the functional properties, in fact no restriction was observed on tertiary conformational changes triggered by homeotropic and heterotropic effectors but the kinetics of ligand-linked quaternary conformational changes are significantly slowed down. It has been shown that Hb in T state encapsulated in wet silica gel binds

oxygen in non-cooperative way both with allosteric effectors and in absence of allosteric effectors. Moreover, two distinct affinity conformations (Shibayama et al., 2001) in T state have been found: a low affinity (LA) and high affinity (HA) (Bruno et al., 2001). In particular, Hb in T state encapsulated in silica gel with allosteric effectors (LA) has a 10 times lower O_2 affinity than in their absence (HA).

Since one of the crucial problems is the behaviour in presence of allosteric effectors, in order to study if there are differences in the tertiary structures of these two T quaternary states, in this work Mössbauer spectroscopy has been used, to get information on the iron surrounding. It has been demonstrated that carboxy-hemoglobin (HbCO) and Hbdeoxy encapsulated in wet silica gel show no differences of the Mössbauer parameters found in solution. The temperature dependence quadrupole splitting of high and low affinity Hb T states have been measured. In fact the temperature dependence of the quadrupole splitting of heme proteins, which was widely studied by Eicher et al. (Eicher et al., 1969; Eicher et al., 1970; Eicher et al., 1974), gives information on the iron geometry and the low–lying electronic levels of Fe^{2+}. Using this theory it is possible to look at the structural differences in the iron surrounding of the high and low affinity Hb T quaternary states.

2 Theoretical Background

2.1 Mössbauer Spectroscopy

In the 1958 R.L. Mössbauer discovered the recoil energy free nuclear resonance fluorescence and for this discovery he was awarded the Nobel Prize three years later. At that time it was expected a development of this new physics branch and actually from that time till nowadays the Mössbauer spectroscopy has been employed in a lot of fields like solid state physics, chemistry, biology, archaeology and many others, providing valuable information. The Mössbauer effect and the methods will be presented. A more complete and deep treatment can be found in specific literature (Danon, 1968; Gonser, 1975; Greenwood and Gibb, 1971).

2.1.1 The Mössbauer Effect

A radioactive isotope usually decays to the stable ground state of a daughter nuclide passing through different excited states of the daughter. The transitions between the different excited states and from excited states to the ground state occur by the emission of electromagnetic radiation-packets, called γ-quanta. A photon with energy E_γ has a momentum $P_\gamma = E_\gamma/c$, where c is the speed of light. In the case of a nuclear transition of an isolated nucleus at rest, the conservation of the momentum requires that the decaying nucleus recoils with a momentum $\mathbf{P_n} = -\mathbf{P_\gamma}$ during the emission of the photon. Thus, the total energy of the nuclear transition E_0 must be divided between the emitted photon and the nucleus that recoils, with an energy E_R given by:

$$E_R = \frac{p_n^{\ 2}}{2M} = \frac{p_\gamma^{\ 2}}{2M} = \frac{E_\gamma^{\ 2}}{2Mc^2} \qquad\qquad \textbf{(2-1)}$$

Because of the conservation of energy, the energy of the emitted photon is $E_\gamma = E_0 - E_R$. For the same reasons, an isolated nucleus can absorb the γ-quantum only if the energy of the absorbed photon is $E_\gamma = E_0 + E_R$. Therefore, the energies of an emitted photon and a photon that can be absorbed differ by the quantity $2 \times E_R$. The recoil energy E_R of γ-rays is usually large compared to the natural width of the nuclear levels. Thus, in the common case of ^{57}Fe (τ_n=141 ns), the natural line width Γ of the emission and absorption line is 4.67×10^{-9} eV, whereas the high energy of the 14.4 keV nuclear transition from the excited state with nuclear moment I=3/2 to the ground state with nuclear moment I=1/2 gives rise to a recoil energy of about 2×10^{-3} eV, which is about six orders of magnitude higher than the natural width of the emission and absorption lines. It follows directly that

the separation between the absorption and the emission energies are by far too large to allow the resonant absorption of γ-quanta by free nuclei. When embedded in a solid lattice, however, an atom cannot transfer recoil as if it was free. In this case, the recoil momentum imparted to the nucleus can be taken up by the whole crystal, which results in a negligibly small recoil energy E_R, because of the large mass of the crystal. The recoil energy free emission and absorption of γ-quanta by nuclei in a solid is known as Mössbauer effect. The probability of recoil-free emission or absorption is known as Lamb-Mössbauer *f*-factor. It is worth noting that *f(T)* decreases strongly with the energy increase of the γ-photons and also with the increase of temperature. In particular one has:

$$f = \exp(-k^2 \langle x^2 \rangle)$$
(2-2)

where k=2π/λ and $<x^2>$ is the mean square displacement which measures the motion of the iron during the absorption or the emission process of the gamma–quantum. Since *f* gives the probability of resonance absorption, an experimental determination of the area of the absorption spectrum allows the determination of the mean square displacement, $<x^2>$, of the iron. Measuring $<x^2>$ as a function of temperature, it is possible to separate different contribution to the motion of the iron and, in this way, to analyse the dynamics of the sample in detail. This property of Mössbauer spectroscopy has been used to investigate protein dynamics (Parak et al., 1971; Huenges et al., 2002; Parak et al., 2003). In order to measure the absorption area and to detect the energy variations caused by the hyperfine interactions of the absorber nuclei as function of the surrounding chemical environment, it is necessary to scan a proper range of energies around the resonance energy. This is usually done by moving the source with respect to the absorber. In particular, when the source is moving with a velocity **v** relative to the absorber, the energy variation of the emitted γ-rays, E_D, produced by Doppler effect is:

$$E_D = \frac{v}{c} E_\gamma$$
(2-3)

In Mössbauer spectroscopy, the energy scales are therefore conventionally reported in mm/s rather than in eV or other energy units.

2.1.2 The Hyperfine Interactions

The high energy resolution of the Mössbauer spectroscopy allows the detection of the interactions between the nucleus and the electrons, hence permitting to obtain information on the chemical environment. The electromagnetic interaction between nucleus and its surrounding electrons is usually treated as multipole expansion. The main interactions, called *hyperfine interactions*, are:

i. the electric monopole interaction, which causes an energy energy shift of the resonance lines (*isomer shift*), and represents the electrostatic interaction between the electronic charge entering the nuclear volume and the protonic charge within the nuclear volume;

ii. the magnetic dipole interaction, which causes a Zeeman splitting of the Mössbauer line (*magnetic hyperfine splitting*);

iii. the electric quadrupole interaction, which also causes a splitting of the Mössbauer line (*electric quadrupole splitting*).

2.1.2.1 Isomer Shift

When the Mössbauer nuclei of source and absorber are in different materials, the absorption line related to the velocity of the Mössbauer transducer v=0 is shifted. This effect, called isomer shift, arises from the Coulomb interaction between nuclear and electronic charge. Lets us assume that the atomic nucleus is spherical, the energy shift can then be given as:

$$\Delta E = \frac{2}{3} \pi Z e^2 \left| \Psi(0) \right|^2 \left\langle r^2 \right\rangle \tag{2-4}$$

where Z is the atomic number, *e* is the electronic charge, $\left\langle r^2 \right\rangle$ is the mean square value of the radius of the nucleus and $\left| \Psi(0) \right|^2$ the electronic density at the nucleus site. In the non-relativistic approximation, the wave function of the s-electrons, in fact, is the only wave function with non-zero amplitude at the nucleus, and therefore with non-zero probability density. Since the atomic nuclei have different radii in the excited and ground states $(r_g \neq r_e)$, the energies in these states are different as well:

$$\Delta E = \frac{2}{3} \pi Z e^2 \left| \Psi(0) \right|^2 \left(\left\langle r^2 \right\rangle_e - \left\langle r^2 \right\rangle_g \right) \tag{2-5}$$

$\left|\Psi(0)\right|^2$ is the s-electron density at the nucleus. It will be affected not only by s-electron population but also by screening effects of p and d electrons, as well as by covalence and bond formation, given by chemical binding of the atom ^{57}Fe. As consequence, the absorption line shift is given by:

$$\delta E = \frac{2}{3}\pi Z e^2 \left(\left\langle r^2 \right\rangle_e - \left\langle r^2 \right\rangle_g \right) \times \left[\left|\psi(0)_A\right|^2 - \left|\psi(0)_S\right|^2 \right] \qquad \textbf{(2-6)}$$

where the A and S indices refer to Absorber and Source. The energy of the nuclear transition therefore changes on addition of electrons to the bare nucleus, and due to the fact that the s-electron density at the nucleus is in general different in the source and in the absorber. Eq. 2-6. contains the product of chemical term and nuclear term, but in practice the nuclear term is constant for a given transition and for chemical application the important equation is

$$\delta = const \times \left[\left|\psi_S(0)_A\right|^2 - \left|\psi_S(0)_s\right|^2 \right] \qquad \textbf{(2-7)}$$

Moreover, the presence of a relativistic temperature dependent contribution to the isomer shift has to be mentioned. The emitting or absorbing atom is vibrating on its lattice site in the crystal. The frequency of the oscillation about the mean position is of the order of 10^{12}, so the average velocity taken over a decay time is zero. However, there is a term in the Doppler shift that depends on v^2, so the mean value $\left\langle v^2 \right\rangle$ is non-zero. This is called "second order Doppler shift", which is shifting the Mössbauer line (Greenwood and Gibb, 1971).

2.1.2.2 Magnetic Hyperfine Splitting

When a nucleus is placed in a magnetic field, there is a magnetic dipole interaction between any nuclear magnetic momentum μ and the magnetic field B, described by the Hamiltonian

$$-\hat{\mu} \cdot \hat{B} = -g_N \beta_N \hat{I} \cdot \hat{B} \qquad \textbf{(2-8)}$$

where g_N is the nuclear Landè splitting and β_N is the nuclear magneton. The total magnetic field experienced by the nucleus is a vector sum of the magnetic hyperfine field and any external applied field. The magnetic hyperfine field at the nucleus arises from any unpaired spin of atomic electrons, and therefore depends on the oxidation and spin state of the atom. This interaction completely raises the degeneracy of a nuclear state with an angular momentum quantum number I>0 and splits it into 2I+1 substates (*Zeeman effect*). In case of ^{57}Fe, the ground state with I=1/2 splits into two substates

and the excited state with I=3/2 splits into four substates. Gamma transitions between the sublevels of the ground state and those of the excited state are subject to selection rules. In case of ^{57}Fe only transitions with $\Delta m_I = 0, \pm 1$ are allowed, giving rise to six transitions altogether. In case of S=1/2, 3/2 and 5/2, the degeneration can be completely resolved, for example in biological compounds, lowering the temperature (5K) and applying a small external magnetic field $B_{ex} \sim 20mT$. This external magnetic field has the duty to define a quantisation axis, and it could even be defined as "weak field stabilization".

2.1.2.3 The Quadrupole Interaction

Any nucleus with a spin I grater then 1/2 has a non spherical charge distribution, which contains a quadrupole term if it is expanded as a series of multipoles. The magnitude of the charge deformation is described by the nuclear quadrupole momentum Q. The sign of Q depends on the shape of the deformation. A negative quadrupole momentum indicates that the nucleus is oblate or flattened along the spin axis, whereas for a positive momentum it is prelate or elongated. In a chemically bound atom, the electronic charge distribution is usually not spherically symmetric. The electric field gradient at the nucleus is defined as the tensor

$$E_{ij} = -V_{ij} = -\left(\frac{\partial^2 V}{\partial x_i \partial x_j} \right) \text{ with } (x_i, x_j = x, y, z) \tag{2-9}$$

where V is the electrostatic potential. The Hamiltonian describing the interaction can be written as

$$\hat{H} = \frac{eV_{zz}Q}{4I(2I-1)} \left[3\hat{I}_z^2 - \hat{I}(\hat{I}+1) + \eta(\hat{I}_x^2 - \hat{I}_y^2) \right] \tag{2-10}$$

where V_{zz} is the electric field gradient in the z direction. In the case of heme protein, due to the heme plane symmetry, the x and y axes are usually chosen to lie on the heme plane while the z axis is taken perpendicular to the heme plane. The orientation of the nuclear axis with respect to the principal axis, z, is quantised. There is interaction energy between Q and V_{zz} which is different for each possible orientation of the nucleus. Moreover, η is the so called *asymmetry parameter*, i.e. a measure of the distortion from axial symmetry of the electric charge cloud about the ^{57}Fe nucleus, and is given by

$$\eta = \frac{V_{xx} - V_{yy}}{V_{zz}} \tag{2-11}$$

Actually, other definition for the x, y, z , axis can be chosen where V_{zz} is the largest component yielding to $\eta \leq 1$.

In the Mössbauer spectroscopy it is necessary to evaluate the eigenvalues of H_Q, which are the energies E_Q for the ground state and for the excited state. Basically, the laws of conservation of angular momentum and of parity lead to the formulation of definite selection rules which characterize the transition between the two states, and these rules ensure that there is a high probability for transitions with $\Delta m = 0; \pm 1$ where $\left[(I_z)_e - (I_z)_g \right] = m$. The electric quadrupole interaction splits the first nuclear excited state of ^{57}Fe into sublevels, with eigenvalues

$$E_Q = \pm \frac{1}{4} eQV_{zz} \left(1 + \frac{1}{3} \eta^2 \right)^{1/2} \tag{2-12}$$

The resultant spectrum will comprise two lines, which are in fact of equal intensity if the sample is in isotropic powder, such as a randomly oriented polycrystalline sample. However, there are cases that exhibit a different intensity for the absorption line even in powder. This effect, known as "Goldanskii- Karyagin effect" (Karyagin, 1963), is due to an anisotropy in the recoil free fraction. In particular, the ratio of the two absorption lines is given by:

$$\frac{I_1}{I_0} = \left[\frac{1}{2} \int_0^\pi f(\theta) \frac{3}{2} \sin^3 \theta d\theta \right] \Big/ \left[\frac{1}{2} \int_0^\pi f(\theta) \frac{3}{4} (1 + \cos^2 \theta) \sin \theta d\theta \right] \tag{2-13}$$

where I_0 is the absorption line for $\Delta m = 0$ and I_1 is the absorption line for $\Delta m = \pm 1$. This ratio is 1 if $f(\theta)$ is isotropic, otherwise the spectra will have a different intensity of the absorption line. Another non-negligible source of quadrupole doublet asymmetry is represented by the *texture effects*. They occur when the EFG (Electric Field Gradient) principle axes are not randomly oriented with respect to the γ-ray direction. The centroid of the doublet corresponds to the energy of γ transition, without the quadrupole interaction, so that we can still measure the chemical isomer shift. The magnitude of the quadrupole interaction is a product of two factors: *eQ*, a nuclear constant for the resonant isotope, and *eq*, a function of chemical environment. In case of the the $3/2 \rightarrow 1/2$ transition, it is not possible to determine neither the sign of $e^2 qQ$ nor the magnitude of η from line position alone. The

electric field gradient is the negative second derivative of the potential at the nucleus of all surrounding electric charge. It therefore includes contribution from both the valence electrons of the atom and from surrounding ions. In ionic complex it is customary to consider these separately, and write:

$$\frac{V_{zz}}{e} = q = (1-R)q_{ion} + (1-\gamma_\infty)q_{latt} \tag{2-14}$$

where R and γ_∞ represent the effects of shielding and anti-shielding respectively of the nucleus by the core electrons. The total electric field gradient from the valence electrons of the ion can be obtained by summing the appropriate wave function contributions. If the orbital population varies with the temperature because of the excitation to low-lying higher states, then the electric field gradient will probably show strong temperature dependence. The quadrupole splitting temperature dependence will be described in detail in the following paragraph, with particular reference to the Hbdeoxy complex.

2.1.3 Temperature Dependence of Quadrupole Splitting in the Iron(II) HS Complex

Hbdeoxy shows a temperature dependence of the quadrupole splitting due to the different Electric Field Gradient (EFG) felt at the nuclear site. The EFG is produced by electrons in the perturbed $3d^6$-configuration and by the second order components of the crystalline electric field. The EFG components of the individual substate are averaged according to Boltzmann statistic (Eq. 2-19) in case of fast relaxation. According to the theory developed by Eicher (Eicher et al., 1970; Eicher et al., 1969; Eicher et al., 1976), it is possible to calculate the eigenvalues and eigenstates of the hamiltonian of the $3d^6$ electrons. The hamiltonian in (Eicher et al., 1969) describes in first approximation a system with a nearly tetragonal point symmetry of the iron cation and the Coulomb repulsion of the 3d electrons, and in a higher approximation the spin orbit coupling of the 3d electrons and the effects of a small rhombic perturbation of the C_{4v} point symmetry (Eicher et al., 1970).
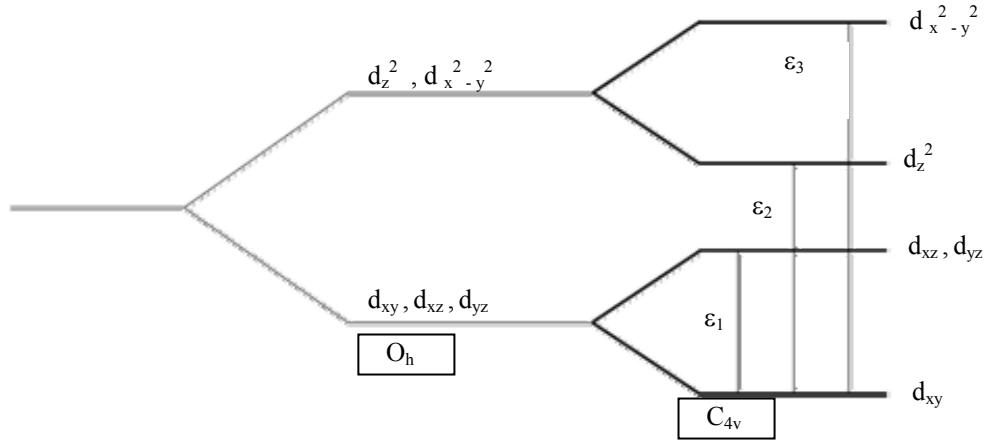
Figure 2.1: Electronic scheme: the degeneracy of e_g and t_{2g} orbitals of Fe in heme protein due to the interaction with neighbouring N-atoms. At first approximation, the symmetry is tetrahedral (C_{4V}). The ε_1, ε_2, ε_3 parameters determine the energy gaps of the antibonding single 3d electron orbitals.

The Hamiltonian that depends on three adjustable parameters ε_1, ε_2, ε_3 describes a system with a nearly tetragonal point symmetry of the iron, a crystalline field with a temperature independent and an axially symmetric Vzz (lattice) term and the Coulomb repulsion of the 3d electrons.

The ε_v are the energy gaps of the antibonding single 3d-electron orbitals:

$$\varepsilon_1 = E(3d_{xz}, 3d_{yz}) - E(3d_{xy})$$
$$\varepsilon_2 = E(3d_{z^2}) - E(3d_{xy}) \hspace{3cm} \textbf{(2-15)}$$
$$\varepsilon_3 = E(3d_{x^2-y^2}) - E(3d_{xy})$$

where E is the energy of the given orbital. In this symmetry the 5-fold degeneracy of the 3d-levels is nearly lifted as shown in Fig. 2.1. The EFG at the nucleus site is produced by six electrons in the antibonding 3d orbitals. Examining the symmetry of the 3d, 4s and 4p orbitals of iron and σ and π orbitals of the surrounding ligands by means of group theory, it follows that the antibonding 3d orbitals are the only involved into the production of the EFG. The energy order is determined by the relative amounts of the antibonding mixing. From the ε_1, ε_2, ε_3 values it is possible to obtain the EFG felt at nuclear site. In particular, it is possible to calculate the eigenvalues of a many-electron wave function that is constructed by the single-electron perturbed wave function. These eigenvalues characterize a many-electron level with a particular energy. The relative position of these many-electron levels of the iron atom describes the electronic shell structure at any fixed

temperature. As reported in (Eicher et al., 1969) it was found that the many-electron levels $^1A_1$, ^3E, $^5B_2$,, and ^5E, lay lowest in energy. The multi-electron terms (Fig. 2.2) can be correlated with the one-electron levels of $3d^6$ via secular equation of the problem.
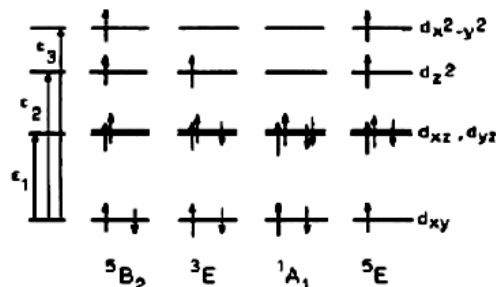

Figure 2.2: Correlation between one-electron levels of the $3d^6$ configuration and the multi-electron term scheme for the C_{4v} point symmetry (Eicher et al., 1976).

The eigenvalues and eigenvectors of these four many-electron levels are used as base vectors for the diagonalization of the relative small spin-orbit interaction and rhombic perturbation. The spin-orbit contribution

$$H_{SO} = -\lambda \mathbf{L} \cdot \mathbf{S} \tag{2-16}$$

- as well as the rhombic perturbation - has to be added to the Hamiltonian. These two interactions remove the degeneracy of the base vectors leading to 22 singlet states that are shown in Fig. 2.3
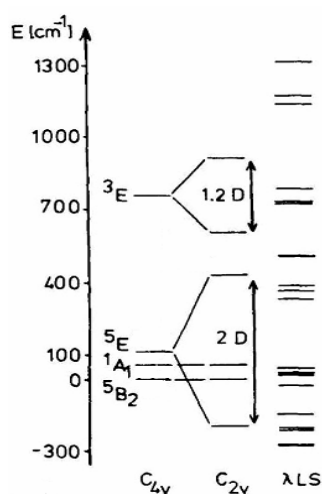

Figure 2.3: Scheme of low energy levels of $3d^6$ configuration of Fe(II) in heme proteins. The degeneracy is raised by rhombic perturbation and by the spin orbital coupling (Eicher et al., 1976).

18

In particular, as reported in (Eicher et al., 1976) the relative energies of the many-electron levels

$$E_1 = E(^5E) - E(^5B_2)$$
$$E_2 = E(^3E) - E(^5B_2) \qquad\qquad (2\text{-}17)$$
$$E_3 = E(^1A_1) - E(^5B_2)$$

can be related to ε_v yielding to the empirical formulas:

$$\varepsilon_1 = E_1$$
$$\varepsilon_2 = 7019.6 + 0.766E_1 + 1.0968E_2 - 1.0622E_3 \qquad\qquad (2\text{-}18)$$
$$\varepsilon_3 = 17942.8 + 1.0474E_1 - 1.0510E_2 - 0.0136E_3$$

where the energies are given in cm^{-1}.

The temperature dependence of the quadrupole splitting is calculated averaging the EFG component of the individual substate according to Boltzmann statistics:

$$\langle V_{zz} \rangle_T = \sum_{i=1}^{22} V_{zz}{}^{(i)} \exp\left(-\frac{E_i}{kT}\right) \bigg/ \sum_{i=1}^{22} \exp\left(-\frac{E_i}{kT}\right) \qquad\qquad (2\text{-}19)$$

The eigenvectors and eigenfunction of these 22 states depend on five adjustable parameters: ε_1, ε_2, ε_3, λ, and D. In particular λ is the spin orbit constant and D is proportional to the splitting amount caused by rhombic perturbation of the orbital doublets ^3E and ^5E. Moreover, the splitting of ^3E and ^5E are 2D and 1.2D respectively (Eicher et al., 1970). So it is possible to obtain the five parameters ε_1, ε_2, ε_3, λ, and D trough the fit, with the least squares procedure, of the measured quadrupole splittings at various temperatures. In this procedure the Electric Field Gradient at the nuclear site is calculated varying the five parameters and minimizing the distance between the calculated EFG value and the measured one, at each temperature. This procedure has been done for many porphyrin compounds and in particular in case of Hb and Mb (Eicher H. et al., 1976). The following conditions for the adjustable parameters must hold in order to have results that are physically significant: the energy gap ε_1 and the rhombic perturbation $|D|$ are much smaller than ε_2 and ε_1 (Eicher et al., 1969); the energy gap ε_2 is greater then ε_3 (Zerner M. et al., 1966). The spin-orbit coupling constant λ must be smaller than $\lambda_0 = 103$ cm^{-1}, that is the value in case of free ion. This reduction is due to the covalency effects in the molecule. Therefore the covalency factor α^2 must be smaller then 1. In addition, λ and α^2 should be nearly the same in all porphyrin compounds. Most important, as it was pointed out in (Eicher et al., 1976), are the considerations about the

structure nearby the iron, which can be deduced from the ε_2 and ε_3 values. The antibonding $3d_{xz}$, $3d_{yz}$ and $3d_{xy}$ orbitals are raised only slightly because they are essentially iron orbital, while $3d_{z^2}$ orbital reacts very sensitively upon the occupation of sixth and fifth position. When tight binding ligand occurs, the energy is lifted up and if the two ligands are quite different as in case of Hb, the iron cation is likely out of the porphyrin plane. The ε_2 value of a_{1g} (d_{z^2}) depends very sensitively on the binding strength of the imidazole nitrogen atom. Therefore the rising of ε_2 is correlated with a shortening of the distance with imidazole nitrogen. On the other hand, $3d_{x^2-y^2}$ orbital interacts solely with the porphyrin σ system (Eicher et al., 1969). In the case of planar Fe-porphyrins the energy gap between the $3d_{xy}$ and $3d_{x^2-y^2}$ orbitals was calculated for model compounds (Zerner et al., 1966) to be around 22000 cm^{-1}. This value is reduced to about 16000 cm^{-1} when the iron is out of the plane. The ε_3 value, that is the energy gap of antibonding single 3d-elecrtron orbitals between $3d_{x^2-y^2}$ and $3d_{xy}$, is rising when the distance between the iron and the heme plane is decreasing. One can think this effect due to a larger overlapping between the 3d antibonding orbitals and the porphyrins σ system: therefore ε_3 is a measure of the bond length between the iron cation and the four nitrogen atom in the heme. According to these considerations, in (Eicher et al., 1976) it was found that the iron cation is a more planar situation in Mb than in Hb. More planar could be correlated with a higher affinity for the ligand.

2.1.4 Analysis of Mössbauer Spectra

2.1.4.1 Spectra Evaluation

When the sample is irradiated with intensity I_0, only a fraction is absorbed by Mössbauer nuclei. The number of quanta in the transmitted beam is given by

$$Z(v) = CR \int_{-\infty}^{\infty} Q(v, E_s, E) \exp\left[-\sigma_a(E_a, E) n_{Fe}\right] dE + CR(1 - f_s) + CU \qquad \textbf{(2-20)}$$

The first term of the equation represents a decrease of the intensity of the transmitted beam due to Mössbauer absorption. The second term represents photons with the improper energy from the 14.4 keV transitions, which loose recoil energy during the emission, and therefore can not perform Mössbauer effect. The final term accounts for photons with the improper energy which cannot be discriminated due to the limited resolution of the detector. Since the energy resolution of the

detector is always much broader then the energy resolution of the Mössbauer effect, U is always non-zero. C is determined by the activity of the source, R is the fraction of detected radiation coming from 14.4 keV transitions, while U is the fraction of detected radiation with energy other the 14.4 keV. In the first term of Eq. 2-20 Q is the emission spectrum of the source centred at the energy $[1 + (v/c)]E_s$:

$$Q(v, E_s, E) = \frac{f_s \left(\Gamma_s / 2\pi \right)}{\left\{ E - E_s \left[1 + \left(\frac{v}{c} \right) \right] \right\}^2 + \left(\Gamma_s / 2 \right)^2} \tag{2-21}$$

and $\sigma_a \left(E_a, E \right)$ represents the cross-section for Mössbauer absorption centred at the energy E_a

$$\sigma_a \left(E_a, E \right) = \sigma_0 f_a \frac{\left(\frac{\Gamma_a}{2} \right)^2}{(E - E_a)^2 + \left(\frac{\Gamma_a}{2} \right)^2} \tag{2-22}$$

The FWHM line widths of the Lorentzian energy distribution emitted by source and absorbed in the sample are given by Γ_s and Γ_a respectively. These are usually slightly broader than theoretical line width. This is due to the fact that each iron ion has generally a slightly different environment. This causes an inhomogeneous broadening. The probability for recoil energy free emission or absorption is given by the Lamb-Mössbauer factors f_s and f_a respectively. For iron $\sigma_0 = 2.56 \times 10^{18}$ cm²/^{57}Fe nucleus, and n_{Fe} gives the number of ^{57}Fe nuclei per cm² in the sample. Unfortunately, the integral of the Eq. 2-20 cannot be solved analytically.

When the sample is thin, which means $\sigma_a \left(E_a, E \right) n_{Fe} \ll 1$, the exponential function can be expanded in a series which is truncated after the linear term of $\sigma_a \left(E_a, E \right) n_{Fe}$.

In the "thin absorber approximation", the Mössbauer spectrum becomes:

$$T(v) = \frac{Z(v)}{Z(\infty)} = 1 - \frac{R}{R + U} f_s t_a \left(\frac{\Gamma_{nat}}{2} \right) \frac{\left(\Gamma_a + \Gamma_s \right) / 2}{\left\{ E_a - E_s \left[1 + \left(\frac{v}{c} \right) \right] \right\}^2 + \left[\left(\Gamma_a + \Gamma_s \right) / 2 \right]^2} \tag{2-23}$$

with $t_a = n_{Fe} \sigma_0 f_a$.

In practice, this equation is often used for a phenomenological description of a Mössbauer spectrum event if the "thin" condition is not rigidly fulfilled. It is common to introduce useful notations. The Mössbauer absorption is given by

$$\eta(v) = 1 - T(v) \tag{2-24}$$

and the maximal absorption becomes

$$\eta(0) = \frac{R}{R+U} f_s t_a \frac{\Gamma_{nat}}{\Gamma_a + \Gamma_s} \tag{2-25}$$

The absorption area A of the Mössbauer spectrum is defined as:

$$A = \int_{-\infty}^{\infty} \eta(v) d\left(\frac{E_s}{c} v\right) \tag{2-26}$$

which gives:

$$A = \frac{R}{R+U} f_s t_a \frac{\Gamma_{nat}}{2} \pi \tag{2-27}$$

This equation is used for the determination of the effective absorber thickness t_a. This parameter, t_a, contains the Lamb-Mössbauer factor f_a and therefore the information about protein dynamics of the sample.

For relative thick absorber ($t_a < 30$), another approach has been developed: in fact the areas under the peak are not proportional to the true intensity or to t_a.

Already Hafemeister (Hafemeister et al. 1965) has calculated the contribution to the area for different $t_a < 30$. In particular, the area

$$A = \frac{R}{R+U} f_s L(t) \frac{\Gamma_{nat}}{2} \pi \tag{2-28}$$

where L(t)

$$L(t) = \sum_{p=1}^{\infty} \frac{(-1)^{p+1}(2p-3)!!t^p}{p!(2p-2)!!}$$ **(2-29)**

In addition to the use of a table where are reported L(t) as function of t_a, another method is used based on the calculation of the transmission integral. According to this method, the cross section $\sigma_a(E_a, E)$ is calculated trough a deconvolution process. In particular, the absorption is:

$$\eta(v) = Rf_s \left[1 - \int_{-\infty}^{\infty} \frac{Q}{f_s} \exp(\sigma_a n_{Fe}) dE \right]$$ **(2-30)**

where

$$\sigma_a n_{Fe} = n_{Fe} f_a \sigma_0 \frac{\left(\frac{\Gamma_a}{2} \right)^2}{(E - E_a)^2 - \left(\frac{\Gamma_a}{2} \right)^2} = t_a \frac{\left(\frac{\Gamma_a}{2} \right)^2}{(E - E_a)^2 - \left(\frac{\Gamma_a}{2} \right)^2}$$ **(2-31)**

hence

$$\eta(v) = Rf_s \left[1 - \int_{-\infty}^{\infty} \frac{Q}{f_s} \exp \left[t_a \frac{\left(\frac{\Gamma_a}{2} \right)^2}{(E - E_a)^2 - \left(\frac{\Gamma_a}{2} \right)^2} \right] dE \right]$$ **(2-32)**

the parameters as t_a and Γ_a are calculated resolving the integral through a deconvolution process. The calculation of the effective thickness t_a gives important information about the Lamb-Mössbauer factor of the absorber f_a and in case of more species about their relative populations.

Apart from thickness effect, vibration etc., the line shape will often be not Lorentzian for more fundamental reasons. These are the static hyperfine parameter distributions (*inhomogeneous broadening*) and the dynamic effect (*homogeneous broadening*) (Rancourt, 1989). The first case is also typical of heterotrophic biological sample. It is likely to find a species with slightly different conformations leading to a line width enlargement and, in principle, to a Gaussian distribution of Lorentzian line as absorption line. In this case, the use of thin approximation $t_a < 1$ or of transmission integral can be combined with the use of Voigt profile. For the analysis of materials

whose spectra consist of a large number of overlapping peaks, the convolution of Lorentzian and Gaussian curves (Voigt) is used to fit the peaks. Dynamic effects are present in Mössbauer spectra when hyperfine interactions vary on a time scale comparable to the intrinsic measurement time. The latter time is the mean time during which the Mössbauer γ-ray interacts with the nucleus, and it is approximately equal to the natural full width at half maximum of the emission (Γ_0) divided by Planck's constant. In the 14.4 keV Mössbauer transition of ^{57}Fe, the measured half life is $t_{1/2}$=97.7ns, such that the decay time is τ=h/Γ_0= $t_{1/2}$/ln2=140 ns (1/τ=1.5×10^7 Hz) and dynamic effects are seen in the frequency window between 10^6 and 10^{11} Hz.

2.2 Conformational Changes of Heme Proteins

The protein conformation is the spatial organization of the protein atoms that depends on the rotation of one or more bonds. The conformation of a protein can change without the breaking of the covalent bonds. If one is considering all the possible rotations of the bonds of each amino acid, the number of possible conformations of one protein molecule is enormous. In reality, the freedom degree of each single residue is restricted. In physiological condition, each protein has only one stable form known as native conformation. The proteins are able to assume different conformations according to their functions, in fact they may shift among several conformations in performing their biological function and these transitions between them are called **conformational changes.** During the last 30 years, many experiments to study the protein kinetics and conformational changes of the hemoproteins have been performed with particular interest on myoglobin. These studies are directed towards the understanding of the correlation between protein structure, dynamics and functions. Examples are given by Hb, which can have a bound dioxygen HbO$_2$ or be in unbound state Hbdeoxy. Each conformation can assume a large number of slightly different structures called Conformational Substates (CS). Proteins in different conformational substates perform the same function albeit with different rate. At non-physiological temperature the protein does not perform its function. Structural protein dynamics has been widely studied with Mössbauer spectroscopy that has contributed significantly to the understanding of the physics of the proteins in two regimes, at temperature lower and higher than the so called *characteristic temperature*, T$_c$. In fact, under T$_c$ the protein is frozen in a particular substate, while above that temperature it is in a flexible state where the structure can fluctuate (Huenges et al., 2002).

2.2.1 Conformational Substates – Ligand Binding Kinetics

Most of the experiments have followed the rebinding of small molecules like CO after the breaking of CO bonding by a light pulse. According to these experiments, the molecules are in an unbound state B and they relax into a bound state A. In case of a binding process from the state B to the state A the rate coefficient k_{BA} can be described by the relation:

$$k_{BA}(T) = \frac{k_B T}{h} \exp\left[-\Delta G^{\#}{}_{AB} / RT\right] \qquad (2\text{-}33)$$

where $\Delta G^{\#}$ is the Gibbs free energy of the reaction, k_B is the Boltzmann, h the Planck constant, and R the general gas constant. Considering that $\Delta G^{\#} = \Delta H - T\Delta S$, it is possible to relate Eq. 2-33 to the Arrhenius relation:

$$k_{BA}(T) = A_{BA}\left(T / T'\right) \exp\left[-H_{AB} / RT\right] \qquad (2\text{-}34)$$

where A_{BA} is a frequency factor, T' is the reference temperature, usually set at 100K, and H_{BA} is the barrier height (activation enthalpy). During the B→A transition, the ligand overcomes the potential barrier. The A_{BA} frequency factor is dependent on the entropy. If the pre-exponential factor A_{BA} and the barrier height H_{BA} have a unique value (the survival probability) then the molecules that have not rebound a ligand at the time t after the light pulse is described by an exponential:

$$N(t) = \exp\left\{-k_{BA}(T)t\right\} \qquad (2\text{-}35)$$

Actually, it is well know that **reaction and relaxation** process of a wide variety of heme proteins are non-exponential in time, and N(t) can be approximated by:

$$N(t) = (1 + k_0 t)^{-n} \qquad (2\text{-}36)$$

where k_0 and n are temperature dependent parameter, as it was postulated by Austin (Austin et al., 1975). It has been demonstrated that this non-exponential behaviour is due to the presence of many different substates characterised by slightly different structure (Alberding et al., 1976; Alberding et

al., 1978; Beece et al., 1980; Doster et al., 1982). The presence of substates is demonstrated also by X-ray diffraction experiment and Mössbauer experiments, as it will be explained in more details afterwards. The conformational substates have a different barrier height H_{BA} for B→A transition. Below the so called characteristic temperature T_c (~200K) each protein molecule is frozen into a particular substate. The probability to find a molecule with barrier height between H_{BA} and $H_{BA} + dH_{BA}$ is defined by $g(H)dH_{BA}$ and the N(t) fraction is given by:

$$N(t) = \int dH_{BA} g(H_{BA}) \exp(-k_{BA} t) \tag{2-37}$$

From measured N(t), the distribution function $g(H_{BA})$ can be determined in terms of k_{BA} by the inverse of Laplace transform (Austin et al., 1975):

$$g(H) = \frac{k_{BA}}{RT} L^{-1}[N(t)] \tag{2-38}$$

where L^{-1} is the inverse of Laplace transform. Since the Austin et al. publication in the 1975, the A value was assumed independent to H value and moreover with a well defined value. In practice, the data from 40K to 300K could be fitted with a single value of A, extrapolated using measurements at different temperatures, for each energy well. In particular, during the CO rebinding experiment the Log(A) was changing from 8.8 to 22, depending on the considered barrier. However, it is clear that there are no hints that if the energy enthalpy is distributed the entropy should be not (Austin, 1975: note 9). Actually, the inversion can be performed analytically if the observed data can be fitted by a function that can be Laplace inverted. Eq. 2.37 can be inserted into Eq. 2.38 leading to a distribution that depends on a Gamma function. This distribution has also been used in the model proposed by Young (Young et al., 1984). According to this proposed model, the substates are in equilibrium and populated according to a Boltzmann distribution. Below the characteristic temperature T_c, the molecules are no longer overcoming the barrier between substates, and remain frozen in a particular substate, with an enthalpy distribution given by

$$g(H_{AB}) = C_c (H_{BA} - H_{min})^{3v-1} \exp\left[-\alpha_c (H_{BA} - H_{min})\right] \tag{2-39}$$

where $C_c = \alpha^{3v}/\Gamma(3v)$ and $\Gamma(3v)$ is the gamma distribution.

In case of $T < T_f$ the enthalpy distribution is independent from temperature, and C_c depend on T_c, while in case of $T > T_c$, the enthalpy distribution $g(H_{AB}, T)$ is temperature dependent and C_c is function of T. The maximum value H_{peak} of the enthalpy distribution is given by:

$$H_{peak} = H_{min} + \left[(3\nu - 1)/\alpha_c\right] \qquad (2\text{-}40)$$

Moreover, in case of high temperature limit around 300K, the experimental monitored fraction N(t) -- as reported in (Young et al., 1984) - is given by:

$$N(t) \approx N_{out} \exp(-\lambda_{IV} t) \qquad (2\text{-}41)$$

where N_{out} is the fraction of photo-dissociated proteins whose ligand have migrated to the solvent, and λ_{IV} is a pseudo-first order rate coefficient that is proportional to ligand concentration. In this model, at high temperature the ligand concentration and the ligand migration to the solvent are taken into account. In this frame the viscosity contribution is important as underlined in (Beece et al., 1980), where it is concluded that in many experiments like flash photolysis, stopped flow or relaxation, the temperature dependence of a reaction will yield information only about the protein solvent system and not on the protein alone - particularly if measurements are only performed in one solvent. Therefore, the barrier height is also a function of viscosity. Nevertheless, other kind of g(H) distribution has been proposed and used (Alberding et al., 1976) such as the Gaussian distribution (Ober et al., 1997; Agmon et al., 1983; Ehrenstein et al., 1992) depending on the model or on the protein measured.

The rebinding kinetic as well as the relaxation of a metastable state can be described using the Gibbs free energy $\Delta G^{\#}$ without the separation of the entropy from enthalpy contribution. This separation was introduced by Austin (Austin et al., 1975) in case of flash photolysis experiments, in order to get an easier treatment. As just mentioned the main point was to keep A fixed at one value at all temperatures, considering only the enthalpy as continuous distribution or vice versa. However, in (Austin et al., 1975) it was also stressed that one could not rule out the idea that both, the frequency factor and the enthalpy have a distribution. Also the introduction of a gamma distribution was carried out at the beginning for "mathematical reasons" since the gamma function can be Laplace inverted. A Gaussian distribution can also be used as the simplest approach.

Therefore it is possible to describe the number of molecules that does not relax into another state as:

$$N(t) = N_0 \int g(\Delta G^{\#}) \exp[-k(\Delta G^{\#}, T)t] d\Delta G^{\#} \qquad \textbf{(2-42)}$$

with $k(\Delta G^{\#}) = \dfrac{k_B T}{h} \times \left[\exp(-\Delta G^{\#}/RT) \right]$ and

$$g(\Delta G^{\#}) = \dfrac{1}{\sigma\sqrt{2\pi}} \times \exp\left(-\dfrac{\left(\Delta G^{\#} - \Delta G^{\#}_{peak}\right)^2}{2\sigma^2} \right) \qquad \textbf{(2-43)}$$

where k_B is the Boltzmann, h the Planck, and R the general gas constant. σ is the standard deviation of the Gaussian distribution and N_0 is the scaling factor taking into account the starting population at different temperatures. In this formulation, the energy distribution includes both the enthalpy and the entropy which is no longer express by the A value.

2.3 Hemoglobin Cooperative Behaviour

Oxygen binding to hemoglobin is distinctly different from its binding to myoglobin. The job of hemoglobin is to bind oxygen efficiently in the lungs, where the partial pressure of oxygen is about 13.3 kPa. However, it needs to release it in the tissues, where the partial pressure is about 5 kPa. Notice that myoglobin is almost fully saturated at 5 kPa pO_2. In fact the binding curve of hemoglobin is not hyperbolic but sigmoidal (Fig. 1.3). This is a sign of cooperativity. The partial oxygen pressure when 50% of heme is bound is defined as p50. At physiological condition, p50 of hemoglobin is around 3.5 kPa. The "Hill plot" permits to evaluate the cooperative behaviour. In particular, the reaction of Hb with oxygen might be represented by the equilibrium equation:

$$Hb_n + nO_2 \leftrightarrow (HbO_2)_n \qquad (2-44)$$

the mass law to this n-th reaction leads to:

$$\dfrac{[HbO_2]_n}{[Hb]_n} = Kp^n \qquad \textbf{(2-45)}$$

that can be also written as:

$$\frac{Y}{1-Y} = K[X]^n$$

(2-46)

where Y is the fractional saturation with O_2 and $[X]$ the ligand concentration. The Hill plot represents the $\log(Y/(1-Y))$ as function of $\log([X])$ and it should give a straight line with slope equal to n, the apparent order of reaction at any point along it (Antonini et Brunori, 1971). Experimentally it has been showed that the reaction of hemoglobin is not a true n-th order reaction. However, the Hill plot is still very useful to get an indication about the degree of cooperativity. The Hill coefficient n_H is the slope of the Hill plot at $p[O_2]$ = p50, when the $\log(Y/(1-Y))$=0. If n_H=1, as in the case of myoglobin, there is no cooperativity, while if n_H is greater than 1 the cooperativity is positive. But if n_H is smaller than 1, it could indicate a negative cooperativity or a different affinity as in case of α and β subunits.
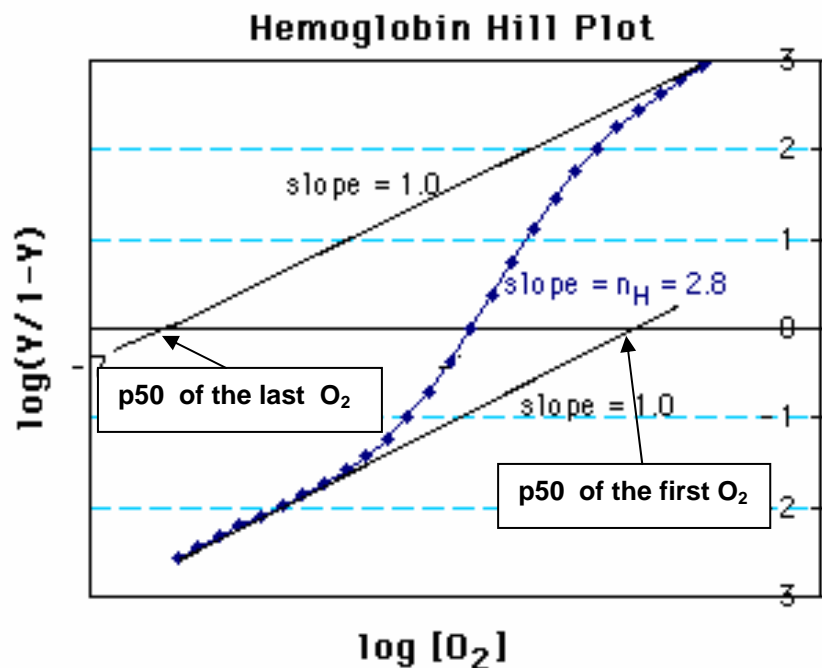

Figure 2.4 : Hill plot of Hemoglobin. The high and low asymptotes have slope equal 1, whereas the Hill coefficient n_H is 2.8. Y: fractional saturation with ligand O_2.

In case of hemoglobin at physiological conditions, at p50 $n_H = 2.8$ (Imai, 1982). In case of Hb the Hill coefficient n_H is varying from 2.8 to 3. In the following, some models are reported to explain the cooperative and allosteric properties of Hb.

2.3.1 Monod, Wyman and Changeux (MWC) Model

Jacques Monod, Jeffries Wyman, and Jean-Pierre Changeux observed that many enzymes are activated and inhibited by substrates and ligands in cooperative fashion and such enzymes contain more than one protein subunit. They actually saw the analogy with hemoglobin and they developed a theoretical model that would apply to many types of multisubunits proteins. As explained also in Perutz (Perutz, 1989), according to the MWC model (Monod et al., 1964), allosteric enzymes would have the biological advantages that no direct interaction need to occur between the substrate of the protein and the regulatory metabolite that controls its activity, because control would be entirely due to a change of structure induced in the protein when it binds its specific effector. The MWC Model can be described by the following statements (Cantor et Shimmel, 1980):

- *Identical protomers occupy equivalent positions in the protein. This implies molecular symmetry.*
- *Each protomer contains a unique receptor site for each specific ligand.*
- *The conformation of each protomer is constrained by the association with the other protomers.*
- *Two (at least two) states are reversibly accessible to allosteric oligomers.*
- *The affinity of one (or several) of the stereospecific site towards the corresponding ligand is altered when a transition occurs from one to the other state.*
- *When the protein goes from one state to another state its molecular symmetry is conserved.*

Therefore according to the previous statements, hemoglobin can exist only in two quaternary structures, an R oxygenated form and a T deoxygenated form. In absence of ligand, the two state T_0 and R_0 are in equilibrium. Moreover according to MWC model, the oxygenation process as well the deoxygenation can be described by two parameters, L and c. *L* is the equilibrium constant for $R_0 \cap T_0$, therefore $L = T_0 / R_0$. The *c* value instead, is the ratio between the oxygen dissociation constant , K_R , relative to R state and the dissociation constant K_T relative to T state, therefore $c = K_T/K_R$. The L value gives information about the stability between the T and R quaternary structures with no oxygen bound. At physiological conditions, $L = 10^4$ and $c = 0.001$. The graphs reported in (Monod et al., 1965) show that the cooperativity of the ligand depend upon the value of L and c. The cooperativity is more marked when allosteric constant L is large and when c is small. In the MWC model the allosteric effects are due to the displacement of equilibrium between discrete states assumed to exist, at least potentially, apart from the binding of a ligand (Monod et

al., 1965). In a successive article (Koshland et al., 1966) Koshland reported for the first time a schematic representation of the MWC model defined as "concerted model" (Fig. 2.5). Although in the original MWC model there were several symmetry requirements, they were not essential in the "concerted model" presented in (Koshland et al., 1966).
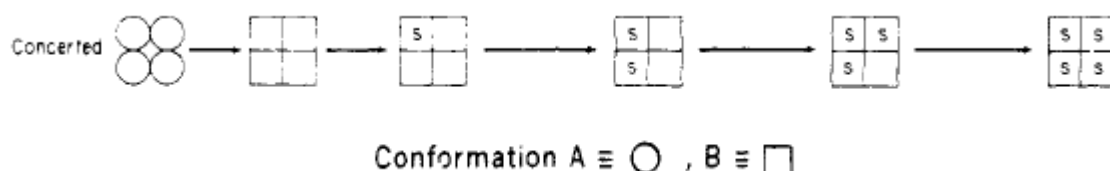

Figure 2.5: Schematic illustration of "concerted" MWC model reported from (Koshland et al., 1966). In the concerted model all conformations change to B together.

2.3.2 Koshland, Nemethy and Filmer (KNF) Model

It was Pauling (Pauling, 1935) that proposed a first structural explanation of cooperative binding. In his model, there was only one constant for oxygen binding and one for the interaction between subunits. Afterwards, since was established that no direct interaction between hemes exists, Koshland, Nemethy and Filmer suggested a more general model defined as "sequential model". In particular, the change in the affinity was the result of some sort of conformational change of subunits upon a ligand binding that is transmitted directly to the adjacent subunits (Koshland et al., 1966). In (Koshland et al., 1966) many models were described: some schematic representation of the presented models (called "tetrahedral", "square" and "linear") are given. All of them have subunits that interact with each other but in a different way. In the "tetrahedral" model each subunit can interact with each of the other subunits. But if some interactions are excluded, this can give a final mathematical result described by "square model". This would be the case for a molecule with 2α and 2β chains in which only α and β interactions occur. In the case of "square" model the subunits are arranged so that each subunit interacts with each of the two neighbours. Whereas in case of the "linear" model there is no interaction between terminal subunits, therefore, each interior subunit interacts with two neighbours while terminal units interact only with one neighbour (Koshland et al., 1966).
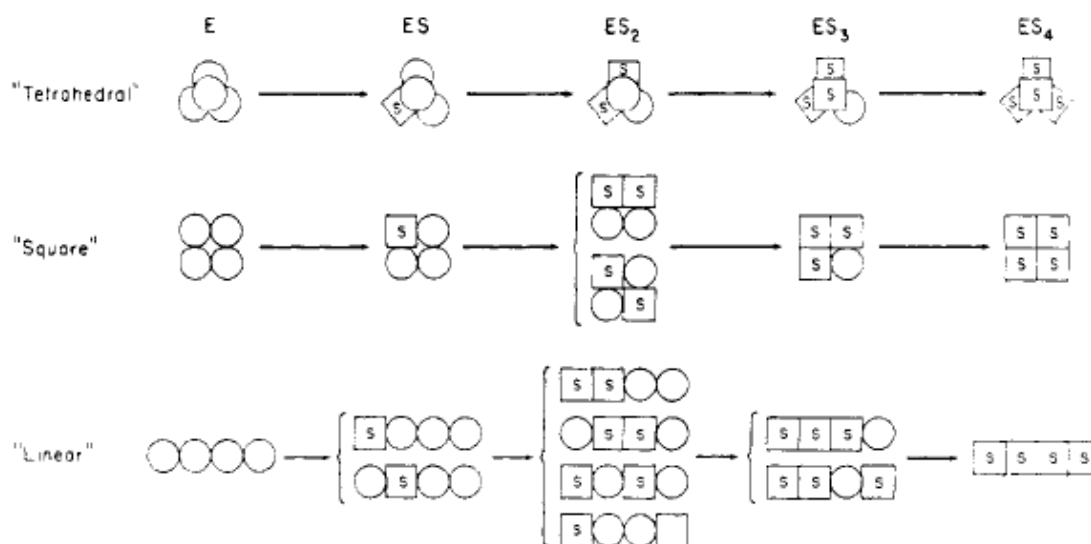
Figure 2.6: Schematic representation reported from (Koshland et al., 1966) of the models of binding the ligand S to the tetrameric enzyme for the three discussed cases: tetrahedral, square, and linear. The square symbol represents the conformation capable of binding S (ligand). The circle symbol represents the conformation of the subunit that is not bound.

The sequential model is generally presented as particular case of the general allosteric scheme shown in Fig. 2.7 (Hammes et al., 1971). This general scheme allows the individual subunits to take freely either of two conformational forms, regardless of the number of ligands that are bound. For a four subunit protein, this allows 25 different forms. The simple sequential scheme involves the forms enclosed by diagonal dotted rectangle in Fig. 2.7.
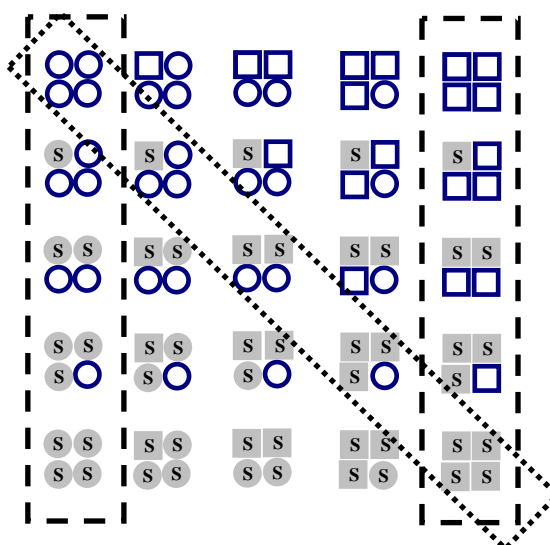

Figure 2.7: A general allosteric scheme in case of a four subunit protein. The **S** stands for the ligand. The simple sequential Koshland model involves the forms enclosed in the dotted rectangle. MWC model is a sub-case of this scheme, involving only the species enclosed by dashed rectangle.

2.3.3 Stereochemical Perutz's Model

The stereochemical mechanism proposed by Perutz (Perutz, 1970; Perutz et al., 1987) was able to combine the MWC as well the KNF model. Identifying the R and T quaternary structures of the MWC model with the structures of oxy- and deoxy-hemoglobin, and describing them in detail, he developed a structural explanation for exactly how hemoglobin worked his 'stereochemical mechanism'. The key finding was a set of salt bridges at the subunit interfaces that are present in the T quaternary structure but absent in R. Perutz described how oxygen binding to the heme in the T quaternary structure with its associated iron displacement could move a helix, break a salt bridge, release a proton, and destabilize the structure at the subunit interface between $\alpha\beta$ dimers of the tetramer, thereby biasing the quaternary equilibrium toward the R. In Perutz's mechanism the salt bridges play three roles: they stabilize the T quaternary structure relative to R, lower the oxygen affinity in T because of the energy required to break them upon oxygen binding, and release protons upon breakage, explaining why the overall affinity is lowered when the pH decreases (the Bohr effect). He viewed the mechanism as a combination of the MWC and KNF models, because in the KNF model ligand binding induces conformational changes in the protein. Although oxygen binding results in conformational changes, there was no structural mechanism for transmitting these changes to the heme of the neighbouring subunits other than through a change in quaternary structure.

2.3.4 MWC – PSK (Perutz – Szabo - Karplus) Model

For homotropic effects Perutz's stereochemical mechanism appeared, therefore, to be pure MWC in that the intrinsic affinity of a subunit is solely determined by the quaternary structure. A mathematical description of this model has been developed by Szabo and Karplus (Szabo and Karplus, 1972). In other words, the MWC modified model became the MWC-PSK model. The model is represented by the scheme in Fig. 2.8. This representation was proposed by Eaton (Eaton et al., 1999) in a review work.
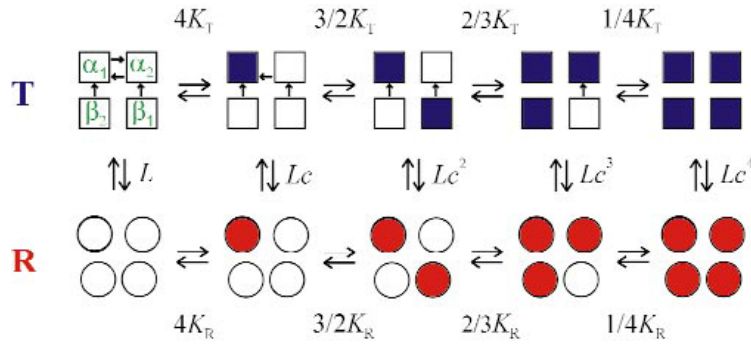
Figure 2.8: Simplified scheme of the MWC/Perutz mechanism. Open symbols designate unliganded subunits and filled symbols liganded subunits. Arrows connecting subunits represent salt bridges - the quaternary bonds of MWC theory that constrain and stabilize the T quaternary structure (Eaton, 1999).

In its simple formulation the partition function for haemoglobin, according to MWC model, is given by:

$$\Xi = L(1+K_T)^4 + (1+K_R p)^4 \tag{2-47}$$

where L is the population ratio of fully deoxygenated T and R quaternary structures, K_T is the oxygen affinity in T quaternary structure, K_R is the oxygen affinity in R quaternary structure, and p is the oxygen pressure.

2.3.5 Tertiary Two-State Allosteric Model (TTS)

The question was clearly if the cooperativity is arising solely from T to R transition or there is also a significant cooperativity in binding to T. This question comes from the evidence that the increase in affinity together with the increase of the oxygen saturation arises from a release of quaternary constrains in the T state tetramers that are responsible for the low affinity. However, crystallization of T structure as well encapsulation of T structure in wet silica gel, have shown that the binding curve is non-cooperative with a Hill coefficient almost exactly 1.0 (Mozzarelli et al., 1991; Rivetti et al., 1993; Mozzarelli et al., 1997). Therefore, there is no cooperative behaviour without quaternary structural changes, and this is in complete agreement with MWC model. In fact, according to MWC model all the conformational changes are associated with the change in quaternary structure. For this reason the MWC model fails to explain heterotropic effects (Bettati et al., 1997; Bettati et al., 1998) such as the decrease in oxygen affinity of the T quaternary

structure with decreasing pH (Minton et al., 1972; Imai, 1982; Imai et al., 1983). Moreover two distinct affinity conformations (Shibayama et al., 2001) in T state have been found: a low affinity (LA) and high affinity (HA) (Bruno et al., 2001). In particular, Hb in T state encapsulated in silica gel with allosteric effectors (LA) has a 10-lower O_2 affinity than in absence of allosteric effectors (HA). Thus, although there is a change in the affinity constant, there is no change in the quaternary state. In order to explain some of these behaviors the Tertiary Two State (TTS) model was introduced by Henry (Henry et al., 2002). In this model, the affinity state corresponds to the tertiary conformation of the subunit, not to the quaternary structure. High and low affinity conformations of individual subunits, called *r* and *t*, exist at the equilibrium within each quaternary structure. The quaternary structure influences the affinity by biasing the t$\cap$r conformational equilibrium, the T conformation favouring t and the R conformation favouring r. In both R and T ligand binding favours r. The net result is that while liganded subunits in R are all in the r conformation and unliganded subunits in T are all in the t conformation, both r and t conformations are significantly populated at equilibrium in unligated subunits in R and liganded subunits in T. A representation of this model is given in (Viappiani, Bettati et al., 2004) as shown in Fig. 2.9. The partition function for this model with the same α and β affinities is given by:

$$\Xi = \frac{L}{l_T^4}\left\{1 + K_r p + l_T(1 + K_t p)\right\}^4 + \left\{1 + K_r p + l_R(1 + K_t p)\right\}^4 \qquad \textbf{(2-48)}$$

where L is the ratio of T to R population in which all the subunits of T are unligated t and all the subunits of R are unligated r, l_T is the ratio of t to r population of the unliganded subunits in T quaternary structure, and K_t and K_r are the affinity of the remaining subunits in t and in r respectively.
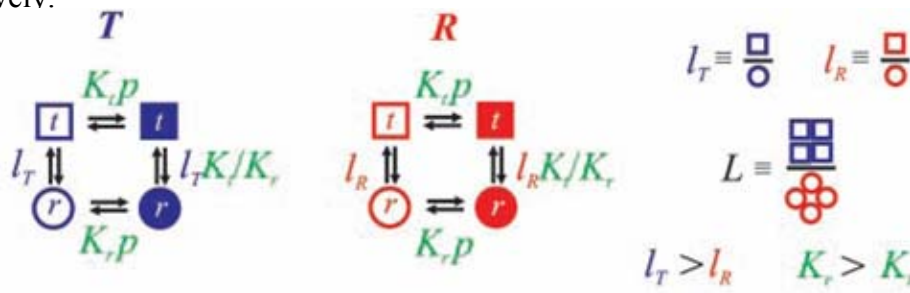

Figure 2.9: Schematic representation of the Tertiary Two State (TTS) model. Open symbol = unliganded subunits; filled symbol = liganded subunits; circles = r tertiary conformation; square =t tertiary conformation; K_t and K_r = affinity of the subunits in t and r conformation in which the liganded subunits remain in t and r, respectively; l_T = ratio of the t to r populations of the unligated subunits in the T quaternary structure; l_R = corresponding equilibrium constant in the R quaternary structure; L = ratio of the T to R populations in which all the subunits of T are unliganded t and all the of the subunits of R are unliganded r (Viappiani et al., 2004).

In this model, heterotropic effectors can influence L, l_R and l_T but not K_r or K_t. It is important to notice that in the limit where the l_T is large and l_R is small Eq. 2-45 and Eq. 2-46 are identical with $K_T=K_t$ and $K_R=K_r$. However, the structural interpretation of the parameters is different because tertiary and quaternary conformations are considered separately in TTS model, rather than together as in the concerted conformational change of the MWC model (Henry et al., 2002).

2.3.6 Allosteric Effectors

Generally, all the heterotropic ligands lower the oxygen affinity stabilizing the T structure (Perutz, 1989). The most important heterotropic ligands are protons. The linkage of the proton uptake to oxygen release and vice versa is known as *Bohr effect*. For example as reported in (Perutz, 1989) for each mole of O_2 released at pH 7.4 and 25°C, human Hb takes up 0.2 mol H^+ in a deionized solution. In this solution all the protons are taken up by His $HC_3(146)\beta$ that donates a hydrogen bond to Asp FG(94) β in a T structure and accepts a hydrogen bond from its own main chain NH in R structure. In consequence, its pK_a rises from 7.1 or less in oxy-hemoglobin to 8.0 in deoxy-hemoglobin. The Hb oxygen affinity is lower in the solution with respect to blood conditions: this behaviour is due to the presence in the red blood cells of 2,3-diphoshoglycerate (DPG), an allosteric effector. This molecule has an affinity constant for the T state that is 40-100 time higher then R state. Therefore, the DPG is changing the equilibrium towards the T state, producing a general lower affinity (Benesch and Benesch, 1967). In the T structure, the two β–subunits form a binding site for the 2,3-diphoshoglycerate. In DPG enters a *cleft flanked b*y N-termini and helix H of the β chain and form ionic bonds with Val $NA_{I(I)}$, His $NA_{2(2)}$, Lys EF6(82) and $His_{21}(143)$ (Fig. 2.10). In the R structure, the gap between the two β chains becomes too narrow to permit the access to the DPG. There are other kinds of allosteric effectors, non-physiological but much more efficient. The most studied are Inositol HexaPhosphate (IHP) (Imai, 1982), Bezafibrate (Bzf) and analogus molecules (LR16, L35, L345) (Lalezari et al., 1988; Lalezari et al., 1990), and RSR-56 (Abraham, 1992). Both DPG and IHP (Fig. 2.10, Fig. 2.11) bind the same site of hemoglobin, that is in the central cavity of the protein and it is formed by residues of β chains. These positive-charged residues interact with the negative charges of the DPG and IHP phosphoric groups. Bezafibrate was studied as antilipidaemic drugs that might prevent the aggregation in deoxy-hemoglobin S in patient with sickle anaemia. This compound and the analogous one stabilize the T structure, binding to symmetric sites of the central cavity formed mainly by residues of α chain. The effect of IHP and DPG on allosteric equilibrium is additive (Perutz et al., 1986).
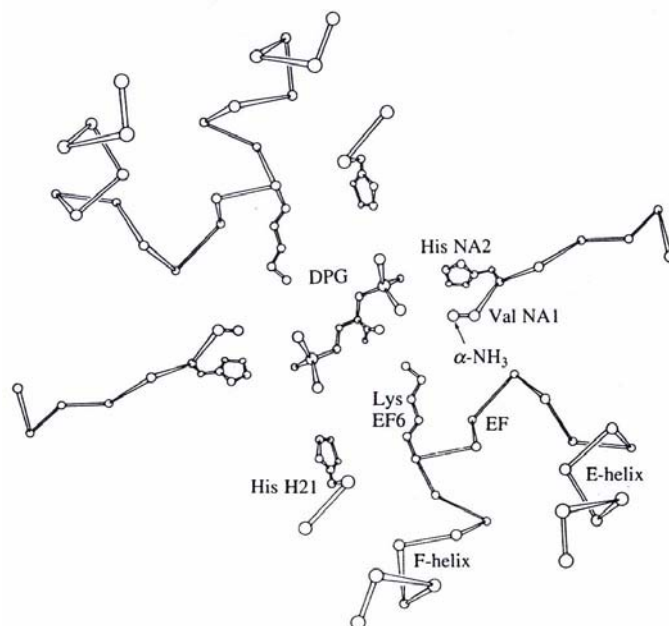
Figure 2.10: Ionic bonds between 2,3-disphosphoglycerate and cation groups of β chain in T structure. In the R structure the gap between EF corners closes and the N-termini move apart (Perutz, 1989).

DPG and IHP change the Hb's p50, and what's more they increase K_T and K_R. As reported by Marden (Marden et al., 1990), in case of DPG and IHP at 1 mM the p50 values are 3kPa (15 mmHg) and 10.4kPa (78 mmHg) respectively.
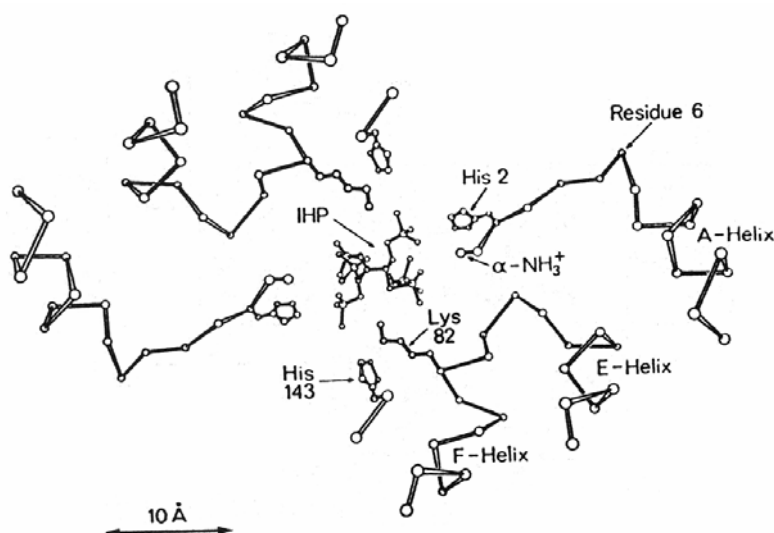

Figure 2.11: Binding of IHP to human Hbdeoxy. The conformation of Lys 82 is different from that in Fig. 2.10 (Arnone et al. 1974)

In addition, they are responsible for an enhancement of acid and alkaline Bohr effect increasing ΔpK_1 and ΔpK_2 (Kilmartin, 1973). A similar effect is produced also by L35 and L36 (Lalezari et al., 1990).
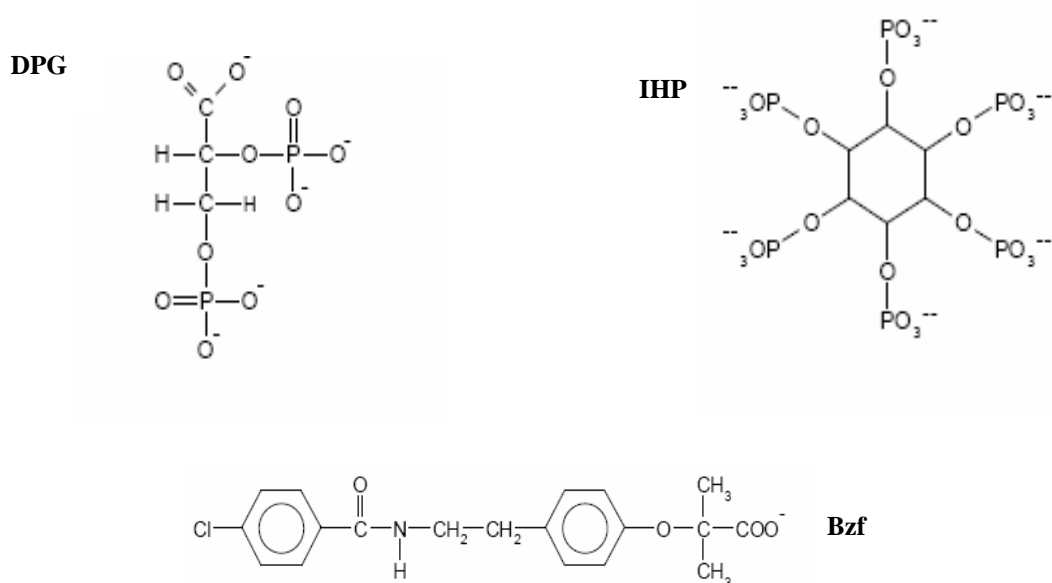

Figure 2.12: Chemical structures of DPG, IHP and Bzf

The effect of allosteric inhibitors is influencing the MWC model. In fact the original MWC two state model is able to explain perfectly the cooperative oxygen binding but does not explain changes in oxygen affinity by allosteric effector, which remains an open question.

3 Sample Preparation and Experimental Device

3.1 Mössbauer Spectrometer

The measurements have been performed with standard Mössbauer spectrometers. The main parts of a Mössbauer system are the cryostat, the transducer and the detector. The cryostat keeps the sample at low temperature since the recoil free fraction f_a is very small at room temperature. Usually two kinds of cryostat are mainly used: a bath cryostat and helium-flow cryostat. In the case of helium flow cryostat, the vacuum pump draws the liquid helium from the can by a vacuum isolated transfer pipe through the cryostat into the exhaust pipe. The helium evaporating in the heat exchanger cools the sample. The transfer pipe has a valve for regulating the flow and consequently the temperature. A helium bath cryostat is filled with liquid helium that is transported by overpressure from the can into the storage volume of the cryostat itself using a vacuum isolated transfer pipe. The sample is thermally connected to the helium bath. To minimise evaporation loss by heat conduction, it has a shield filled with liquid nitrogen and an isolating vacuum chamber. Both kind of cryostat have been used during the experiments although most of the measurements have been done with the bath cryostat. A representation of the cryostat used is reported in Fig. 3.1. In the specific case, the cryostat was made by Cryophysics SA. The absorber is mounted on a support rod in a central exchange gas space and is cooled by conduction through the static helium or with nitrogen gas. The temperature control ($\pm 0.1K$) is connected with the rod sample support. The sensor is a silicon diode (DT 500) placed nearby the sample. The isolating vacuum (10^{-6} mbar), controlled by Penning and Pirani gauge heads, is obtained with an oil diffusion pump and a rotative pump. The sample is irradiated with a radioactive source. It consists of ^{57}Co in a Rhodium matrix that decays to ^{57}Fe emitting a gamma Mössbauer line with 14.4 keV energy. The source is fixed to an electromechanical transducer that is placed on a metallic support guides to allow source substitution.
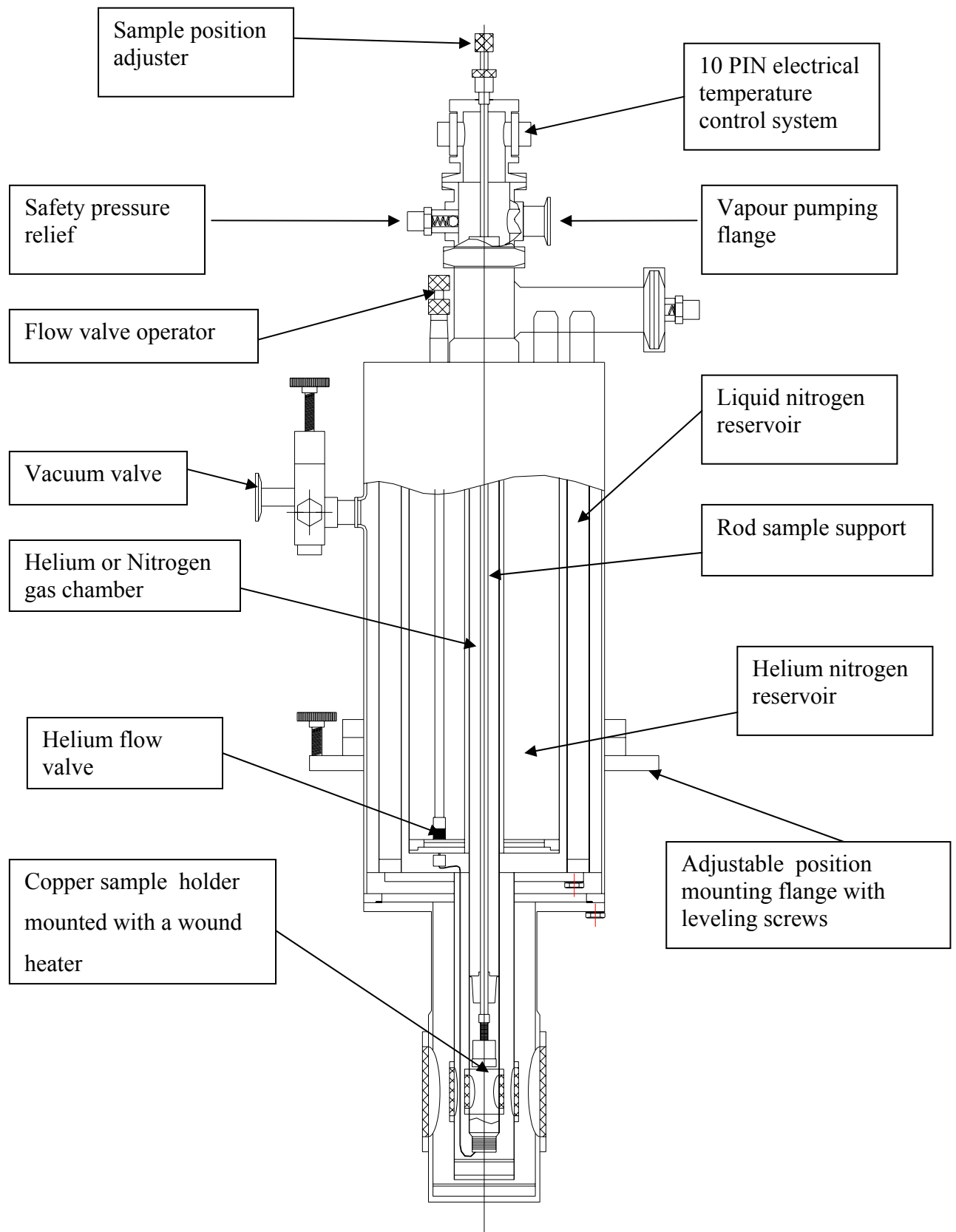
Figure 3.1: Helium bath Mössbauer cryostat made by Cryophysics SA. The absorber is mounted on a support rod in a central exchange gas space and it is cooled by conduction through the helium or with nitrogen gas. This gas is fill in through the vapour pumping flange. The temperature control (±0.1K) is connected with the rod sample support. The sample is thermally connected to the helium bath reservoir. To minimize evaporation loss by heat conduction, it has a shield filled with liquid nitrogen and an isolating vacuum chamber (10^{-6}mbar).
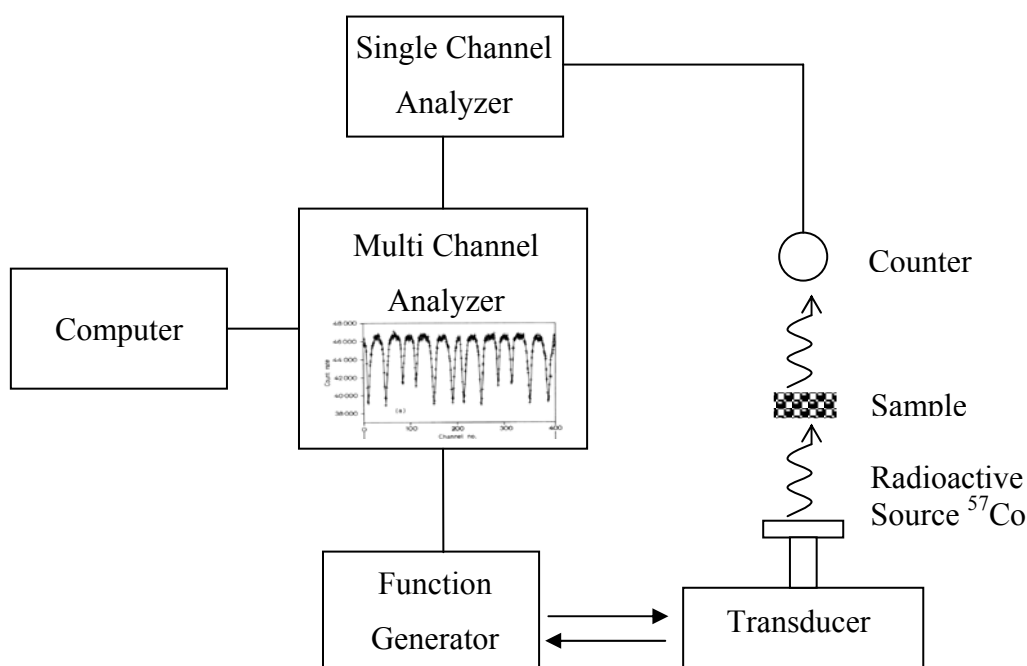
Figure 3.2: The transducer and electrical acquisition system of a Mössbauer spectrometer is represented in the flow chart. The function generator gives signal to the transducer in such a way that - at present - the source velocity is determined, thus the energy of the emitted radiation is determined. With the help of a feedback signal, the radiation detected by the counter at each time is associated to a defined velocity. The association of the counting rate with the defined transducer velocity is done by the Multi-Channel Analyser. In particular, the velocity range is divided in 1024 channels. In the Single-Channel Analyser the resonance Mössbauer line is selected from the complete spectrum that includes Compton shoulder and the X–ray discrete emission line and the background.

The transducer is placed in a lead cylinder. Moreover, next to the transducer there is a collimator to efficiently reduce the radiation emitted from the source in such a way to attenuate the strong background. The transducer is driven by a function generator that produces a periodical waveform, which serves as a reference for the motion of the source through the desired velocity range. In the Mössbauer system reported in Fig. 3.2 the generator produces an electric signal with a triangular waveform, while in the other system used during the experiments the waveform was sinusoidal. The transducer is regulated by a feedback system comparing the voltage from the pickup coil with the reference voltage and feeding the difference signal back to the driving coil of the transducer after suitable amplification. Due to the Doppler Effect the emitted quanta experience an energy shift.

The γ-photons passing through the absorber are detected by a gas proportional counter filled with Xenon. The voltage applied to the proportional counter is around 2 kV. The detector signals are amplified and discriminated in the region of interest with a single-channel analyser and finally stored in a multi-channel analyser synchronized to the motion of the source. The spectrum, usually stored in 1024 channels, is transferred to a personal computer at the end of the measurement. In Fig. 3.2 a scheme of the electronic acquisition system is reported.

3.2 Sample Preparation

The low concentration of ^{57}Fe is a source of difficulties measuring biological specimen. In fact the natural abundance is only about 2%. In order to have a good signal-to-noise ratio the hemoglobin and myoglobin samples studied in this work have been enriched in ^{57}Fe. Human hemoglobin, conserved as met-hemoglobin (Hbmet) in ammonium sulphate $(NH_4)_2SO_4$ solution 4M, is dialysed relative to bi-distilled water before enrichment procedure. The Hb sample has been enriched with ^{57}Fe following the Acid-Butanone-Method (Teale, 1959). According to this procedure, the heme group of natural Hbmet is removed chemically and replaced by ^{57}Fe hemin. The Hbmet(^{57}Fe) obtained is concentrated by pressure filtration. The sample is checked by optical measurements and the Hbmet concentration is calculated using the molar extinction coefficient of the Soret–Band.

Myoglobin from sperm whale, was stored as crystals in 4M ammonium sulphate $(NH_4)_2SO_4$ 4M solution with pH=6.8. Before the enrichment procedure, myoglobin is dialyzed against bi-distilled water. Similarly to Hb enrichment procedure met-myoglobin (Mbmet) has been enriched in ^{57}Fe following the Acid-Butanone-Method. After the sample preparation, which is described in the following section, the samples are placed in a suitable holder. The Mössbauer holder has the total volume of 390 mm^3. The Mössbauer sample holder is done with a round plastic part, with two Mylar windows and two brass washers. The plastic part has a hole with area of 1 cm^2. Each window is placed between the plastic part and the brass washer. The sample holder is airtight with indium wires. Each wire is allocated between the brash washer and plastic part. In the case of hemoglobin samples the concentrations are referred to the concentration of the single chains.

3.2.1 ^{57}FeMetHb Samples

After the ^{57}Fe enrichment procedures, two samples of ^{57}FeHbmet have been prepared. To prevent free radical formation and to create CO molecules with X-ray low temperature irradiation, 50%

glycerol/water (v/v) of glycerol has been added to the two ^{57}FeMetHb (pH=7.4) concentrated samples. One sample (1) has the final concentration of 1.06mM/ml and has been frozen in condensed propane, in order to increase the high to low spin ratio, and then placed into a Mössbauer holder at T=77K. To condensate the propane it is necessary to blow the propane gas in a container that is kept roughly at nitrogen temperature. When the propane was condensed the concentrated sample was dropped into liquid propane. Afterwards the drops were collected into a Mössbauer sample holder kept in liquid nitrogen. The sample holder has been closed remaining inside the liquid nitrogen. The other ^{57}FeMetHb sample (2) has the final concentration of 2.5mM/ml and has been frozen in liquid nitrogen.

3.2.2 ^{57}FeHbdeoxy Samples

The Hbdeoxy sample has been prepared in argon atmosphere inside a glows-box adding dithionite to ^{57}FeMetHb concentrated solution (pH = 6.9) and 50% glycerol/water (v/v) as in the case of the ^{57}FeMetHb glycerol samples. After the final concentration, the samples were placed in the Mössbauer sample holder and immediately frozen in liquid nitrogen with a final concentration of about 2.5mM/ml.

3.2.3 ^{57}FeMbdeoxy Samples

Two samples of Mbdeoxy have been prepared in argon atmosphere inside a glows-box. One with glycerol (Mbdeoxy$_{gly}$) was obtained adding to ^{57}FeMetMb concentrated solution (pH = 6.7), 50% glycerol/water (vol/vol) with diluted dithionite. The other one without glycerol (Mbdeoxy$_{wat}$) was obtained adding dithionite sodium phosphate solution 0.1M to ^{57}FeMetMb concentrated solution (pH = 6.7). The samples were placed in a Mössbauer sample holder and immediately frozen in liquid nitrogen, with a final concentration of about 3 mM/ml.

3.2.4 Encapsulation of Hemoglobin Sample in Wet Silica Gel

Human hemoglobin was purified as described in (Rivetti et al., 1993) and conserved as Hbmet in 4M ammonium sulphate buffer. It was dialysed with bi-distilled water before enrichment procedure to remove the buffer. Hbmet was enriched with ^{57}Fe following the Acid-Butanone-Method (Taele, 1959). The sample preparation of enriched ^{57}FeHbmet was checked with optical measurements.

3.2.4.1 ^{57}FeHbdeoxy Samples Encapsulted in Silica Gel in High and Low Affinity T Structure

The encapsulation of deoxyhemoglobin was carried out using an already reported method (Bettati et al., 1997; Bruno et. al., 2001; Viappiani et al., 2004), in presence and in absence of allosteric effectors. The low affinity (LA) deoxyHb was prepared with the following procedure. A solution containing 10 mM N-(2-hydroxyethyl)piperazine-N-(2-ethanesulfonic acid) (HEPES) and 1 mM ethylenediamine tetraacetic acid (EDTA) at pH 6.2 was added to an equal volume of TetraMethyl OrthoSilicate (TMOS). This solution was thoroughly mixed and vortexed for a few minutes. The resulting solution was deoxygenated by continuous mixing under nitrogen flow for 90 min at 4°C. This process removes the fear of oxidation and denaturation of ferrous hemoglobin, because any methanol produced is eliminated from the solution. Finally, a deoxygenated solution containing 2.7% (wt/vol) deoxyhemoglobin, 10 mM HEPES, 30 mM sodium dithionite, 1 mM EDTA, and the allosteric effectors was added to the solution anaerobically in the ratio 1.5 to 1 at pH 6.2. In particular, the allosteric effectors were 10 mM inositol hexaphosphate (IHP), 2 mM bezafibrate and and 0.2 M chloride ions. A homogeneous mixture of this solution was distributed on a glass (solid) support vial. Gelation occurred within a few minutes at room temperature. A solution containing 100 mM HEPES, 30 mM dithionite, 1 mM EDTA, 10 mM IHP, 2 mM bezafibrate and 0.2 M chloride ions at pH 7 was poured on the gel, which was stored anaerobically at 4°C.

The encapsulation of the high affinity (HA) T-state hemoglobin is similar to the protocol used for the low affinity T-state hemoglobin, except that the negative heterotropic allosteric effectors IHP, bezafibrate and chloride ions were not used.

3.2.4.2 ^{57}FeHbCO Samples in Silica Gel in R Structure

To study the HbCO in the R quaternary structure, CO was added to a deoxygenate solution containing Hbdeoxy before encapsulation. After gelification, the samples were immediately put in a Mössbauer sample holder and frozen in liquid nitrogen.

3.3 X-ray Irradiation

The samples used in the conformational relaxation experiments first have been measured at different temperatures. Afterwards, they have been irradiated by X-rays. The irradiation system is

represented in Fig. 3.3. The sample was placed in a support attached to a cold finger that was put inside a dewar filled with liquid nitrogen.
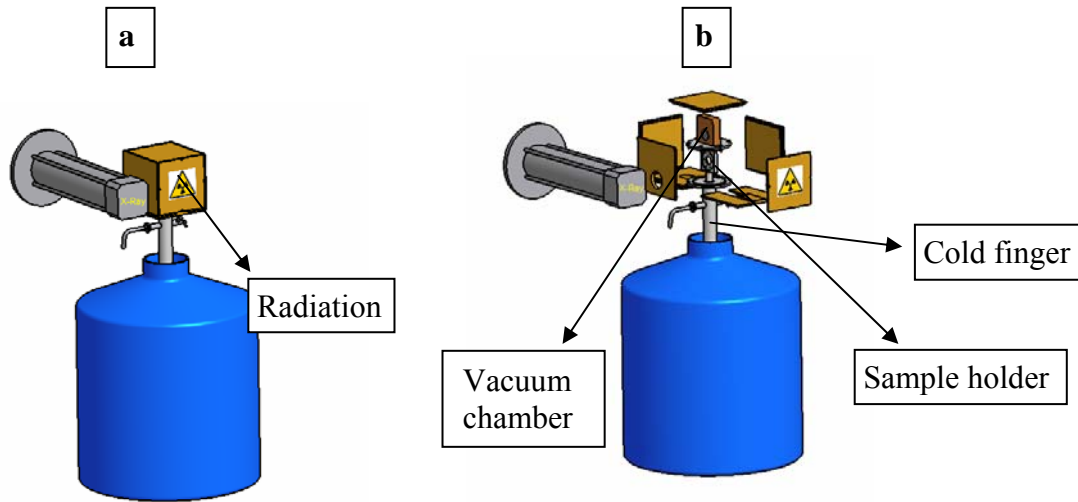

Figure 3.3: System as it appears when it is irradiating [a], and while the sample is mounted [b]. The sample is placed on a cold finger, and is closed in a vacuum chamber to prevent ice formation. In addition, another external box prevent radiation hazard.

To prevent ice formation the sample support is closed to form a vacuum chamber (10^{-2} mbar) connected with a vacuum rotative pump. The vacuum chamber has two beryllium windows to permit the X-ray irradiation. The sample holder and the vacuum chamber are closed in a brass box to prevent radiation hazard. Within the support of the sample holder is placed a silicon diode sensor connected to a remote temperature control system, in order to check the temperature of the sample during the irradiation (Fig. 3.4).
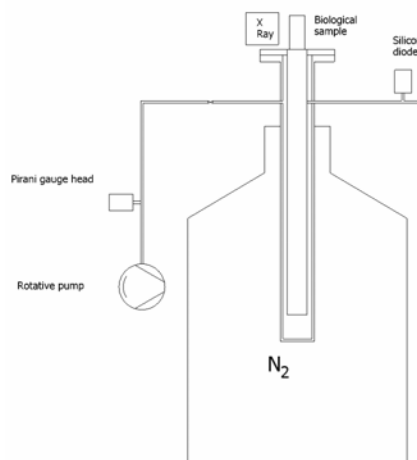

Figure 3.4 The irradiation system is formed by an X-ray tube, cryogenic system, a rotative pump, and a temperature control system.

The irradiation was carried out from both sides of the samples to provide homogeneous X-ray absorption. The uniformity of irradiation was checked placing a Kodak film inside the vacuum chamber in the position of the sample. All the samples have been irradiated with 30 mA and 40kV peak voltage.

4 Hemoglobin and Myoglobin Conformational Changes

The Hbdeoxy spectra have been interpreted with the transmission integral method due to the high number of ^{57}Fe nuclei; in fact the Mössbauer absorption is about 12%. On the contrary, in the case of Hbmet and Mbdeoxy samples, the thin absorber approximation was used with the Lorentzian profile for the absorption line. The Isomer Shift (IS) values are given relative to α-iron. The values obtained from the fit are reported with their error bars. The absence of this error bar means that the value was kept fixed during the fitting procedure, which was necessary mainly because of the low abundance of the species.

4.1 Mössbauer Spectroscopy of X-ray Irradiated Methemoglobin Samples

Hbmet(1) has been measured at T=6K and T=78K before irradiation. For the computation of Mössbauer spectra the Lorentzian approximation has been used, showing a χ^2 between 0.9 and 1.3. This proves the goodness of the fit.
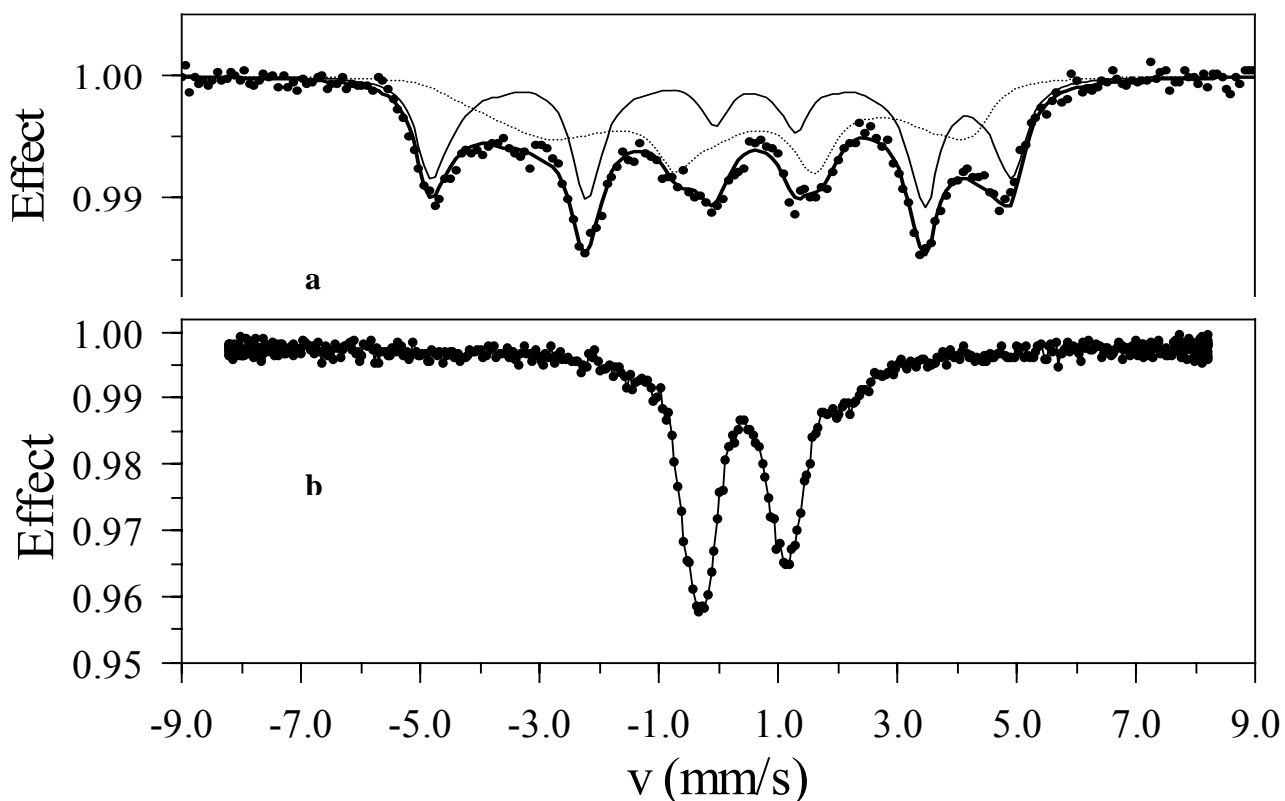

Figure 4.1: a: Hbmet(1) sample before irradiation at T=5.6K: —— (solid line) - Fe(III)HS high spin component; ------ (dashed line) - Fe(III)LS low spin component; **b:** Hbmet(1) sample after X-ray irradiation. The spectrum collected at 6K shows that Fe(III) has been quite completely reduced to Fe(II).

Measurement done before the irradiation of the sample exhibits the presence of Fe(III) high spin and low spin components as shown in Fig. 4.1a. The ratio between high and low spin depends on the velocity of freezing. Sample [57]FeHbmet(1) has been irradiated at 90K for 70 hours. The electrons produced by irradiation at T lower than 100K convert Fe(III) into Fe(II). After irradiation almost all the high and low spin Fe(III) components are reduced to Fe(II) low spin as it is shown in Fig 4.1b. After the X-ray irradiation the spectrum can be fitted with five components (Fig. 4.2). The main one is due to the reduction of Fe(III) to Fe(II). In particular, the spectrum of the freshly irradiated sample of Hbmet(1) is fitted with 84% of Fe(II) low spin (LS), 10% of Fe(II) high spin (HS) - Hbdeoxy - and 1% of HbCO (Fig. 4.2). However, just after irradiation there is still about 5% Hbmet that could not be reduced. The relative abundances of each component used during the fit are reported in Table 6 (Appendix). The hyperfine values used to fit the spectrum that is shown in Fig. 4.2 are reported in Table 1.
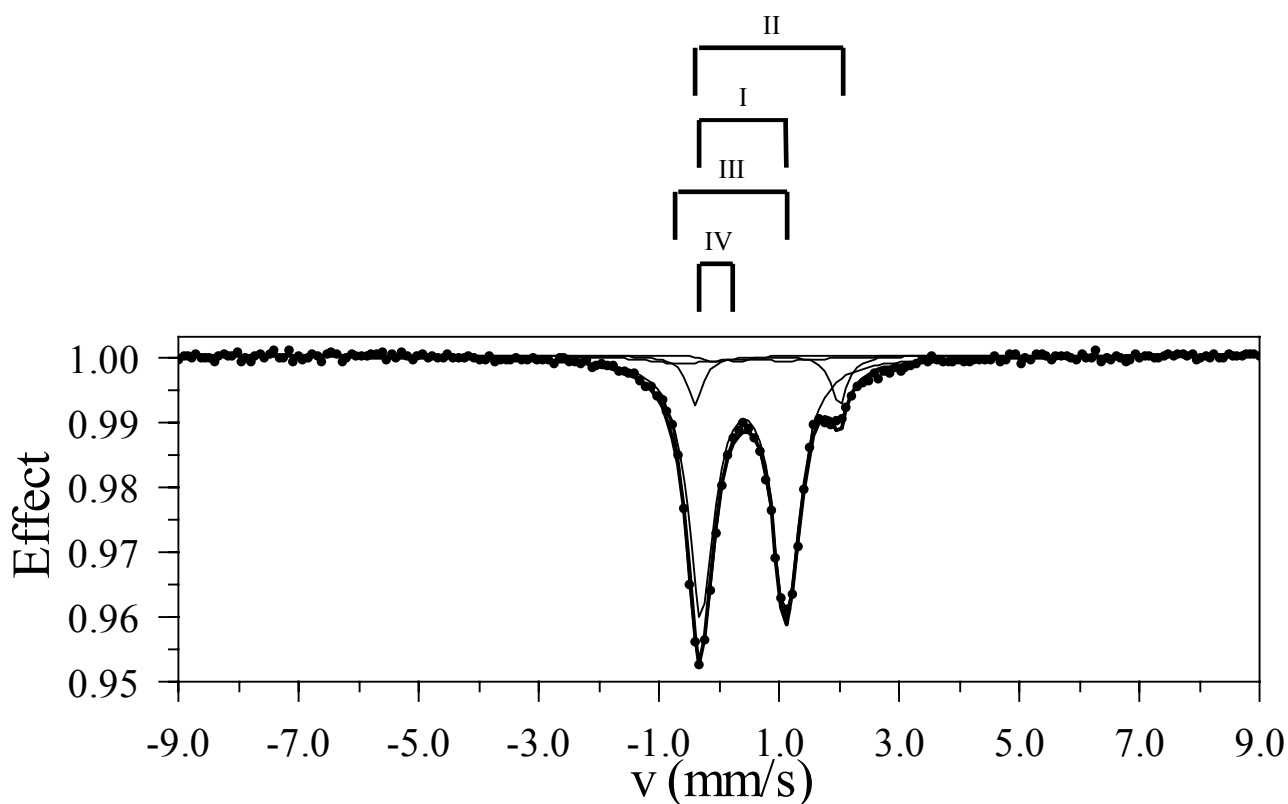

Figure 4.2: Hbmet(1) sample just after irradiation at T=78K. Different components are used to fit the spectra: I - Fe(II)LS due to the metastable state, II - Hbdeoxy, III - Hbmet Fe(III), IV - HbCO. The velocity scale is referred to Rh source matrix.

Table 1: Values used to fit the spectrum of Hbmet(1) measured at T=78K, just after irradiation. In the columns are reported for each component: line width, Isomer Shift (IS), Quadrupole Splitting (QS) and intensity ratio of the right line to the left line. The IS is reported with respect to α-Fe and in brackets with respect to a Rh source matrix, obtained from Fig. 4.2.

Irradiated Hbmet(1) at heating time t=0	line width (mm/s)	$IS_{\alpha.Fe}$(mm/s)	QS (mm/s)	line intensity ratio
Fe(II) LS	0.531 (±0.005)	0.503 ±0.002 (0.414) $_{Rh}$	1.41 (±0.003)	1
Fe(II) HS Hbdeoxy	0.32 (±0.02)	0.884 ±0.006 (0.796) $_{Rh}$	2.4	1
Fe(II)LS HbCO	0.4	0.234 (0.146) $_{Rh}$	0.42	1
Fe(III) Hbmet	1.47	0.36 (0.27) $_{Rh}$	1.84	0.6

Afterwards, many thermal cycles have been performed. They consist of raising the sample temperature for a different time and cooling again to nitrogen temperature, keeping the sample in the Mössbauer cryostat. All the measurements were done at T=78K. These cycles allow the metastable Fe(II)LS state to relax into stable states. Thermal cycles for the Hbmet(1) sample have been done from 140K to 200K. Few representative spectra collected during thermal cycles at T=170K are reported in Fig. 4.3. Hbmet(2) has been irradiated at 120K for 90 hours. The sample Hbmet(2) showed the same behaviour. In particular, just after irradiation the spectrum could be fitted with 65% of Fe(II)LS, 12% hemochromes and 12% Fe(II)HS of the Hbdeoxy, and about 11% is not reduced Hbmet (Fig. 4.4a). Particularly, to fit the non-reduced Hbmet two components have been used. This procedure takes into account the presence of both, Fe(III)HS and LS. The Fe(III)HS is fitted with an asymmetric doublet. The values used to fit the spectra shown in Fig. 4.4 are reported in Table 2.
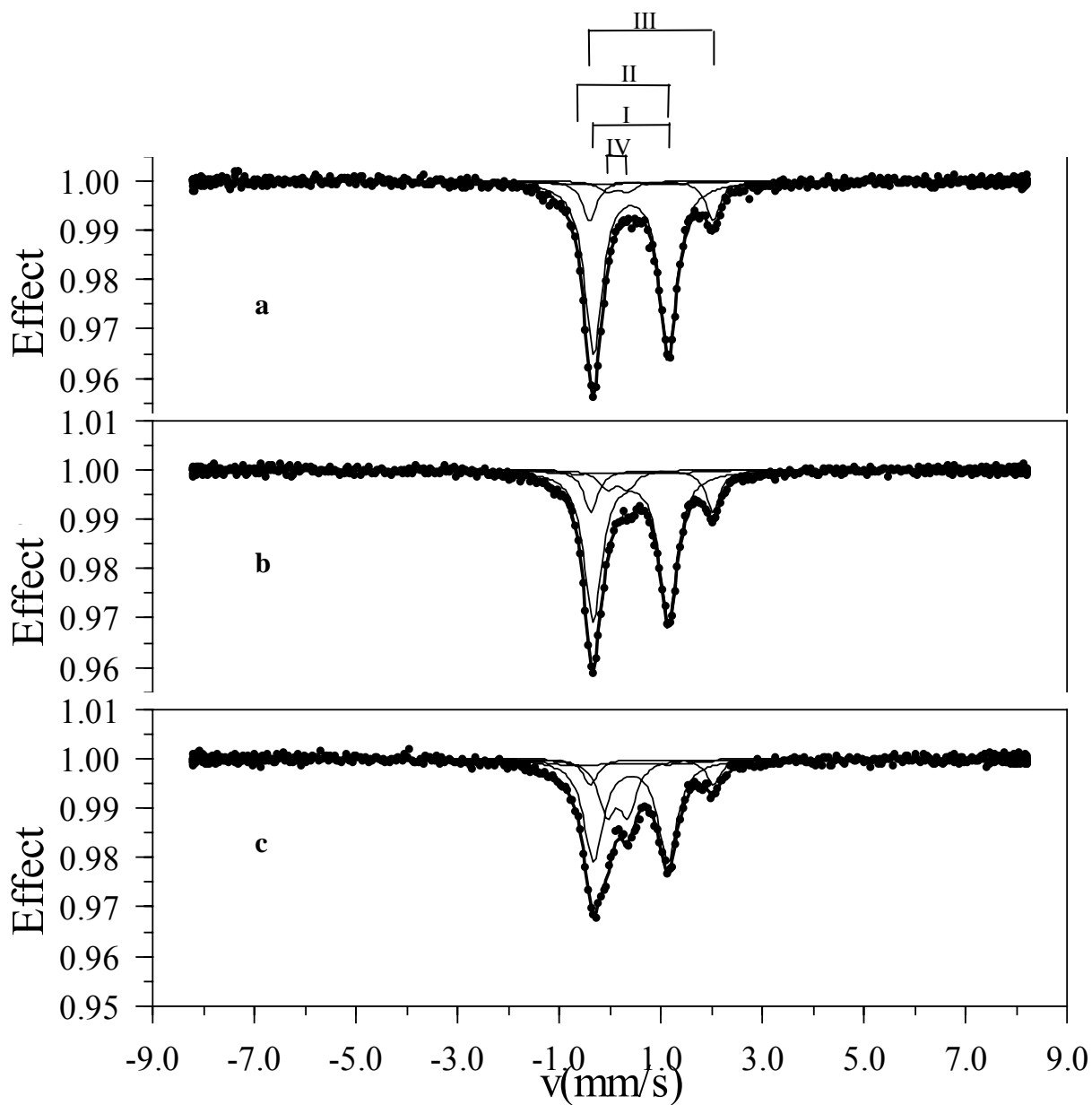
Figure 4.3: Hbmet(1) after irradiation measured at T=78K. **a:** after 0.5h heating at 170K; **b:** after 10.5h heating at 170K; **c:** after 80.5h heating at 170K. The spectra are fitted with the following components: I - Fe(II)LS, metastable state; II - Fe(III) not reduced Hbmet; III - Fe(II) HS (Hbdeoxy), IV - HbCO. The velocity scale is with respect to a Rh source matrix.

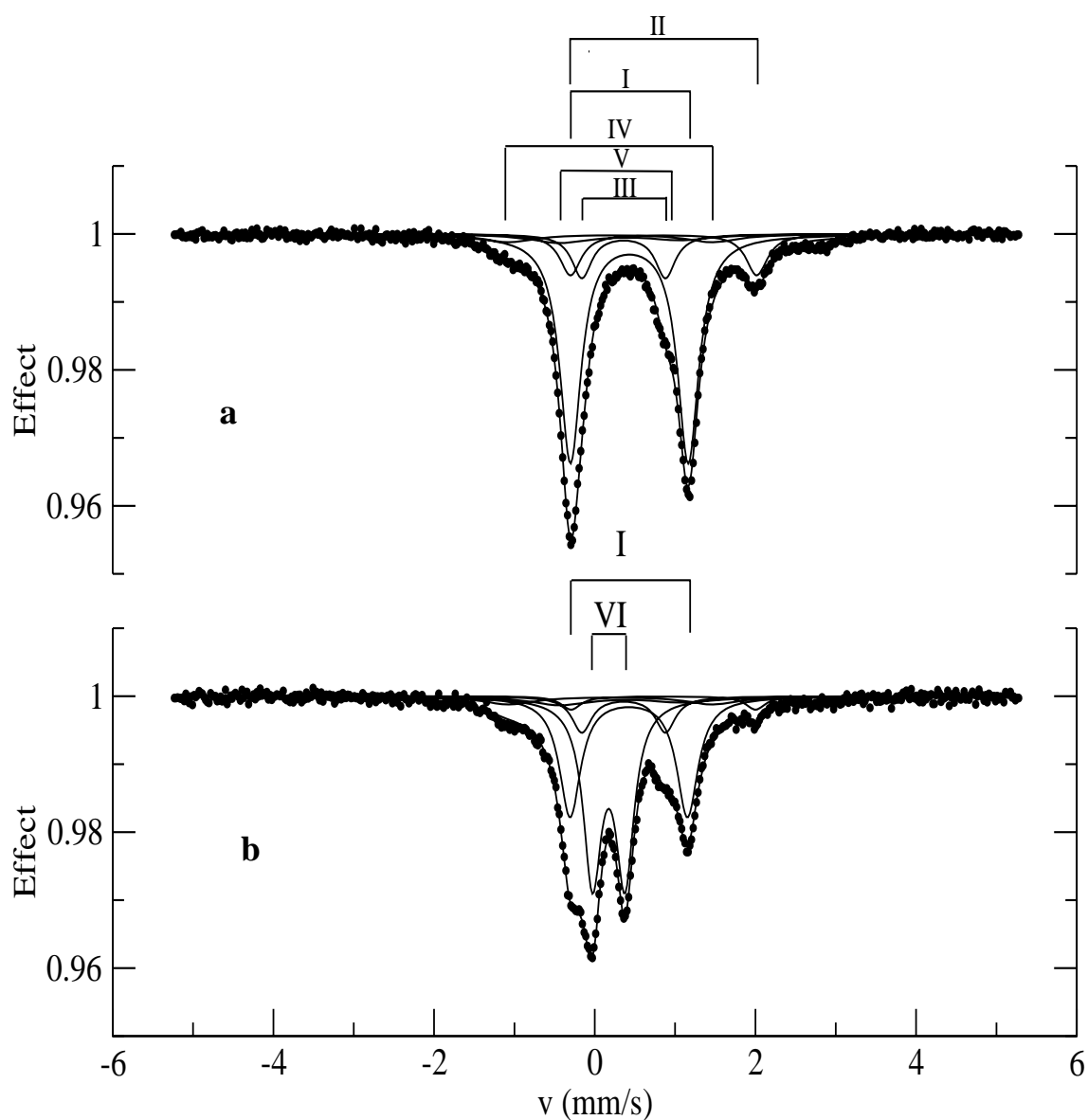**Figure 4.4:** Hbmet(2) after irradiation at T=78K. **a:** spectrum just after X-ray irradiation fitted with the following components: I - Fe(II)LS due to the metastable state; II - Fe(II) HS (Hbdeoxy); III - hemochromes; IV - Fe(III) LS; V - Fe(III) HS, (unreduced Hbmet). **b:** spectrum after 6h heating at 180K is fitted with the same components used for spectrum (a) plus the component VI - HbCO.

Table 2: Values used to fit the spectra of Hbmet(2) measured at T=78K, just after irradiation and after 6h of heating at T=180K. In the columns are reported the line width, the Isomer Shift (IS), the Quadrupole Splitting (QS), and the intensity ratio between the of the right line respect to the left line of each component. The IS is reported with respect to α-Fe and in brackets with respect to the Rh source matrix. These components are used to fit the spectra of the Fig 4.4.

Irradiated Hbmet(2) after heating time t=0	line width (mm/s)	$IS_{\alpha\text{-Fe}}$ (mm/s)	QS (mm/s)	line intensity ratio
Fe(II) LS	0.32	0.52(0.43)$_{Rh}$ ±0.02	1.46 (±0.05)	1.00
Fe(II) HS Hbdeoxy	0.32 (±0.02)	0.9(0.8)$_{Rh}$ ±0.1	2.32(±0.3)	1.00
Fe(III) Hbmet HS	0.90	0.41 (0.32)$_{Rh}$	1.50	0.66
Fe(III) Hbmet LS	0.80	0.29(0.20)$_{Rh}$	2.53	1.00
Fe(II) hemochroms	0.30	0.45(0.36)$_{Rh}$	1.04	1.00
Irradiated Hbmet(2) after heating time t=6h at T=180K	line width (mm/s)	$IS_{\alpha\text{-Fe}}$ (mm/s)	QS (mm/s)	line intensity ratio
Fe(II) LS	0.32	0.51(0.42)$_{Rh}$ ±0.01	1.47 (±0.02)	1.00
Fe(II) HS Hbdeoxy	0.30	0.94(0.85)$_{Rh}$ ±0.05	2.3 (±0.1)	1.00
Fe(III) Hbmet HS	0.90	0.41(0.32)$_{Rh}$	1.50	0.66
Fe(III) Hbmet LS	0.89	0.28(0.20)$_{Rh}$	2.50	1.00
Fe(II) hemochroms	0.30	0.45(0.36)$_{Rh}$	1.04	1.00
Fe(II) HbCO	0.284 (±0.002)	0.261(0.173)$_{Rh}$ ±0.001	0.411 (±0.002)	1.00

The amount of Hbdeoxy component produced during irradiation is very similar in both samples. In case of Hbmet(1), hemochromes have not been created. Differently from Hbmet(1), the irradiated Hbmet(2) has been heated only at T=180K and T=190K. A spectrum collected during the heating cycles at T=180K is reported in Fig. 4.4. Looking at this figure, it is evident that during the heating procedure there is a decrease of the Fe(II)LS component and an increase of HbCO. In both samples, the Hbdeoxy component is decreasing with the increase of heating time and temperature. The relative area of each component is proportional to the number of iron resonant nuclei that are in a specific configuration. To follow the change of a specific iron conformation, the relative population of each component, N(t), is reported as function of heating time. In particular the area of each component of Hbmet(1) and Hbmet(2) irradiated samples are reported in Fig. 4.5 and in Fig. 4.6 respectively. The numerical values are given in Table 6 and Table 7 (Appendix).
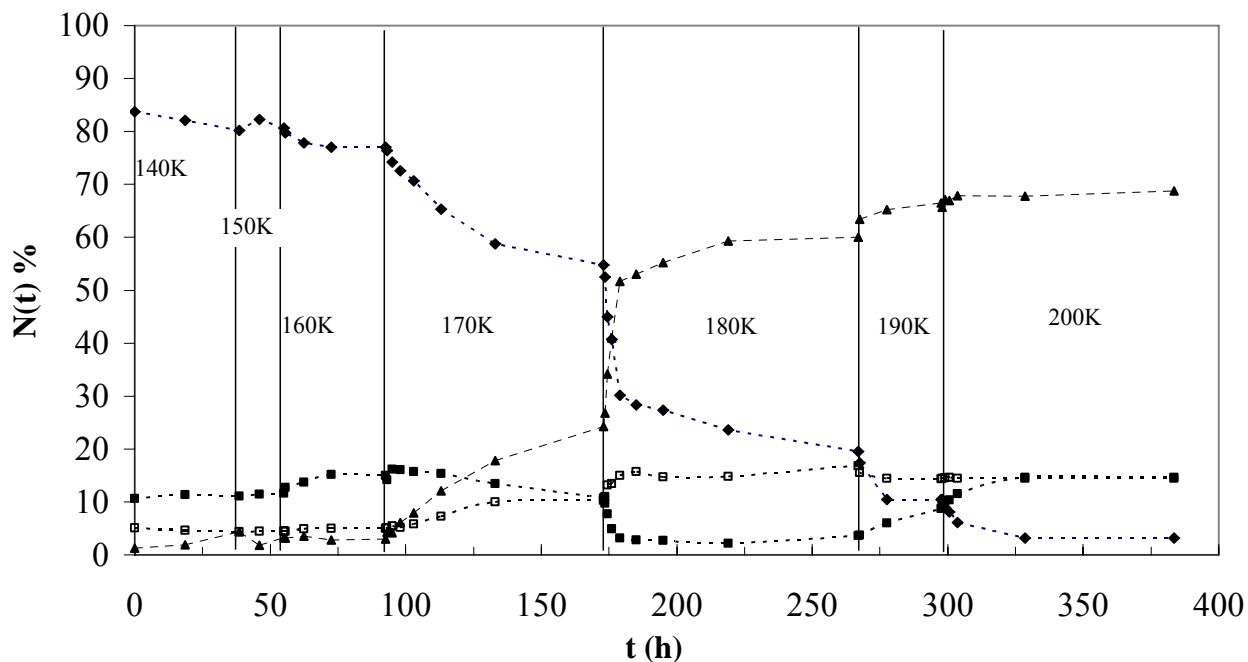
Figure 4.5: The relative area, N(t), of the different components of the irradiated Hbmet(1) sample as a function of heating time t: (◆) Fe(II)LS, (▲) HbCO, (■) Hbdeoxy and (□) sum of Fe(III)HS and Fe(III)LS components. Dashed lines are eye guide lines. All Mössbauer spectra were taken at T=78K. Vertical lines separate experiments performed at the same heating cycle temperature.

In case of Hbmet(1) during thermal cycles at 140K and 150K there is no decay of the Fe(II)LS metastable component as well as no change of the other components. The decrease of the Fe(II)LS is starting at 160K, but the biggest variation is during the heating at T=180K. For this reason, and to check the influence of previous heating cycles, the second sample was heated only at 180K and 190K. Regarding the other components – still in the Hbmet(1) case – Hbdeoxy increases at 160K and starts to decrease at 170K, while HbCO start to increase at 170K till 200K. In the case of the second sample – Hbmet(2), the Hbdeoxy is increasing during the first half hour at T=180K and then is decreasing while HbCO is rising since the beginning of heating at 180K. In Fig 4.6 the Fe(III)HS and the Fe(III)LS unreduced Hbmet are added and represented by a single value. In particular hemochromes and the Fe(III) Hbmet are constant during all the measurements.
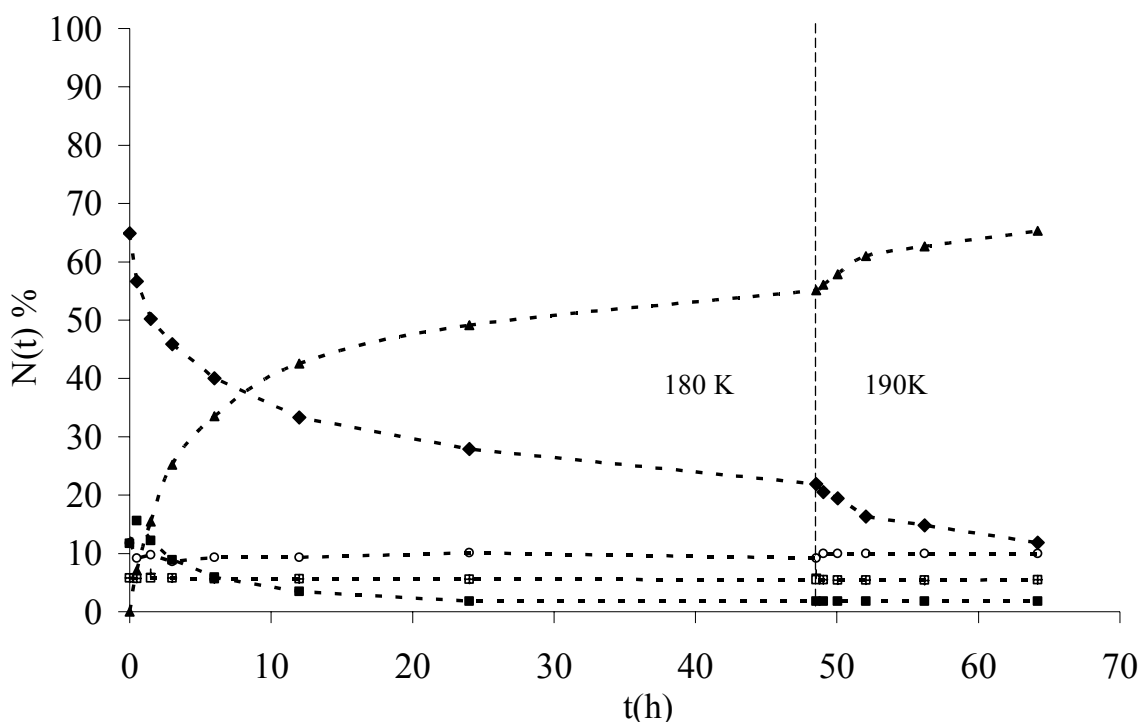
Figure 4.6: The relative area N(t) of the different components of the irradiated Hbmet(1) sample as a function of heating time : (♦) Fe(II)LS, (▲) HbCO, (■) Hbdeoxy, (◊)hemochromes and (□) unreduced Hbmet-Fe(III) components. Dashed lines are eye guide lines. The graph is divided by a dashed vertical line into two parts characterized by the same heating temperature: 180K and 190K. All the measurements are performed at 78K.

4.2 Mössbauer Spectroscopy of X-ray Irradiated Mbdeoxy Sample without Glycerol

Mbdeoxy$_{wat}$ from sperm whale prepared without glycerol, has been measured at 78K before the irradiation (Fig. 4.7a). The Mbdeoxy$_{wat}$ spectra can be well fitted with a single Lorentzian doublet with typical hyperfine parameters of Mbdeoxy. The exposure to X-rays has been done on both sides of the sample for 48h at each side to obtain a uniform irradiation. During the irradiation the temperature was kept below 100K.
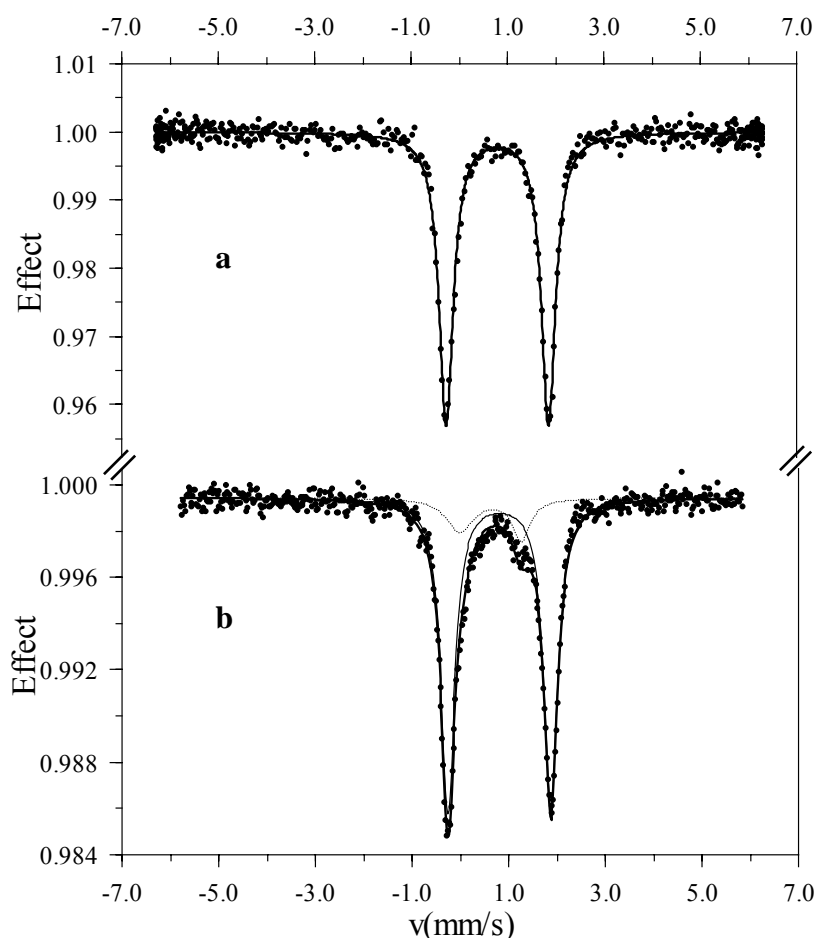
Figure 4.7: Mbdeoxy$_{wat}$ measured at T=78K prepared without glycerol. **a:** spectrum before irradiation, fitted with one component with QS=2.120 (±0.002) mm/s and IS$_{\alpha-Fe}$=0.88 ±0.02 (0.79)$_{Rh}$ mm/s. **b:** spectrum just after X-ray irradiation, fitted with two components. <u>Solid line</u>: Mbdeoxy with QS=2.129(±0.002) mm/s and IS$_{\alpha-Fe}$=0.89 ± 0.02 (0.76)$_{Rh}$ mm/s. <u>Dashed line</u>: metastable component with QS=1.27 mm/s and IS$_{\alpha-Fe}$=0.71 (0.63) $_{Rh}$. The velocity scale of the graph is referred to Rh matrix source.

A spectrum has been collected at 78K, just after the irradiation: it can be fitted with two components (Fig. 4.7b). The component with the larger quadrupole splitting is characteristic for Mbdeoxy (87%), the remaining area of 13% represents a metastable component. The latter is formed during irradiation. At T equal to 78K this component is asymmetric and has a QS=1.25 mm/s and IS=0.71 mm/s respect to α-iron. At T higher than 240K another symmetric component appears, and has QS=1.27 and IS=0.61 mm/s respect to α-iron. These values are characteristic of Fe(II)LS state. Afterwards, thermal cycles have been done from T=140K to T=280K, still performing all the measurements after cooling down to 78K. Low temperature irradiation of the Mbdeoxy sample prepared without glycerol has clearly shown that the binding of CO molecules is formed only at temperatures higher than 170K (Fig. 4.8). In addition, when the temperature is

raised to 140K, part of metastable component that is produced after irradiation is converted to Mbdeoxy. The relative area values of each component are reported in the Table 8 (Appendix).
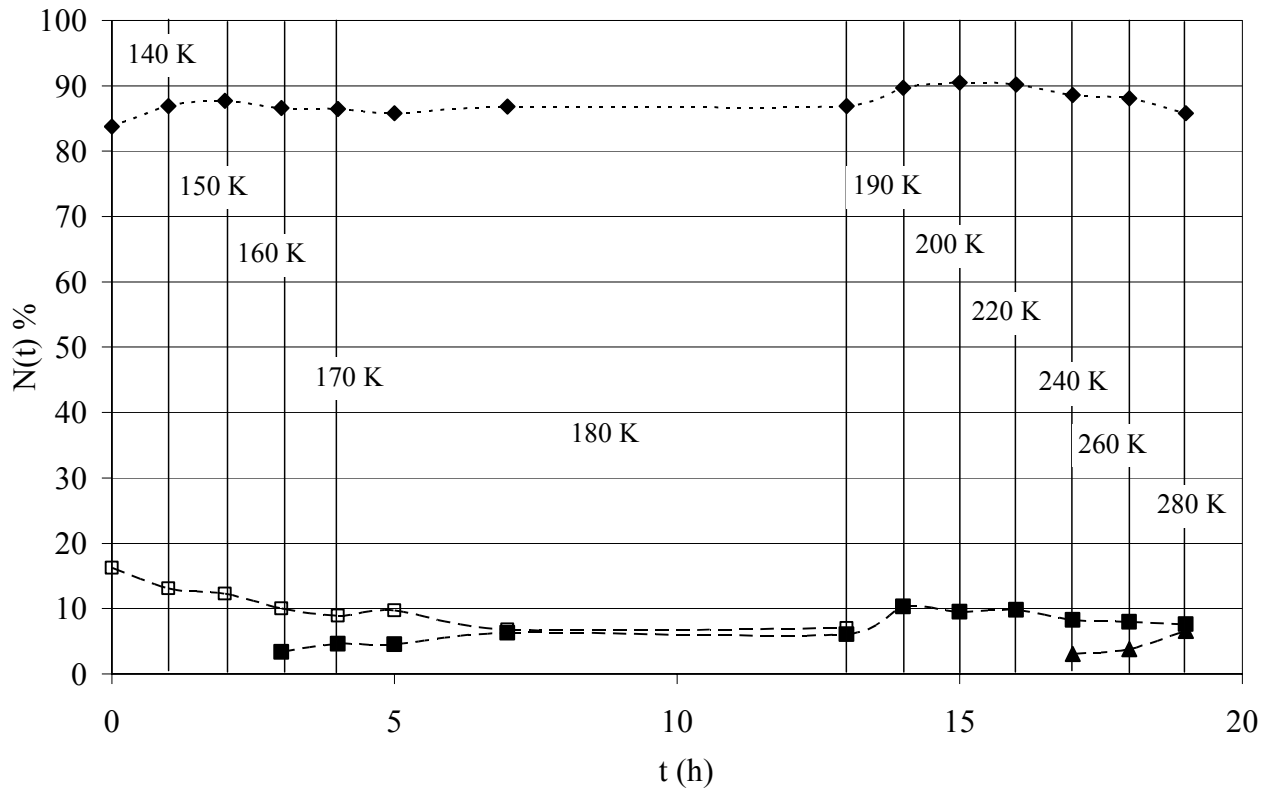

Figure 4.8: Relative population - N(t) - of each state as function of heating time, t, during different thermal cycles performed on Mbdeoxy$_{wat}$ after X-ray irradiation: (♦) Mbdeoxy; (■) MbCO; (□) asymmetric metastable components; (▲) symmetric components Fe(II)LS. Dashed lines are eye guide lines. The graph is divided by vertical lines into parts characterized by the same heating temperature. Thermal cycles are performed from 140K to 280K. All the measurements were done at T=78K.

4.3 Mössbauer Spectroscopy of the X-ray Irradiated Mbdeoxy Sample with Glycerol

The Mbdeoxy sample prepared with glycerol has been measured at 78K before X-ray irradiation (Fig. 4.9). Following the same procedure used for the other samples, the exposure to X-rays has been done on both sides of the sample (48h at each side). The irradiation temperature was below 100K. After the irradiation, spectra have been collected at 78K(Fig.4.10)
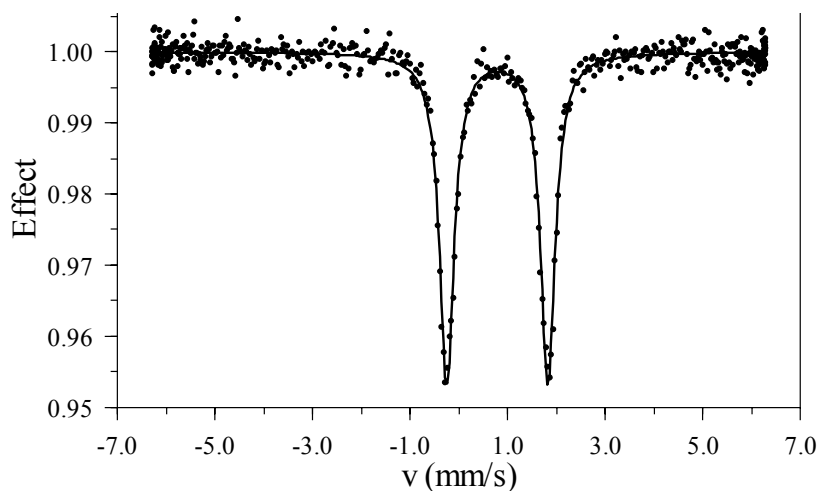
Figure 4.9: Mbdeoxy$_{gly}$ spectrum prepared with glycerol and measured before irradiation at T=78K. The velocity scale is referred to Rh matrix source. The spectrum is fitted with Quadrupole Splitting (QS) = 2.070 (±0.003) mm/s and IS$_{\alpha\text{-Fe}}$=0.879 ±0.001 (0.791)$_{Rh}$ mm/s.

The irradiation has created 37.4% of an asymmetric metastable component (Fig. 4.10). The parameters of the Mbdeoxy component were the same as those obtained in the sample before the irradiation.

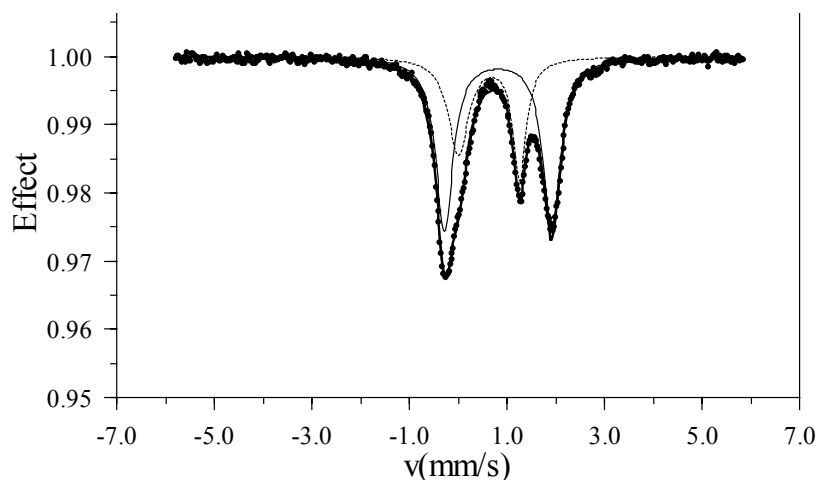**Figure 4.10:** Mbdeoxy$_{gly}$ sample prepared with glycerol and measured just after irradiation at T=78K. The velocity scale is with respect to a Rh source matrix. <u>Solid line</u>: Mbdeoxy component with IS$_{\alpha\text{Fe}}$=0.905±0.002 (0.816)$_{Rh}$ mm/s and QS=2.19 ± 0.005mm/s; <u>dashed line</u>: metastable state component with IS$_{\alpha\text{-Fe}}$=0.715 ± 0.004 (0.626)$_{Rh}$ mm/s and QS=1.25±0.008 mm/s.

After the irradiation, two thermal cycles at 150K have been performed (Fig. 4.11a and Fig. 4.11b). During these cycles no MbCO was formed, but some of the metastable component was already converted to Mbdeoxy. The QS and IS value of the two component are reported in Table3.
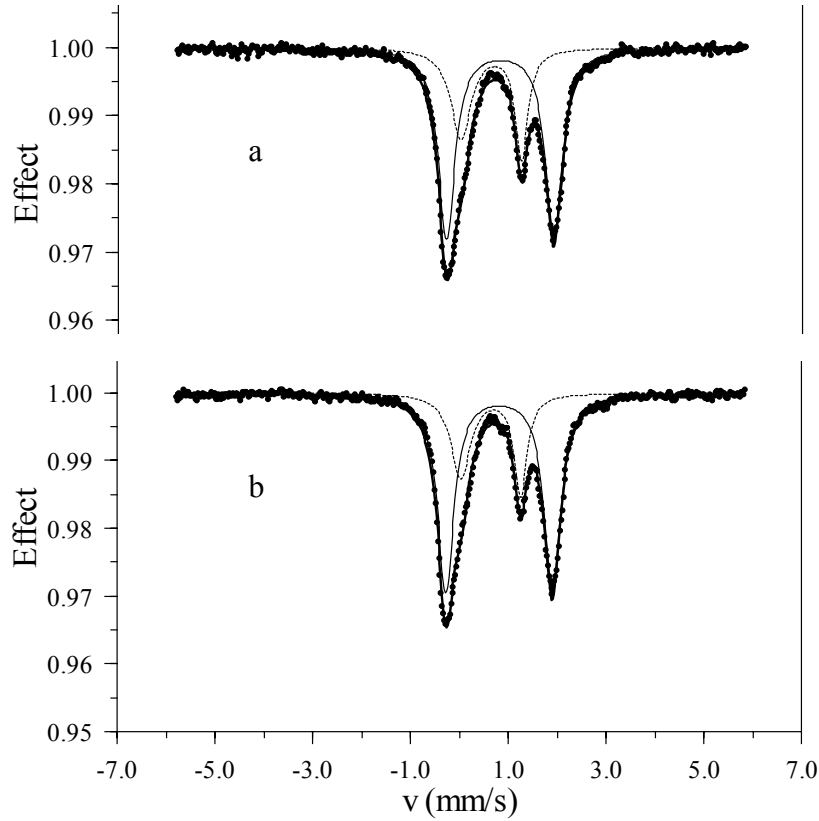
Figure 4.11: Mbdeoxy$_{gly}$ sample measured at T=78K. **a:** after t=0.5h at T=150K. **b:** after t=3h heating at T=150K. Solid line: Mbdeoxy component; dashed line: metastable state component. The values of the QS and IS of each components are reported in Table 3. The velocity scale is with respect to an Rh source matrix.

Table 3: Values used to fit the spectra of Mbdeoxy$_{gly}$ sample of Fig 4.11. Mbdeoxy measured after 0.5h and after 3h of heating at T=150K. In the columns are reported: heating time, IS of Mbdeoxy, QS of Mbdeoxy, IS of metastable component, QS of metastable component. The IS is reported with respect to α-Fe and in bracket with respect to Rh matrix source.

Irradiated Mbdeoxy with glycerol	Heating time (h) at T=150K	IS$_{\alpha.Fe}$(mm/s) Mbdeoxy	QS (mm/s) Mbdeoxy	IS$_{\alpha.Fe}$ (mm/s) metastable component	QS (mm/s) metastable component
	0.5	0.905±0.002 (0.816)$_{Rh}$	2.19 ±0.004	0.715±0.004 (0.626)$_{Rh}$	1.24 ±0.01
	3	0.905±0.002 (0.816)$_{Rh}$	2.19 ±0.004	0.715 ± 0.004 (0.626)	1.25±0.011

Thermal cycles were then performed from 180K to 280K to be sure that the entire CO was bound to the Mbdeoxy. Fig. 4.12 shows some representative spectra collected during the thermal cycles at 180K. It is evident that already after only 0.5h at 180K more then 50% of MbCO was formed.
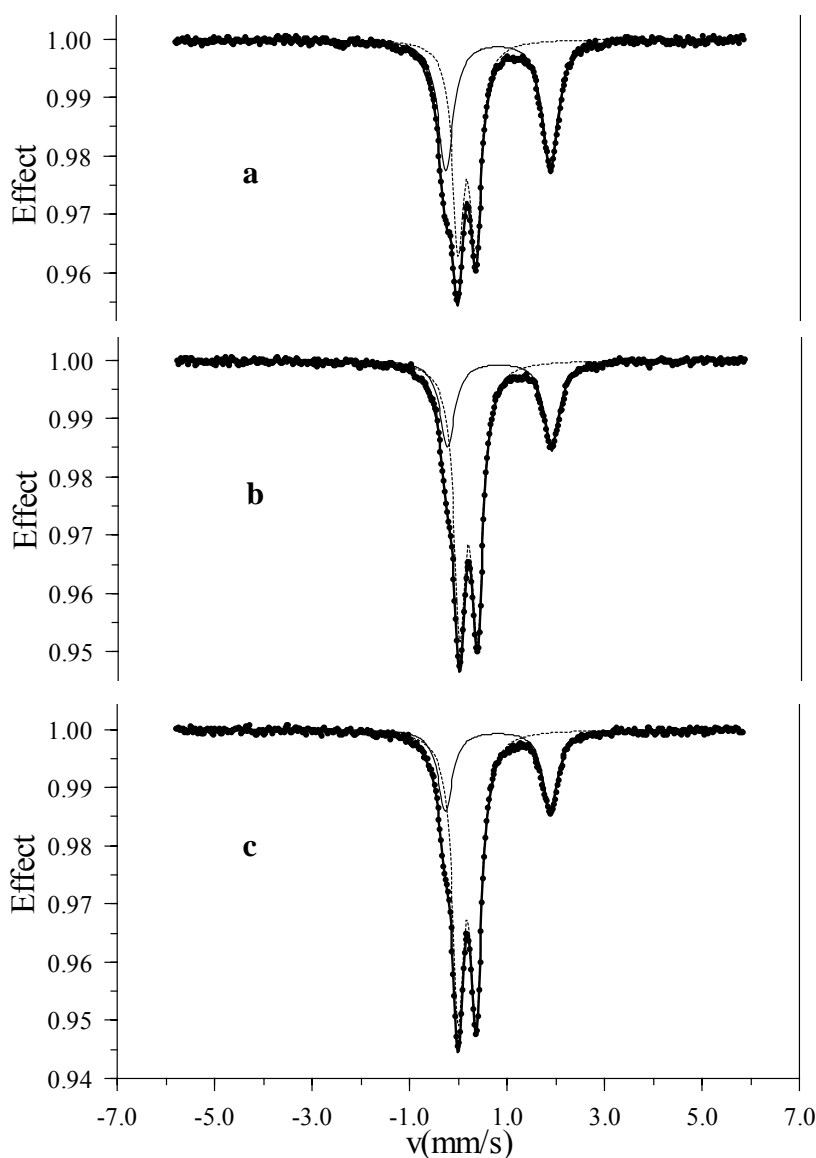
Figure 4.12: Mbdeoxy sample measured at T =78. **a:** spectrum after t=0.5h heating at T=180K; **b:** spectrum after t=12h heating at T=180K. **c:** spectrum after t=96h heating at T=180K. All the three spectra are fitted with two components. <u>Solid line:</u> Mbdeoxy component with $IS_{\alpha\text{-}Fe}$=0.899±0.004 (0.810)$_{Rh}$ mm/s QS=2.13±0.01 mm/s. <u>Dotted line:</u> MbCO component with $IS_{\alpha\text{-}Fe}$=0.270±0.006 (0.181)$_{Rh}$ mm/s QS=0.36±0.01mm/s.

Moreover, after 0.5h at 180K no metastable component is present any longer. In Fig. 4.13, the relative areas of the various components are plotted against heating time during the different thermal cycles. The relative area of each component is given in Table 10 (Appendix).
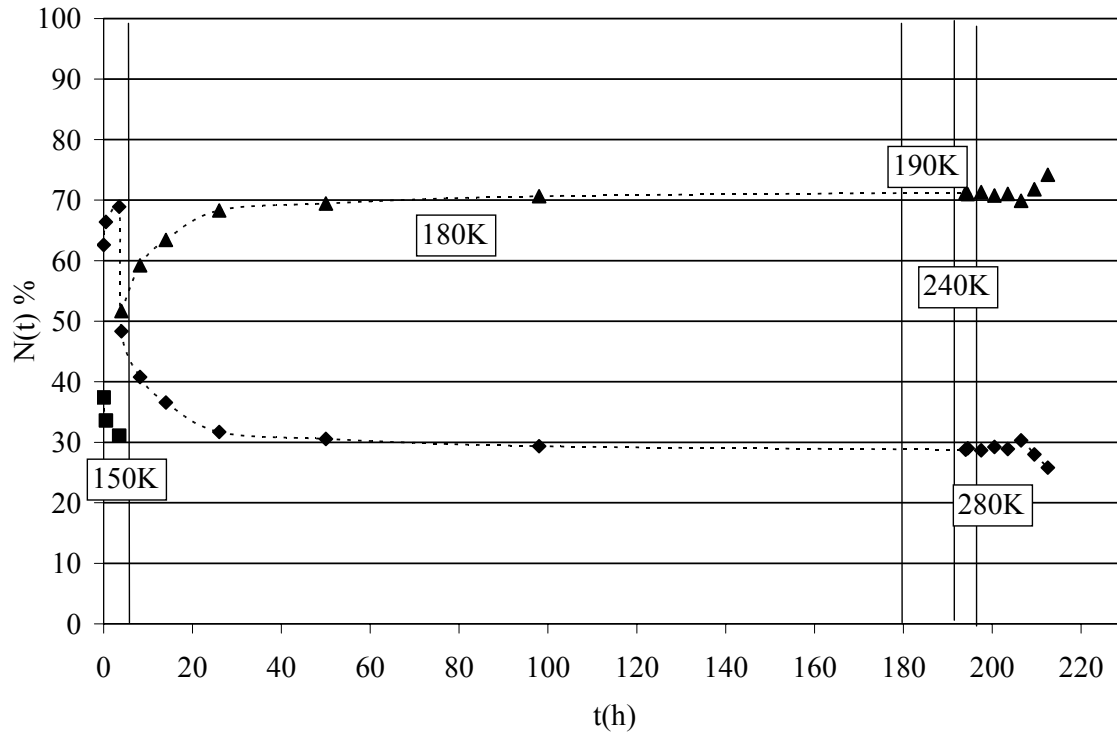
Figure 4.13: Relative population N(t) of each state as function of heating time, t, during different thermal cycles performed on Mbdeoxy: (♦) Mbdeoxy; (▲) MbCO; (■) metastable state. Dotted lines are eye guide lines. The graph is divided by vertical lines into parts characterized by the same heating temperature. The thermal cycles are performed from 150K to 280K. The measurements were done at T=78 K.

4.4   Mössbauer Spectroscopy of X-ray irradiated Hbdeoxy Sample

The human Hbdeoxy(1) sample has been measured before irradiation at 77K (Fig. 4.14). As already mentioned, the fitting was done by using the transmission integral with a Voigt profile due to the high intensity of the sample. The spectra show an asymmetric doublet, moreover the line widths of the doublet are different and also their relative intensity is different (Fig. 4.14). This unusual behaviour will be analysed in the following chapter.
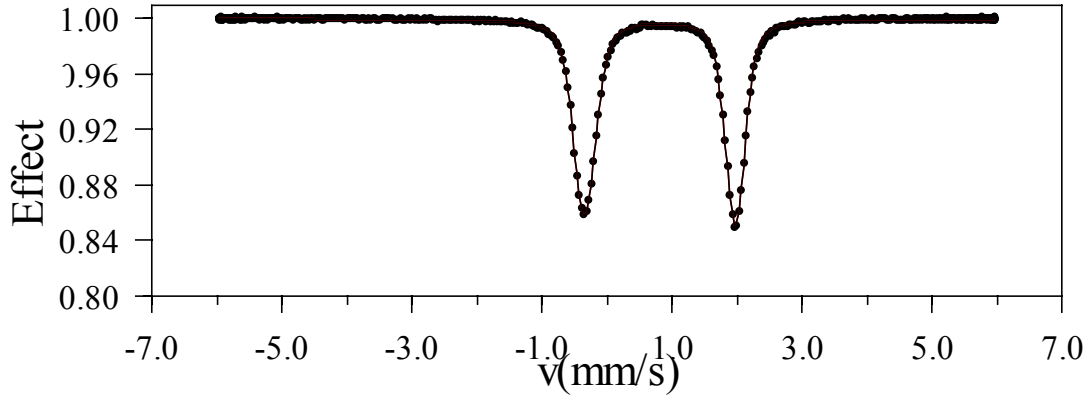
Figure 4.14: Hbdeoxy sample measured at 77K, and fitted with one asymmetric component. The velocity scale is referred to Rh matrix source.
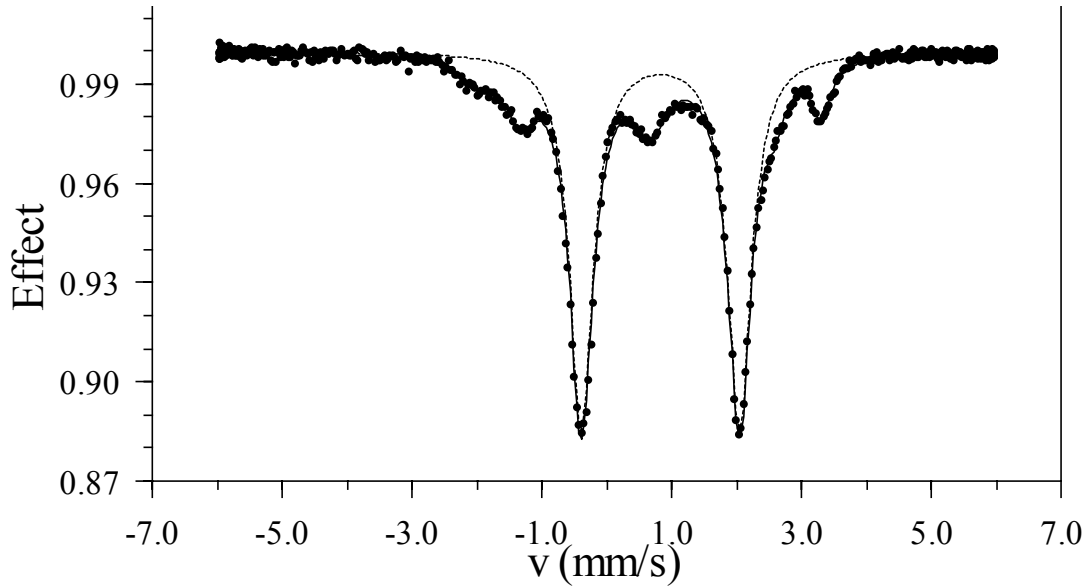
Figure 4.15: Hbdeoxy sample after X-ray irradiation, measured at T=5K and with a magnetic field B_{ex}=20mT. <u>Dashed line</u>: Hbdeoxy component.

Fig. 4.15 shows the spectrum after irradiation measured at T=5K with an applied low intensity magnetic field of 20mT perpendicular to the beam. The spectrum just after irradiation has also been measured at T=78K (Fig. 4.16a). The fitting of the Hbdeoxy component was done with one asymmetric doublet that has two different line widths and two different intensities with QS = 2.31 mm/s and IS = 0.89 mm/s respect to α- iron at 78K. These QS and IS values are completely in accord with the values found in literature. The spectrum of the **irradiated sample** exhibits a metastable component with a magnetic hyperfine splitting at low temperature, representing about 35% of the iron population and a clear Hbdeoxy component. At T=5K the metastable component shows the hyperfine splitting due to spin-orbit coupling, since the spin-lattice relaxation time

61

increases when lowering the temperature. The spectrum corresponds to an effective magnetic field of about 15T. This is a small value for Fe(III). This metastable component corresponds at 78K (Fig. 4.16a) to the doublet with the smallest QS. At 78K the spin-lattice relaxation is still sufficiently slow to see a residual of magnetic spitting. Moreover, the isomer shift with respect to α-iron can be estimated to be around 0.86 mm/s and QS is 0.9 mm/s at T=78K similar to a Fe(II) LS. On the other hand, this metastable component is very unstable since after 0.5h heating at T=180K it is almost completely relaxed to HbCO.
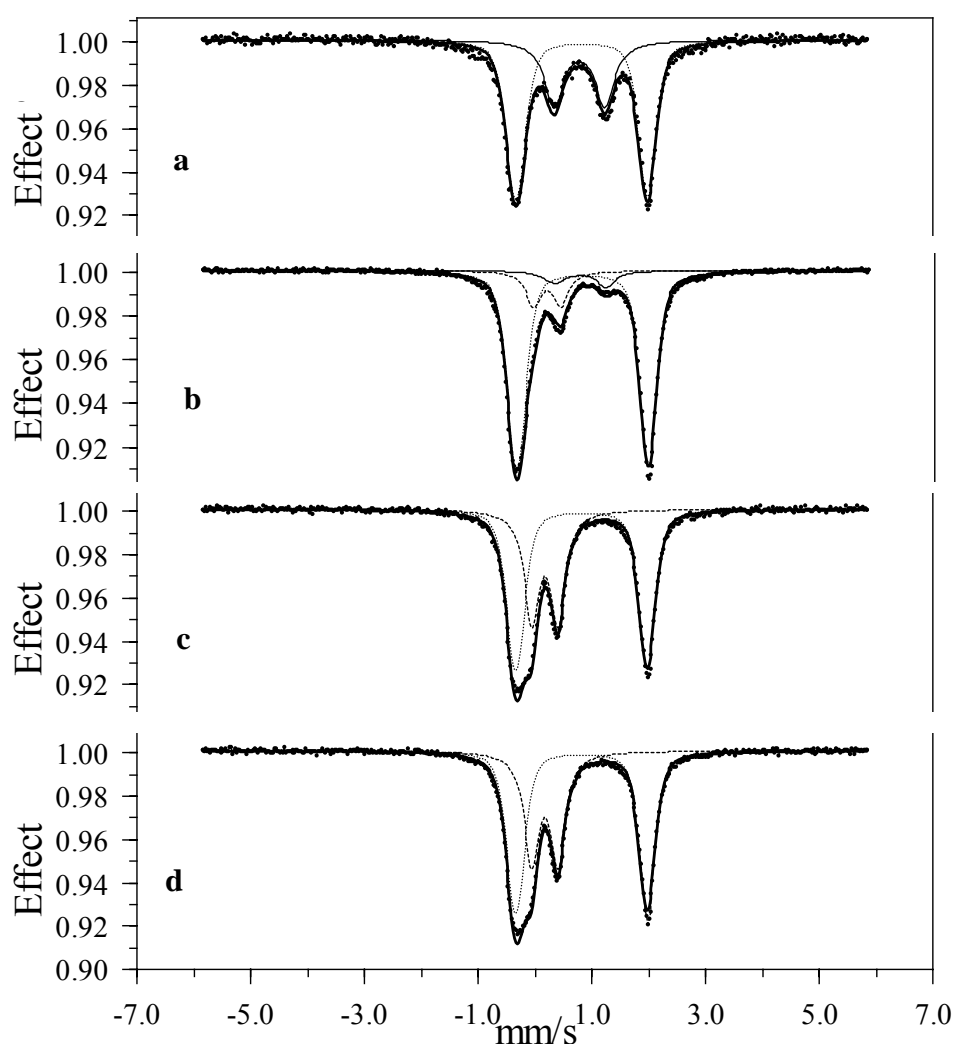
Figure 4.16: Hbdeoxy sample after irradiation measured at T =78K. **a:** before heating; solid line - metastable state, dotted line – Hbdeox. **b:** after t=0.5h heating at T=180K; solid line - metastable state, dotted line – Hbdeoxy, dashed line – HbCO. **c:** after t=6h heating at T=180K; dotted line – Hbdeoxy, dashed line – HbCO. **d:** after t=24h at T=180 K; dotted line – Hbdeoxy, dashed line- HbCO. The values of QS and IS used to fit the spectra are reported in Table 4.

Table 4: Values used to fit the spectra of the Hbdeoxy sample of Fig 4.16. Hbdeoxy measured just after irradiation and after 0.5h, 6h, 24h of heating at T=180K. In the columns are reported: heating time, IS of Hbdeoxy, QS of Hbdeoxy, IS of metastable component, QS of metastable component and IS of HbCO, QS of HbCO. In case of the IS in brackets are reported the value respect to a Rh source matrix.

	Heating time(h) T=150K	$IS_{\alpha.Fe}$ (mm/s) Hbdeoxy	QS (mm/s) Hbdeoxy	$IS_{\alpha.Fe}$ (mm/s) metastable component	QS (mm/s) metastable component	$IS_{\alpha.Fe}$ (mm/s) HbCO	QS (mm/s) HbCO
Irradiated Hbdeoxy	0	0.90 $(0.81)_{Rh}$	2.31	0.86 $(0.78)_{Rh}$	0.9	/	/
	0.5	0.90 $(0.81)_{Rh}$	2.31	0.86 $(0.78)_{Rh}$	0.9	0.28 $(0.20)_{Rh}$	0.48
	6	0.90 $(0.81)_{Rh}$	2.31	/	/	0.26 $(0.17)_{Rh}$	0.45
	24	0.90 $(0.81)_{Rh}$	2.31	/	/	0.26 $(0.17)_{Rh}$	0.45

The parameters of the asymmetric component are also similar to that ones of the asymmetric metastable components formed after irradiation of Mbdeoxy with and without glycerol (Fig 4.10 and Fig. 4.7b). Two are the possible interpretations of this component. It could be a Fe(I) with S=1/2, in fact although the literature data (Greenwood and Gibbs, 1971) gives a different value for the IS, a study on (TPP) Fe(I) complex reported a IS equal to 0.65mm/s (A Read et al., 1982). It could also be that an unpaired electron is delocalized in the pyrrolic rings causing a small magnetic field at the nucleus. Both interpretations could explain the metastable behaviour. With these evidences there are not enough clues to establish which iron configuration is produced after irradiation. Thermal cycles were performed from 180K to 280K. At these temperatures the occurrence of CO binding is evident. Representative spectra during the thermal procedure are given in Fig. 4.16. After 0.5h, the metastable state is nearly completely relaxed into HbCO. Also the Hbdeoxy component binds CO, as it appears clearly in Fig. 4.16. At the end of the thermal cycles around 20% of the Hbdeoxy has bound CO molecules. Nevertheless, at the end of the heating cycles more than 40% of the hemoglobin subunits have bound CO. It is interesting to notice that within the first 0.5h of heating, the Hbdeoxy component increases and the HbCO is already build up by the relaxation of the metastable component. The relative area of each component is reported in Table 9 (Appendix).

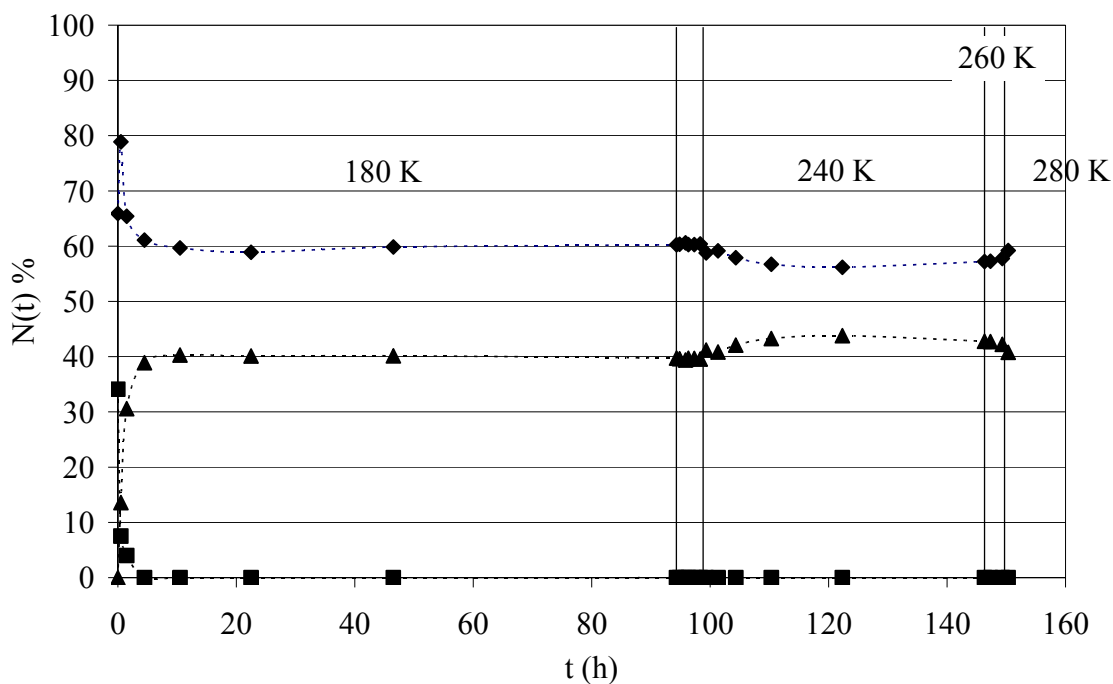**Figure 4.17:** Relative population N(t) of each state as function of heating time during different thermal cycles performed on Hbdeoxy: (♦) Hbdeoxy; (▲) HbCO; (■) metastable state. Dotted lines are eye guide lines. The graph is divided by vertical lines into portions characterized by the same heating temperature. The thermal cycles are performed from 180K to 280K. The measurements are done at T=78K.

5 Temperature Dependence of the Quadrupole Splitting: Hbdeoxy in Wet Silica Gel

5.1 Mössbauer Spectroscopy of HbCO in Silica Gel

HbCO in the quaternary R state encapsulated in wet silica gel has been measured at T=78K. The spectrum has been fitted with Lorentzians since we can consider the sample in the thin absorber approximation. The Mössbauer spectrum of HbCO e (Fig. 5.1) has a quadrupole splitting QS=0.38 mm/s and isomer shift $IS_{\alpha\text{-Fe}}$ =0.25 mm/s, and presents a linewidth Γ=0.33mm/s in agreement with literature values of HbCO in solution (Greenwood and Gibb 1971).
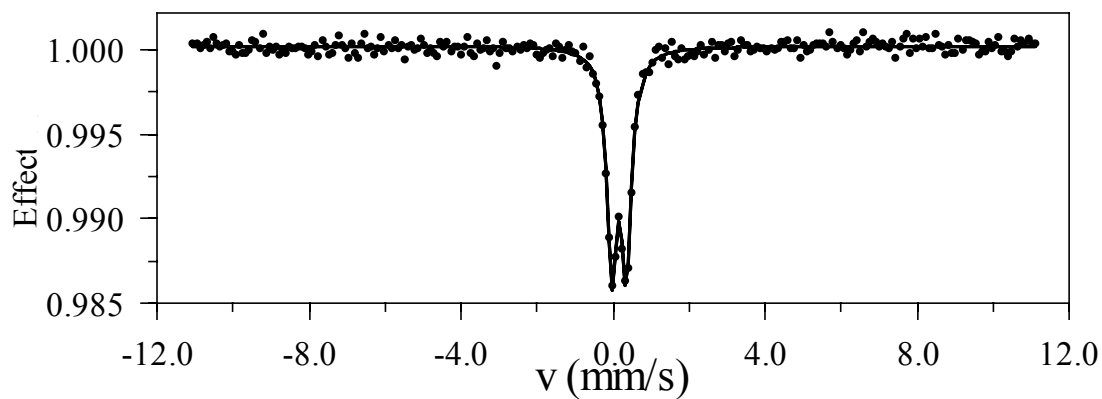
Figure 5.1: HbCO encapsulated in wet silica gel and measured at 78K.

5.2 Mössbauer Spectroscopy of Hbdeoxy in Solution

Hbdeoxy in solution was measured at 5K, 77K, 98K, 150K, and 180K (Fig.5.2), in this way it is possible to compare the QS temperature dependence of Hbdeoxy in solution with that obtained from Hbdeoxy encapsulated in silica gel. The Hbdeoxy spectra show an asymmetric doublet that depends on the temperature (Fig.5.2). In particular with the increase of the temperature, the ratio W21 of the linewidth of the second line (at higher velocity) with respect to the first one (at lower velocity) is increasing from 0.83 at T=5K to a value of 1.05 at T=180K. Moreover, the ratio A21 between the intensity of the second line with respect to the first one is going from a value of 0.9 to 1 (Fig. 5.3).
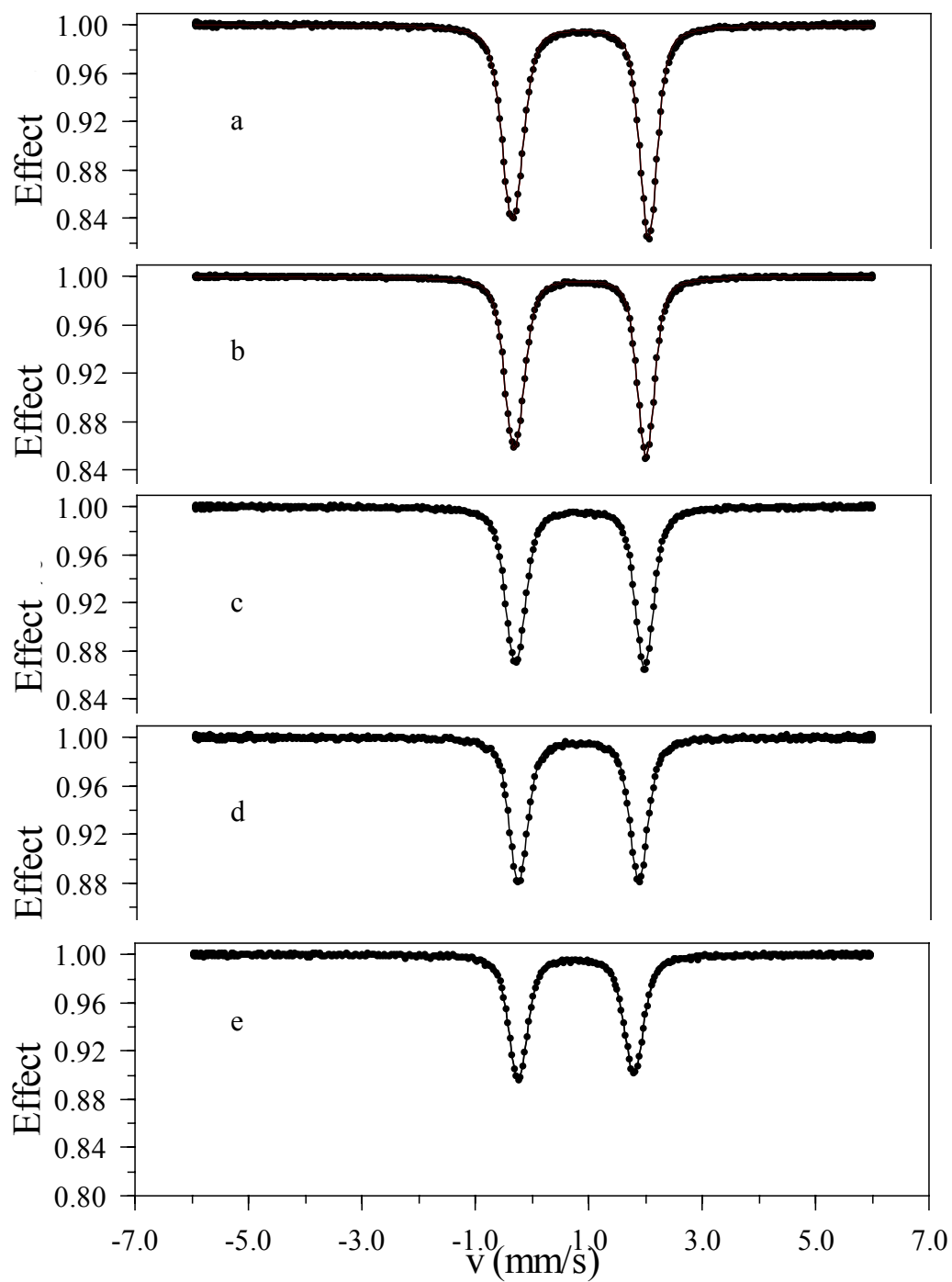
Figure 5.2: Hbdeoxy sample measured at **a:** T=5K; **b:** T=78K; **c:** T=98K; **d:** T=150K; **e:** T=180K, and fitted with one asymmetric component. The velocity scale is referred to a Rh source matrix.
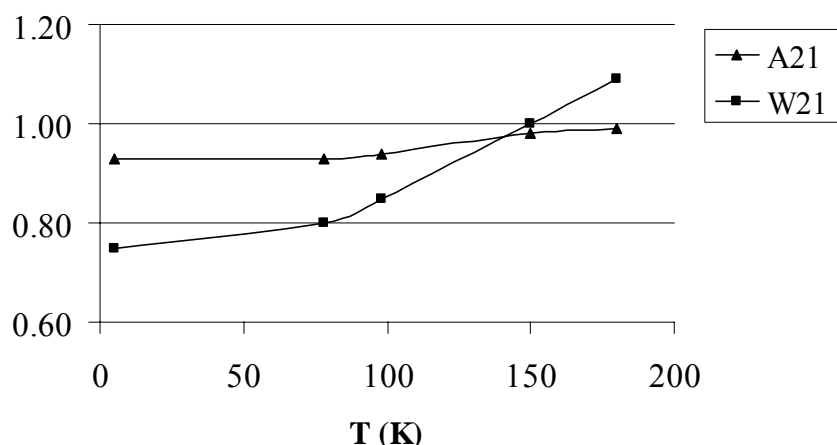
Figure 5.3: Values used to fit the spectra of the Hbdeoxy sample in Fig. 5.2. W21: ratio of the line width of the second line with respect to the first one as a function of temperature. A21: ratio between the intensity of the second line with respect to the first one.

The values of the QS of the spectra fitted with a single asymmetric component are reported as a function of temperature in Fig. 5.5. Some attempts have been done to fit the spectra with two doublets with the same area (Fig. 5.4). The values of the QS and IS of each component are reported in Table 13(Appendix).
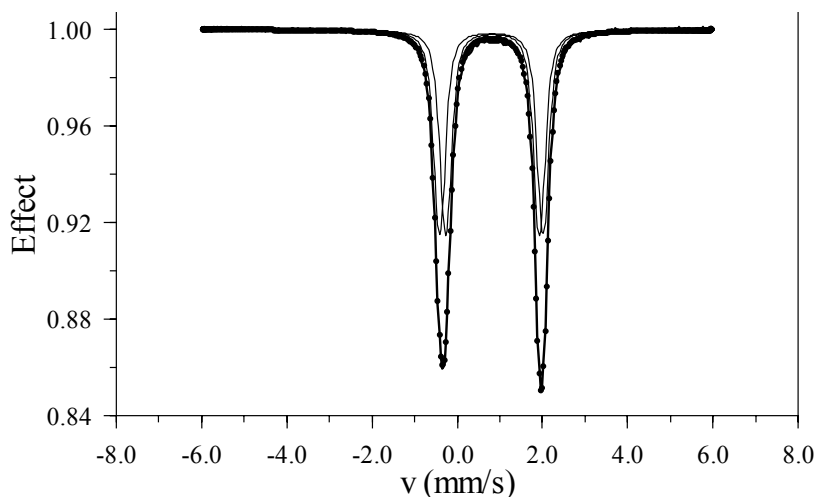
Figure 5.4: Hbdeoxy sample measured at T=78K before irradiation, fitted with two doublets having the same area. The velocity scale is referred to a Rh matrix source.

5.3 High and Low Affinity Hbdeoxy in Wet Silica Gel

The Hbdeoxy sample without allosteric effectors **called Hbdeoxy HA** (High Affinity) has been measured from 5K to 200K.
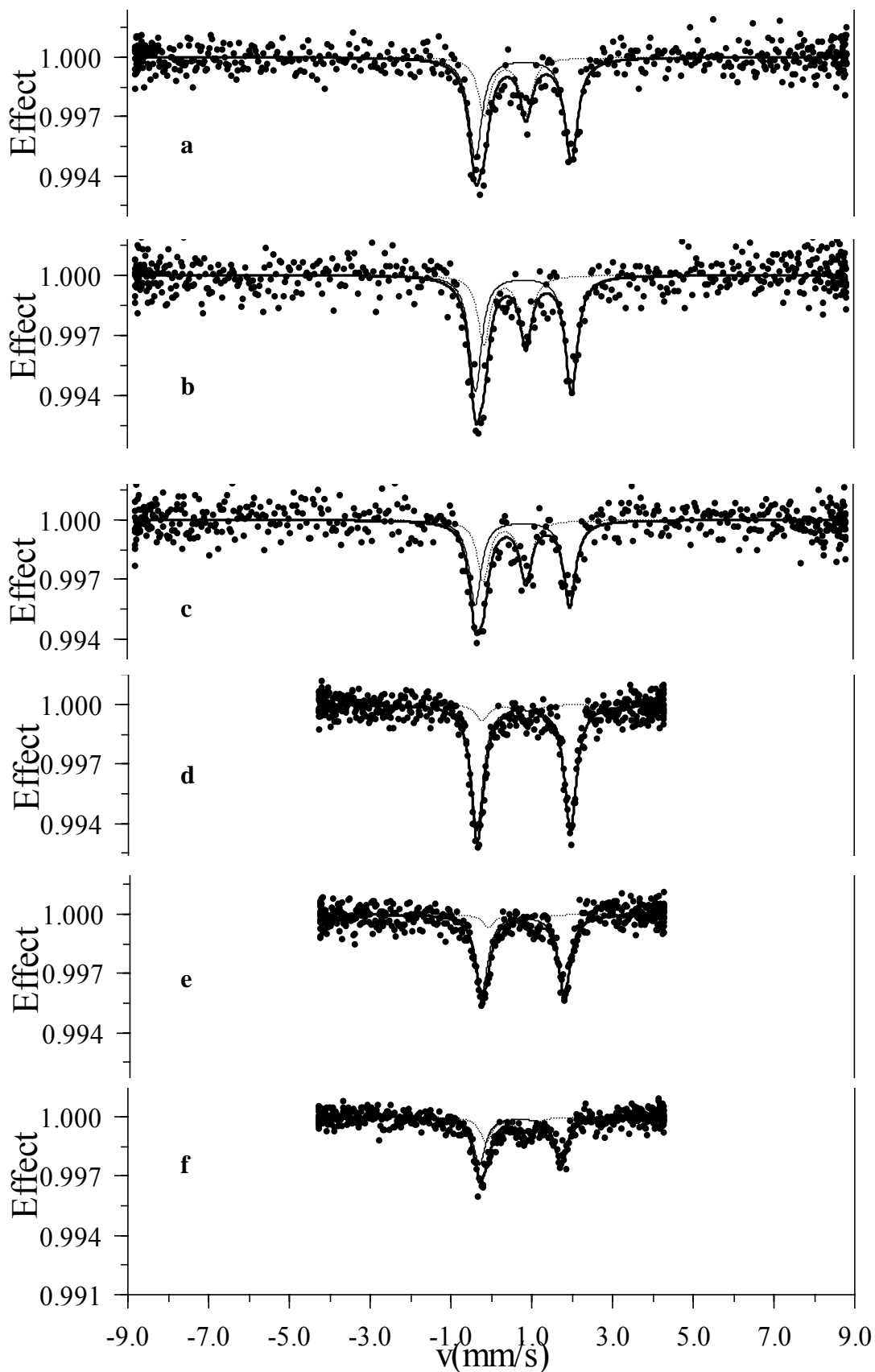
Figure 5.5: Hbdeoxy HA encapsulated in wet silica gel at **a:** 5.5K; **b:** 14.5K; **c:** 39K; **d:** 77; **e:** 180K; **f:** 200K. The least squares fit is done with two components: <u>dashed line</u> – Low Spin complex coordinated with the N^ε-His E7; <u>solid line</u> – Fe(II)HS Hbdeoxy. The velocity scale in the graph is referred to a Rh matrix source.

The spectra have been fitted with Lorentzians since we can consider the sample in the thin absorber approximation. The sample was first measured from 77K to 200K. Then, measurements at 5.5K, 14.5K, 39K, and 20K were conducted. In Fig. 5.5 few representative spectra of this Hbdeoxy HA sample are reported. The order of the measurements is very important, as explained in the considerations that follow. The spectra in Fig. 5.5 are fitted with two components: one is characteristic of Fe(II) high spin, the other represents a low spin complex coordinated with N^ε-His E7, which is the only available globin coordinating group on the distal side of the heme iron (Levy et al., 1985). In particular at 77K, the Hbdeoxy component is fitted using QS=2.31 mm/s, $IS_{\alpha\text{-}Fe}$=0.89 $(0.80)_{Rh}$ mm/s and Γ=0.36 mm/s. The Fe(II)LS complex has QS=1.01mm/s, $IS_{\alpha\text{-}Fe}$=0.42 $(0.33)_{Rh}$ mm/s and Γ= 0.35 mm/s. This complex can be formed if the sample is heated at T equal or higher than 200K (Levy et al., 1985). That's why it was important to stress the order followed in collecting these spectra. In fact, the first measurements were performed from 77K to 180K and the bis(histidine) complex were around 10%. At 200K the component reaches 33%, which is practically the same abundance that we find in the measurements from 5.5K to 39K. It is a reversible complex that can be reconverted in to Fe(II)HS if the sample is thawed and again rapidly cooled at 77K. To check this hypothesis, the sample was heated at 288K for 20 minutes and then cooled and measured at 5.5K. The spectra are reported in Fig. 5.6.
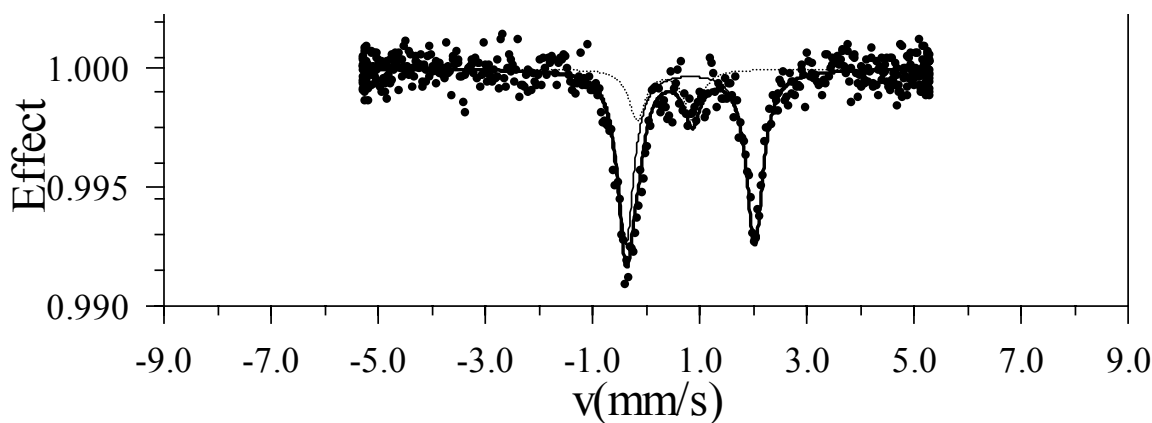
Figure 5.6: Hbdeoxy HA encapsulated in wet silica gel measured at 5.5 K after heating at T=288K for 20 min. The fitting is done with two components: <u>dashed line</u> - low spin complex coordinated with the N^ε-His E7; <u>solid line</u> - Fe(II) HS Hbdeoxy.

From Fig. 5.6 it is clear that the component mainly produced during heating at T=200K, has been reduced by thawing the sample: in particular, it decreased from 33% to 22% according to the literature. In the case of Hbdeoxy HA sample, the relative area of the single component and their QS and IS are reported in Table 11 (Appendix).

The sample prepared with allosteric effectors, **Hbdeoxy LA** (Low Affinity), showed a similar behaviour. It was measured at 6.5K and from 77K to 210K. Also in this case after the measurement at 210 K it was warmed up to 288K and cooled again at T=77K. Afterwards, measurements were performed at 20K, 55K and 77K. Some representative spectra are given in Fig.5.7
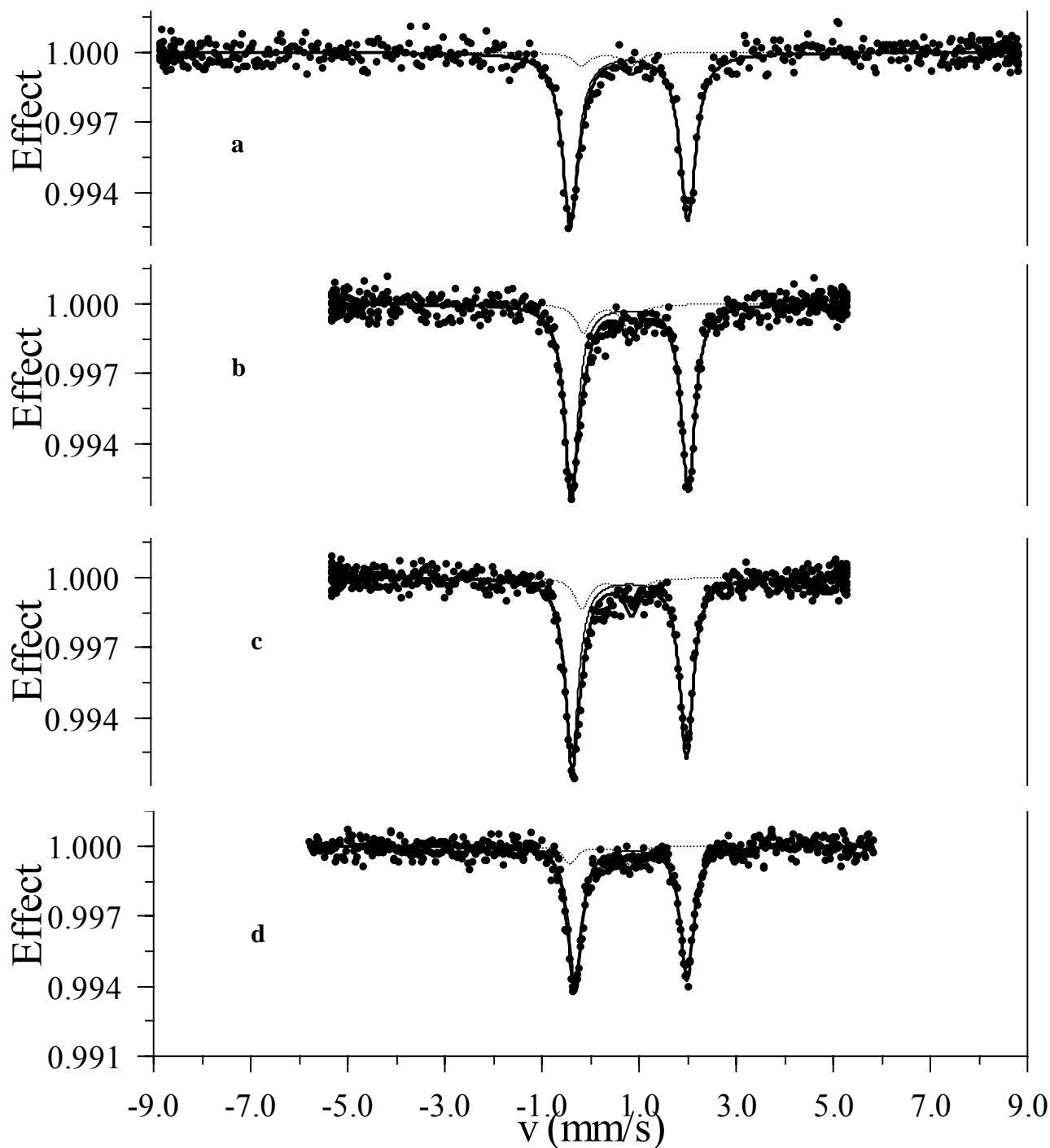
Figure 5.7: Hbdeoxy LA encapsulated in wet silica gel at **a:** 5.5 K; **b:** 20K; **c:** 55K; **d:** 78K. The fitting is done with two components: <u>dashed line</u> – Low Spin complex coordinated with the N^{ε}-HisE7; <u>solid line</u> – Fe(II) HS Hbdeoxy.

Also in this case the spectra were fitted with two components. One is characteristic for Hbdeoxy with QS= 2.33 mm/s, $IS_{\alpha\text{-Fe}}$=0.91 (0.82)$_{Rh}$ mm/s and Γ=0.31 mm/s. The other is characteristic for a Fe(II)LS (N^{ε}-His E7) complex with QS=0.98 mm/s, $IS_{\alpha\text{-Fe}}$=0.36 (0.27)$_{Rh}$ mm/s and Γ=0.28mm/s at T=77K. In the case of Hbdeoxy LA sample, the relative area of the single component and their QS and IS are reported in Table 12 (Appendix). As expected, the quadrupole splitting of the Hbdeoxy HA and LA shows strong temperature dependence. The quadrupole splitting of the two samples as function of the temperature are reported in Fig 5.8. A least squares fit according to the Eicher theory (Eicher et al., 1976) is also shown.
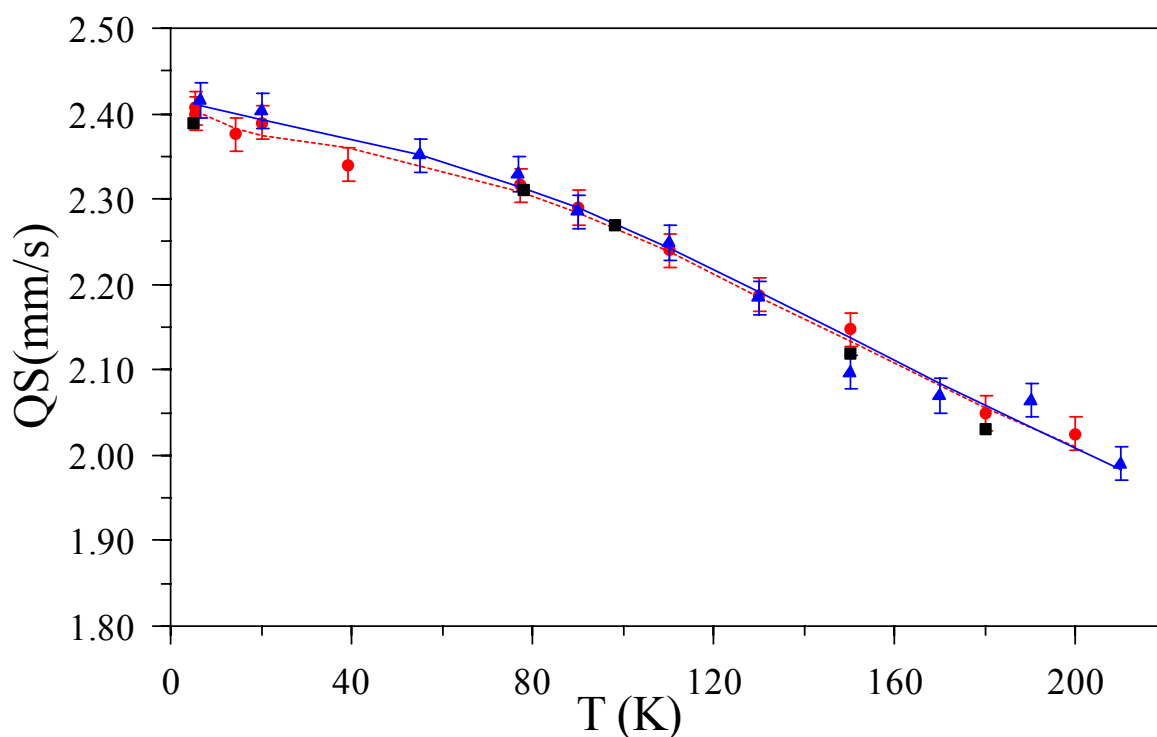
Figure 5.8: Quadrupole Splitting function of temperature. Square (■): Hbdeoxy in solution; Circles (●): Hbdeoxy LA sample. Dashed line: least squares fit of Low Affinity Hbdeoxy QS values. Triangles (▲):Hbdeoxy HA sample. Solid line: least squares fit of High Affinity Hbdeoxy QS values.

6 Data analysis and Discussion

6.1 Free Energy Barrier of the Metastable Hbmet Relaxation, Comparison with Mbmet Data

The irradiation is used to create a metastable Fe(II) LS state in case of Hbmet (Fig. 4.2) and Mbmet samples (Prusakov et al., 1995). Both the samples, Hbmet(1) frozen in liquid propane and Hbmet(2) frozen in liquid nitrogen, were reduced to Fe(II)LS and some percent of Hbdeoxy. In both Hbmet samples, the Fe(II)HbH$_2$O metastable state completely relaxes to HbCO stable state during thermal cycles. In the case of the irradiated Hbmet samples, the strong decrease of the intermediate Fe(II)LS state, after the thermal cycles, is not exponential in time.
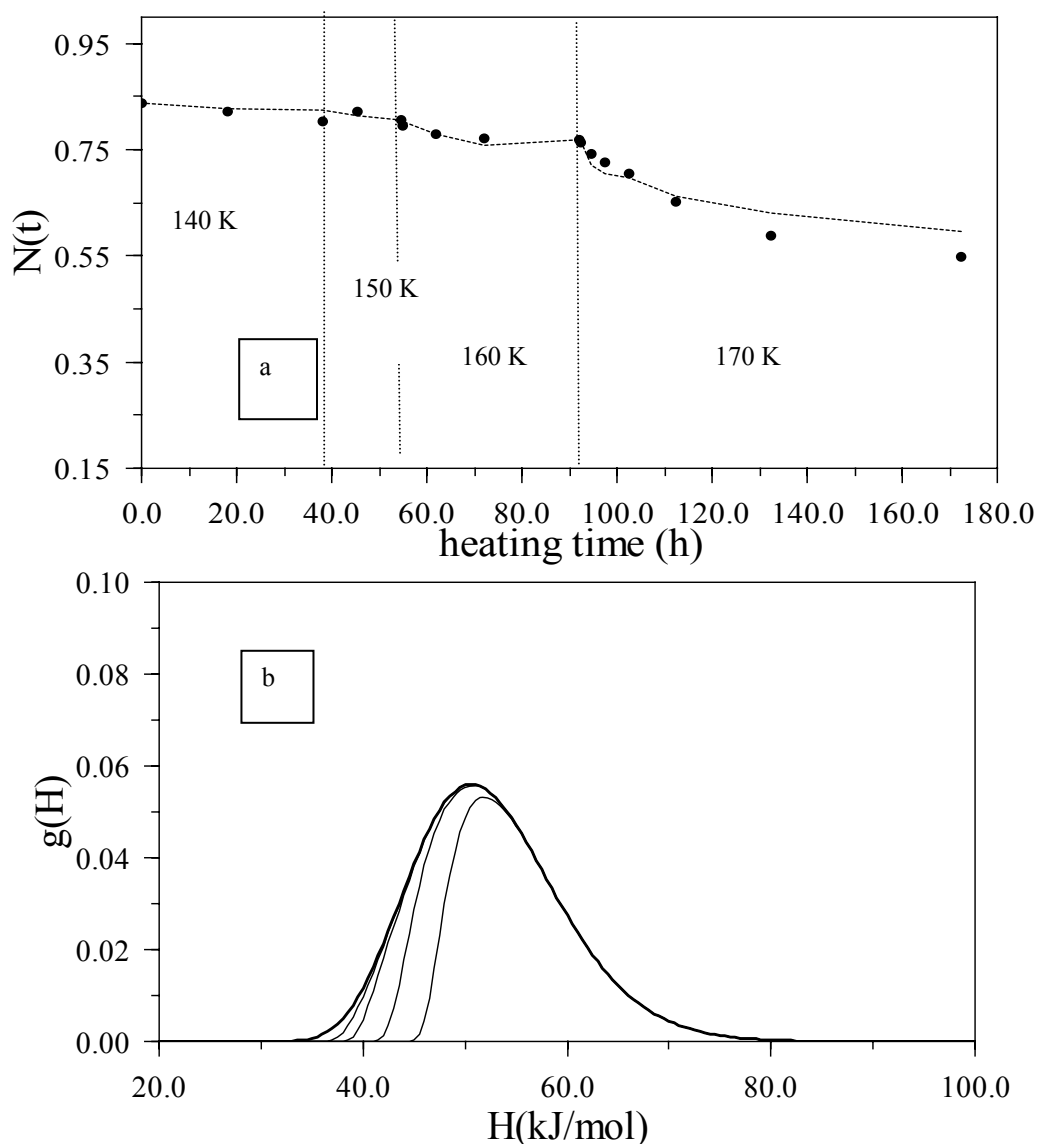
Figure 6.1: a: Hbmet(1) Fe(II)LS relaxation from T=140K to T=170K (circles) fitted with the same starting distribution - dashed line. **b:** enthalpy distributions at the beginning of relaxation at T=140K, at the end of 140K, 150K, 160K, and 170K heating cycles.

Similar to the case of Mbmet sample (Prusakov et al., 1995) the decreasing of this metastable component has been fitted with an enthalpy distribution according to Eq. 2-39.

Temperature cycles on the irradiated Hbmet(1) have been performed from 140K to 200K. For the thermal cycles at 140K, 150K, 160K, and 170K it is possible to fit the decreasing population of Fe(II)LS using the same starting enthalpy distribution as shown in Fig 6.1.
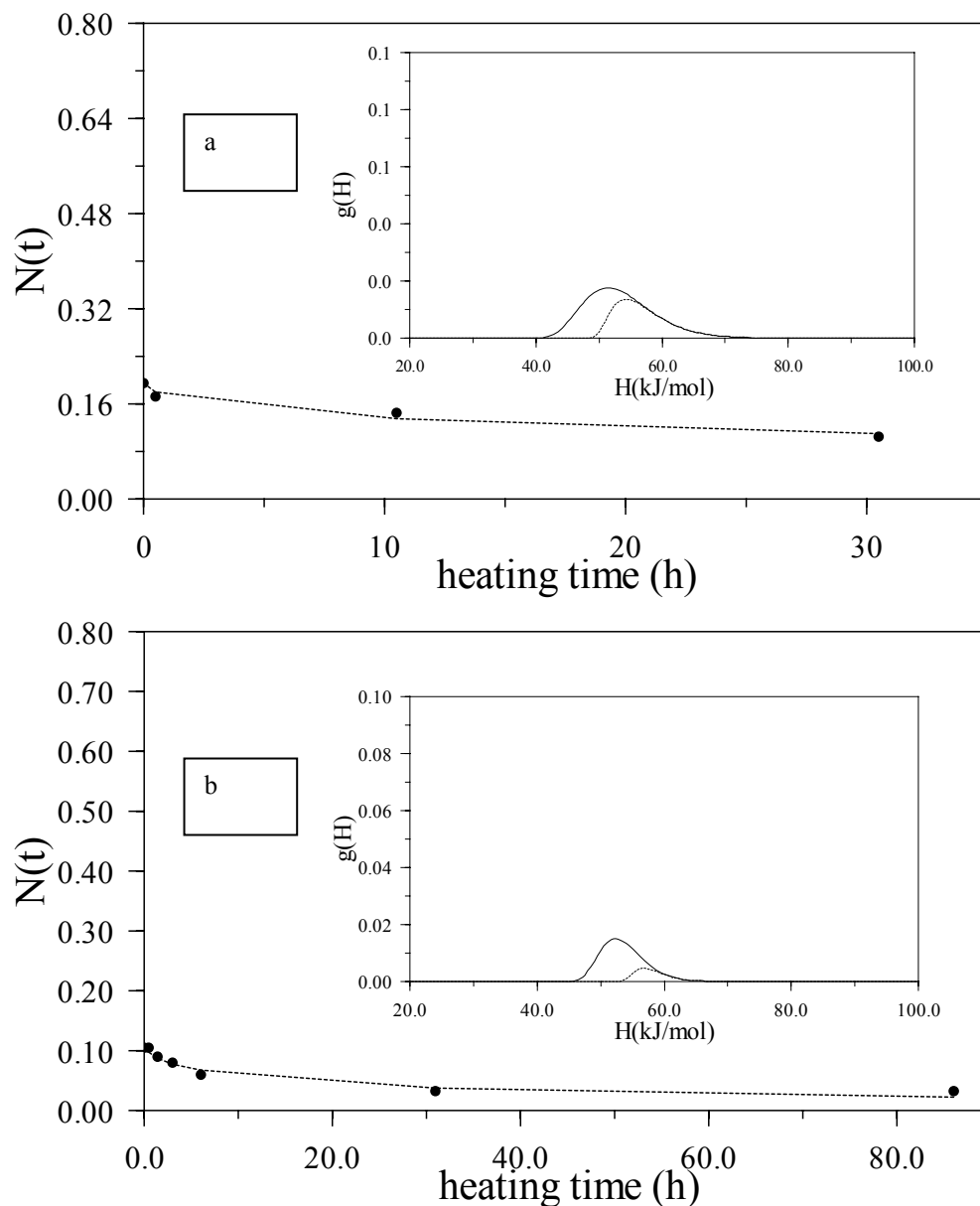
Figure 6.2: a: circles - Hbmet(1) Fe(II) LS relaxation at T=190K;   **b:** circles -Hbmet(1) Fe(II) LS relaxation at T=200 K. Two distributions are represented in each inset, solid line and dashed line are representing the starting and the ending distribution that are used to produced the fitting curves reported in **a** and **b**.

The data obtained during the thermal cycles at T equal 180K can be fitted with a similar - but not identical - enthalpy barrier used to fit the data heated in the range of temperature from 140K to 170K. Also in the case of the fit of the data at 190K and 200K, it is necessary to use a new fresh starting distribution. Fig. 6.2 reports the fit of the data at 190K and 200K using a value of $A=10^9$. However, also in these cases a wide range of A values gives a satisfactory fit.

The Hbmet(2) sample was heated only at 180K and 190K. It shows (Fig 6.3) practically the same behaviour of Hbmet(1). The barriers used to fit the Fe(II)LS decreasing population are not the same at 180K and 190K, even if they have similar values, as reported in Table 5.
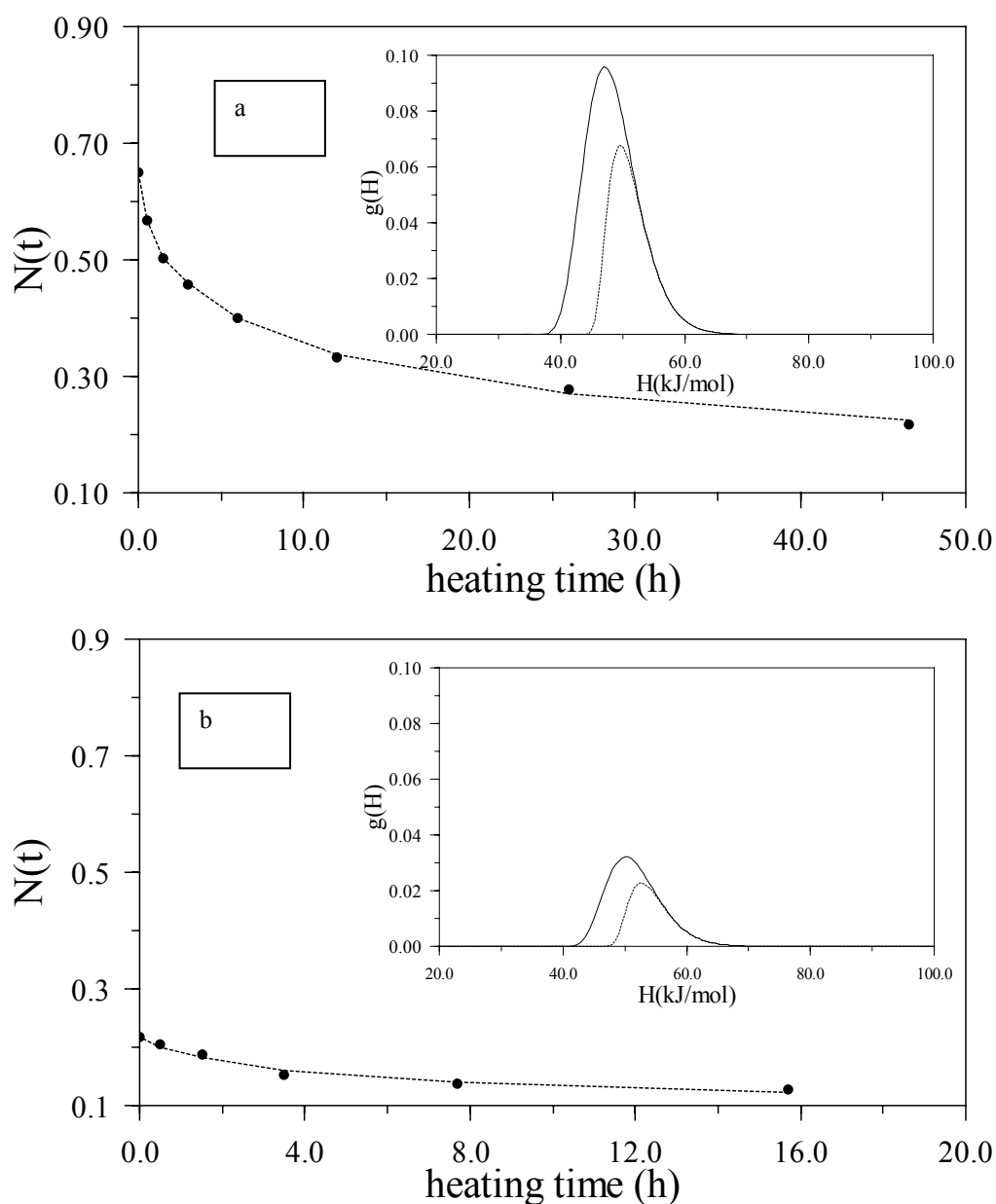
Figure 6.3: a: <u>circles</u> - Hbmet(2) Fe(II) LS relaxation at T=180K**; b:** <u>circles</u> **-** Hbmet(2) Fe(II) LS relaxation at T=190K, fitted with the enthalpy distributions that are shown into the inset. Two distributions are represented in each inset; solid line and dashed line represent the starting and the ending distribution.

During the data fitting, it became clear that it is not possible to obtain one unambiguous set of values that defines the barrier distribution and the pre-factor A. In fact, at each temperature the fitting of the Fe(II)LS relaxation can be done with different enthalpy energy distributions correlated with a different value of A. Fig. 6.4 shows some examples of the fitting of irradiated Hbmet(1) at 180K. The parameters of the enthalpy distributions and the pre-factor A are reported in Table 5. It has to be noticed that (Fig. 6.4) an increase in the value of A moves the barrier to higher enthalpy values. Moreover, a decrease of the α value as well as the increase of ν moves the enthalpy peak towards higher values.
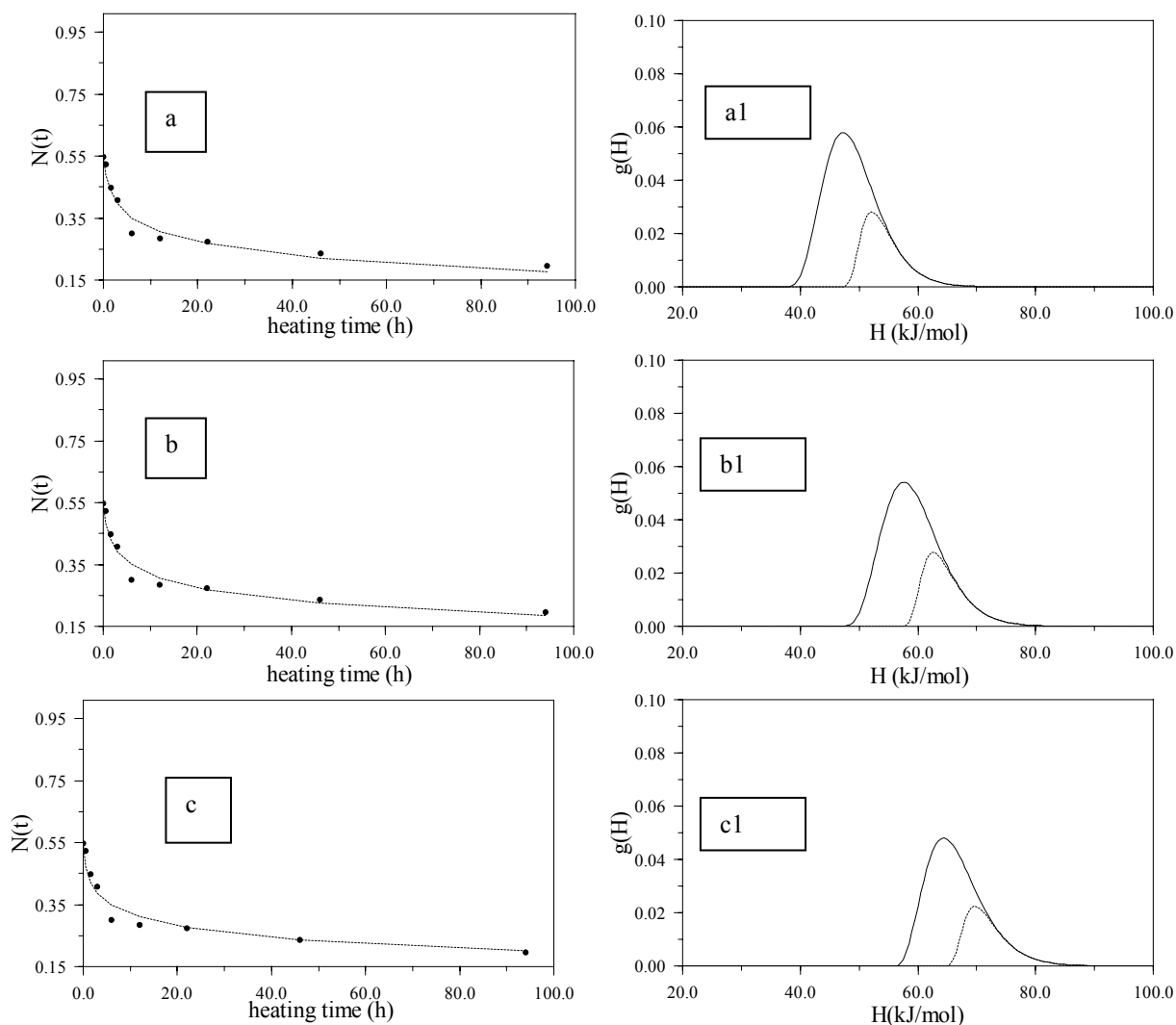
Figure 6.4: a, **b**, **c:** Hbmet(1) Fe(II)LS relaxation at T=180K fitted with different enthalpy distributions with different A values - **a1:** A=10^9; **b1:** A=10^{12}; **c1:** A=10^{14}. <u>Solid line</u>: beginning of relaxation. <u>Dotted line</u>: end of relaxation.

Table 5: Parameters of the enthalpy energy distributions used to fit the decay of the metastable Fe(II)LS state. First column: sample names, **a**, **b** and **c** refer to three different enthalpy distributions used to fit the Fe(II) LS decay data obtained during the thermal cycles at 180K (Fig. 6.4). Second column: heating cycle temperatures. Next columns: parameters A, ν, α and Hpeak that define the barriers used to fit the data.

Sample	T heating cycles (K)	Hmin (kJ/mol)	A	ν	α	Hpeak (kJ/mol)
Hbmet (1)	140	24.81	1.00E+09	4.76	0.51	50.85
Hbmet (1)	150	24.81	1.00E+09	4.76	0.51	50.85
Hbmet (1)	160	24.81	1.00E+09	4.76	0.51	50.85
Hbmet (1)	170	24.81	1.00E+09	4.76	0.51	50.85
Hbmet (1) a	180	36.37	1.03E+09	2.37	0.55	47.48
Hbmet (1) b	180	43.76	1.00E+12	2.34	0.55	54.71
Hbmet (1) c	180	50.47	1.01E+14	2.55	0.47	64.62
Hbmet (1)	190	38.06	1.02E+09	2.53	0.49	51.51
Hbmet (1)	200	43.95	1.03E+09	2.52	0.78	52.36
Hbmet (2)	180	34.68	1.06E+09	3.35	0.73	47.08
Hbmet(2)	190	38.99	9.83E+08	2.78	0.65	50.28

From Fig 6.4 and Table 5, it is clear that the A determination is afflicted by large errors. In fact it is possible to change the A value by about 5 orders of magnitude still yielding a good fit. Since it is the Gibbs free energy $\Delta G^{\#}$ which determines the activation, in principle there is no reason to separate enthalpy and entropy a priori. Although the enthalpy distributions fit quite well our experimental data, it is not necessarily the best description of our experiments. Our relaxation experiments depend on a completely different range of time. The relaxation, in these experiments, takes place during hours while in the case of flash photolysis it occurs between μs and 1000s. Consequently the data are analyzed using a Gaussian distribution of the Gibbs free energy according to Eq 2.42 and Eq. 2.43.

The fitted data of Hbmet(1) from 140K to 170K with a $\Delta G^{\#}$ distribution are reported in Fig. 6.5. It has to be noticed that to fit the data at the four different temperatures, 140K, 150K, 160K, and 170K, only one starting distribution has been used. In particular, the remaining distribution of molecules at the end of the 140K measurement is used as starting distribution for 150K and so on for the other temperatures till 170K.
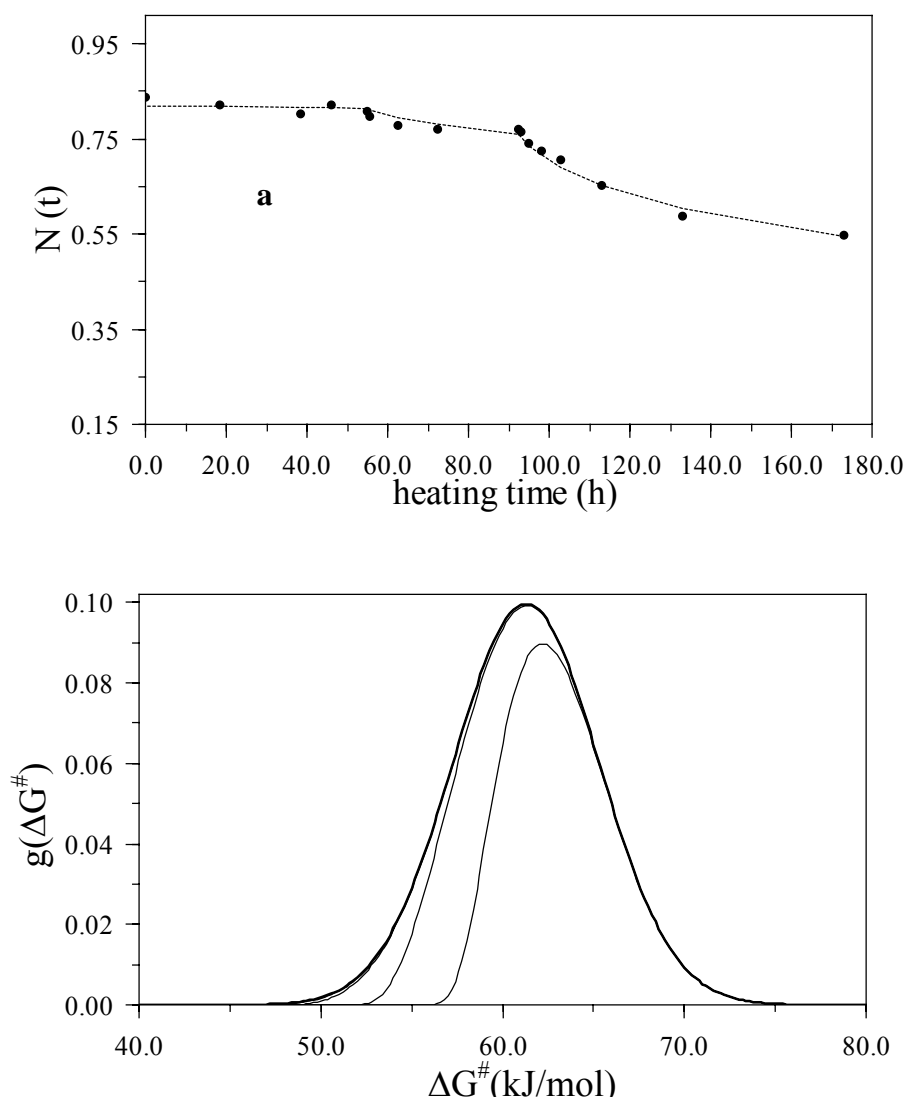
Figure 6.5: a: Hbmet(1) Fe(II)LS relaxation from T=140K to T=170K fitted with the same starting distribution; **b:** free Gibbs energy distributions at the beginning of relaxation at T=140K and at the end of 140K, 150K, 160, 170K.

The starting barrier reported in the Fig.6.5 is centred at $\Delta G_0^{\#}$=61kJ/mol and has a line width σ=4kJ/mol. Due to the relaxation of the Fe(II)LS population, the energy barrier distribution decreases its area with the increase of temperature and also changes its shape. In fact, the starting barrier distribution has a Gaussian shape but with the increase of the heating temperature the shape is changing and it is not any longer symmetric, because only the states with lower energy are relaxing. Evidently at these temperatures a repopulation of the lower energy states does not occur on the time scale of the experiment. The conformational substates are "frozen" in defined energy barrier state. At temperatures above 170K it is no longer possible to fit the data with the same starting distribution. The barrier used at the end of relaxation process at 170K was not able to fit the data at 180K. Therefore, it has been necessary to start with a new, fresh distribution. From

comparison between Fig. 6.6a1 and Fig. 6.5b it is evident that the barrier at 180K is very similar to the starting barrier used at 140K. In fact, it is centred at $\Delta G_0^{\#} = 61$kJ/mol with σ about 4kJ/mol. This shows that the lower energy states have been repopulated. Also for the relaxation data at 190K and 200K it was necessary to use a new barrier shifted at higher temperatures, as represented in Fig. 6.6. The barrier obtained from the heating cycles at 190K is centerd at $\Delta G_{peak}^{\#} = 65$kJ/mol while the barrier at 200K is centered at $\Delta G_{peak}^{\#} = 67$kJ/mol. The line width did not change significantly. In Fig. 6.7 the fits of Hbmet(2) sample together with barriers used at 180K and 190K are shown. In both samples the energy barrier distributions are normalised to 1, that means that the first barrier of the irradiated Hbmet(1) at 140K has the area equal to 1. At 180K (Fig.6.6) the area is the same of last distribution at 170K. In the same way, the area of the distribution at 190K is the same of the last distribution at 180K and so on. The other barriers from 150K to 170K have the areas that are decreased by the exponential factor present is Eq. 2-42. This is always the case when there is not a new starting distribution. In the case of the irradiated Hbmet(2) the first heating cycle is performed at 180K, therefore the first energy distribution at 180K is normalised to 1. In Fig. 6.7 the barrier at 180K and 190K of the irradiated Hbmet(2) are centred at $\Delta G_{peak}^{\#} = 60.9$kJ/mol and $\Delta G_{peak}^{\#} = 64$kJ/mol respectively. Comparing Fig. 6.6 and Fig. 6.7 the energy distribution at 180K and at 190K are practically the same, that means that the previous heating cycles, performed in case of Hbmet(1) sample, did not influence the relaxation process. This is strictly connected with the repopulation of the lower energy states: in fact the thermal history of the sample could be important only at T lower than 180K. At T equal or higher than 180K even the states with lower energy are repopulated, showing no differences whether the sample has been heated before or not. The first distribution at 180K is practically the same of the first distribution at 140K. In this case the repopulation of the lower energy state is clear. At temperatures higher than 180K this repopulation it is not so evident, this is due to the fact that during the repopulation time the protein is relaxing. In practice there are two competitive events, one is the repopulation of the low energy states and the other is the decay from that states. In other words, if the relaxation time is faster then the repopulation time there is no way to see the complete repopulation of the low energy states.
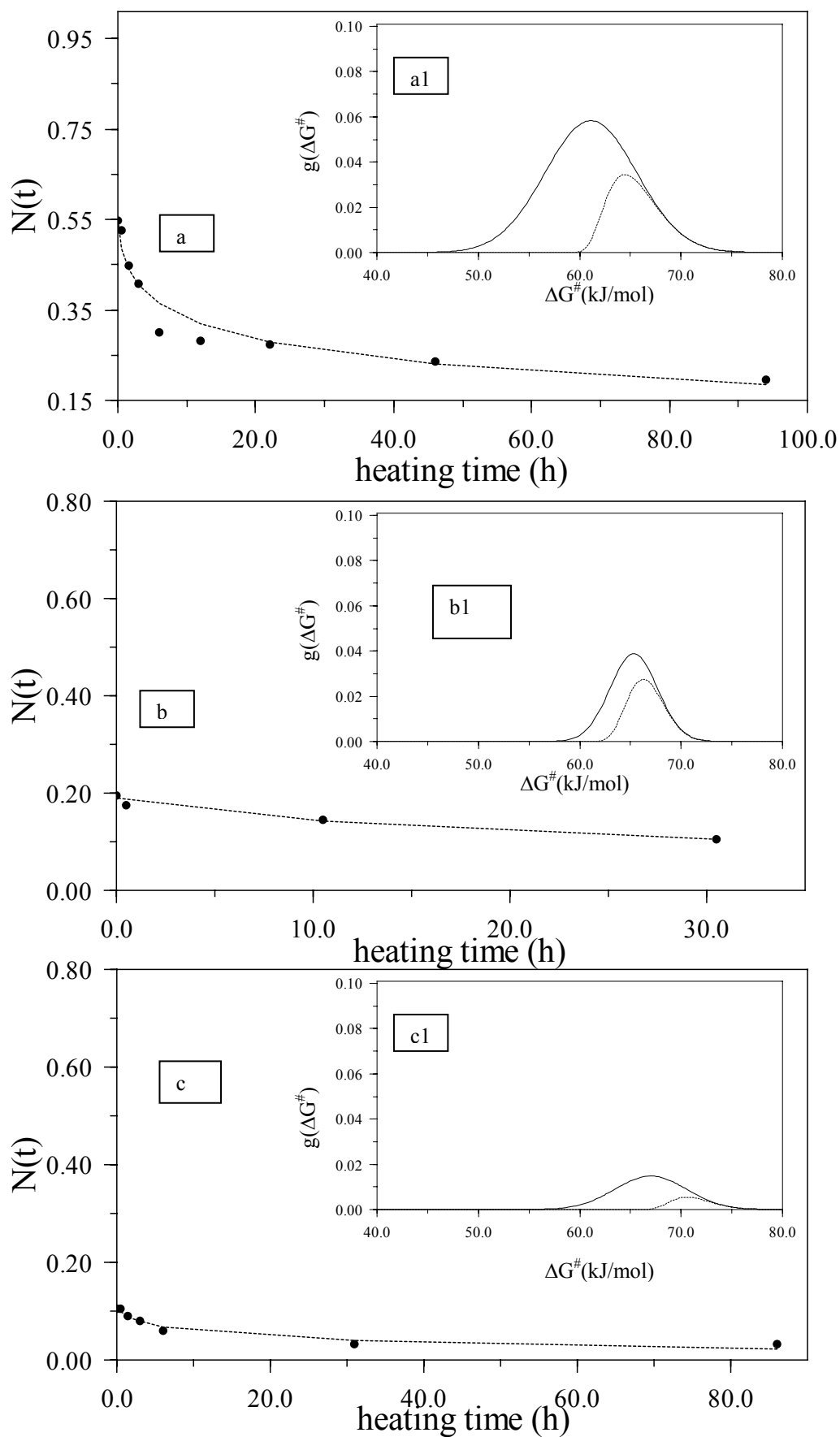
Figure 6.6: Hbmet(1) Fe(II) LS relaxation at **a:** T=180K; **b:** T=190K, and **c:** T=200K, fitted with the Gibbs free energy distributions **a1, b1, c1** respectively.

At T equal to 180K there is the biggest decrease of the metastable component. Since it is no longer possible to use the same starting energy barrier to fit the data at T higher than 180K, this means a rearrangement of protein structure. Structural relaxations occur within the Fe(II)LS state, in agreement with the results of (Engler et al., 2000). Also CO rebinding experiments in myoglobin after flash photolysis have shown that above 180K the barrier height distribution becomes temperature dependent (Young et al., 1984). This temperature dependence recalls the fact that the temperature of about 180K is a characteristic temperature (T_c) where structural fluctuations of proteins become visible on the time scale of nanoseconds to picoseconds (Parak, 2003).
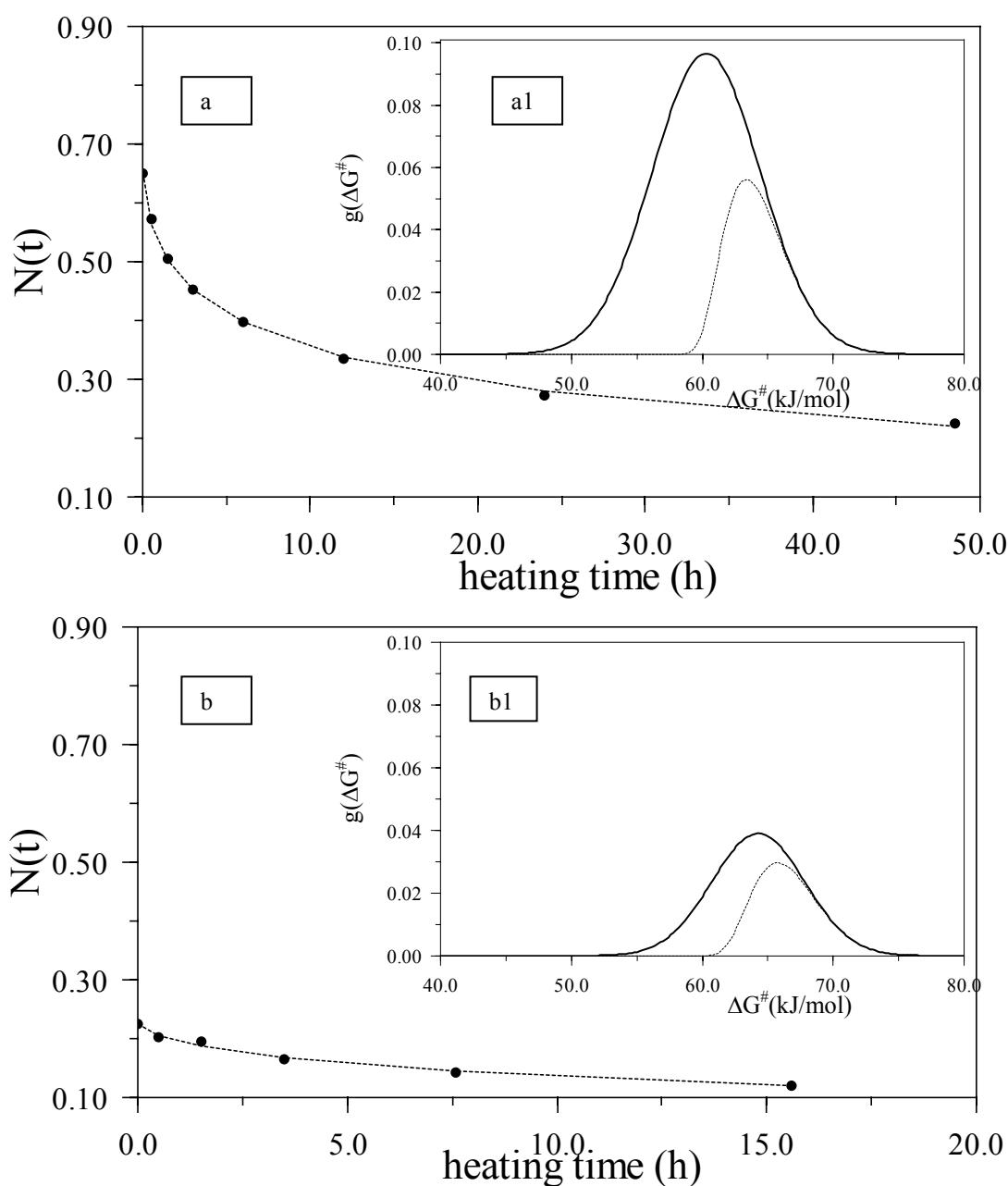
Figure 6.7: a: Hbmet(2) Fe(II) LS relaxation at T=180 K**; b:** Hbmet(2) Fe(II) LS relaxation at T=190 K, fitted with the Gibbs free energy distributions **a1, b1,** respectively.

An experiment similar to the Hbmet experiment just discussed was performed by Prusakov (Prusakov et al., 1995) on met-myoglobin (Mbmet). Te sample was prepared and irradiated in the same way as the Hbmet samples. For comparison the published data were fitted with a free activation energy distribution. Two samples of Mbmet were prepared by Prusakov (Prusakov et al., 1995). The first was irradiated and heated at 147K and 174K, while the second was heated at 180K, 190K and 195K. As in case of Hbmet, a Fe(II)LS state was created and it relaxed to Mbdeoxy and to MbCO during the heating cycles. The fitted data of the decay of metastable Fe(II)LS component are reported in Fig. 6.8. The fit is performed with the same starting distribution at 147K and 174K. The data at 180K, 190K and 195K stem from another sample. In this case it is not possible to use the same starting distribution to fit all the data simultaneously. The barrier height distributions had to be fitted independently.
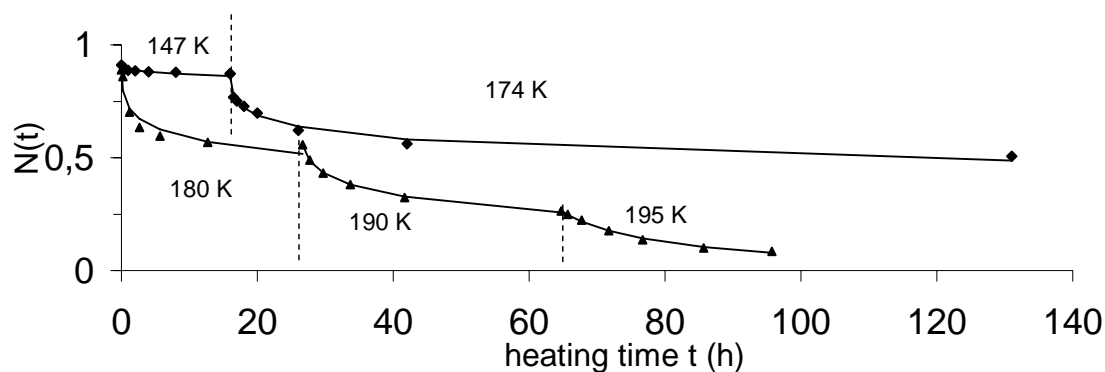
Figure 6.8: Decay of metastable Fe(II)LS component of irradiated Mbmet (Prusakov et al., 1995) as function of heating time: (◆) Fe(II)LS component of the sample heated at T=147 and T=174K; (▲) Fe(II)LS component of a second sample irradiated at 180K, 190K and 195K. The solid lines are the fit curves obtained using Eq. 2-42.

The $g(\Delta G^{\#})$ distributions for 147K, 174K and 180K are practically equal. $g(\Delta G^{\#})$ is centred at 62.7 kJ/mol, the half width of the Gaussian is 7 kJ/mol. At higher temperatures the distributions $g(\Delta G^{\#})$ become more narrow (4.24 and 1.7 kJ/mol respectively) and a shift to higher energies (64.9 kJ/mol and 65.4 kJ/mol respectively) occurs. A comparison of these results with the ones obtained from the irradiated Hbmet is reported in Fig. 6.9.
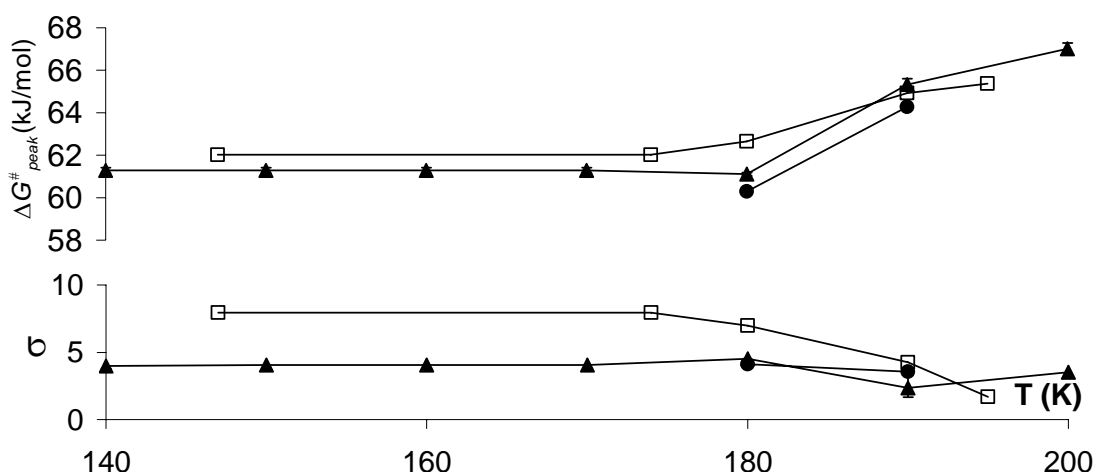
Figure 6.9: Gaussian distributions as a function of temperature to fit the decay of the metastable Fe(II)LS component of the irradiated Hbmet(1) (▲), Hbmet(2) (●), and Mbmet (□). $\Delta G^{\#}_{peak}$: peak value of the mean free energy distribution value. σ: energy barrier half width.

From Fig. 6.9 it is evident that the relaxation of Fe(II)LS state is the same in both Hbmet and Mbmet sample. From our investigation of the relaxation of the intermediate state, we obtain the Gibbs free activation energy. It is distributed with an average $\Delta G^{\#}$ - at 180K - of about 61 kJ/mol. This value has two contributions. For decay, the binding of the water molecule to the heme iron has to be broken. However, this does not suffice. As we know from (Lamb et al., 1998) the water rebinds after flash photolysis at 150K. The barrier height distribution which has to be surmounted in this process is rather similar to that of CO after photolysis. Only if the molecule obtains a certain degree of flexibility the water stays away from the iron and the molecule can change its structure. In case of myoglobin, we can estimate the energetic cost of these two processes. At 180K the ΔG_{flex} to reach the flexible state is about 7.4 kJ/mol: this value is deduced from the probability of the molecule to stay in the flexible state in case of Mbmet crystal (Knapp et al., 1983; Huenges et al., 2002). This leaves more than 53.6 kJ/mol for the water binding: it seems astonishingly high. However, one may compare this with the binding energy of one water molecule in a Fe-hexaquo complex at 298K. It is 35.08 kJ/mol for Fe(II) and 60.42 kJ/mol for Fe(III) (Helm et al., 1999). From the temperature dependence of ΔG it is possible to calculate 37.6 kJ/mol for Fe(II) and 61.84 kJ/mol for Fe(III) at 180K. In addition, in hemoglobin the free energy of binding of CO at 293K is equal to 40 kJ/mol (Antonini and Brunori, 1971). From values reported in (Austin et al., 1975), it is possible to deduce a value around 69 kJ/mol as free binding energy of CO to Mb at 310K and around 83 kJ/mol at 50K.

Comparing the Gaussian parameters obtained from Hb and Mb samples, there is the evidence of a different behaviour of the distribution width as shown in Fig. 6.9. In case of Mb, at temperature below 180K, the σ value is larger than in the case of Hb by about 3 kJ/mol. This is an indication of a broader CS starting distribution and indicates the existence of more different conformational substates with respect to Hb. It could appear strange that a smaller protein has more different conformational substates with respect to a four times bigger one. The explanation of this apparent contradiction can come from the presence of the quaternary structure. Salvay (Salvay et al., 2003) showed that the content of water molecules bound per Hb tetramer at 98% relative humidity when oxygenation is completed is about 1410 in presence of NaCl and 1425 in the absence of NaCl. That means: each Hb subunit is surrounded by about 352 or 356 water molecules depending on NaCl presence. In fact, the hemoglobin subunits are less exposed to the solvent than Mb, because of the contact surface between α and β subunits. Mb studies with Monte Carlo calculation of water position in a myoglobin crystal leads to 814 water molecules for unit cell, thus around 407 water molecules for each Mb molecule (Schmidt et al., 1996; Parak et al., 1993; Parak et al., 1992), while osmotic stress study (Salvay et al., 2003) reports a value of around 480. Therefore, in case of Hb the monomers are surrounded by a lower number of water molecules with respect to the Mb monomers. Many studies showed the relation between the entropic and enthalpic contribution of water to the protein function (Bulone et al., 1992). In particular Bulone et al. found that 75 additional water molecules are present in the protein hydration shell during hemoglobin T→R transition in solution. This result is confirmed by Salvay et al. (Salvay et al., 2003) who reported a value of 80 additional water molecules after oxygenation of Hb films. It has to be mentioned that in case of Mössbauer spectroscopy there is no difference between Mb monomers assemble and subunits of Hb molecules, if the iron nucleus feels the same interactions. In fact these measurements give information about the near surrounding of iron nucleus that means within the heme pocket. Following the idea that more water molecules are present in myoglobin, more different conformational substates can exist.

6.2 CO Binding to Mbdeoxy Samples

During the heating cycles performed on the irradiated Hbmet samples, the HbCO was produced as it is shown in Fig. 4.5 and Fig. 4.6 although the samples did not contain CO molecules in their solution. Somehow the X-ray irradiation procedure has created them. To clarify how the CO is produced, we prepared two Mbdeoxy samples in solution with glycerol (Mbdeoxy$_{gly}$) and without glycerol (Mbdeoxy$_{wat}$). In order to show the effect of low temperature X-ray irradiation, they have been measured before and after the irradiation at 78K. Before the irradiation the spectra collected

from both samples can be well fitted with one Lorentzian doublet with typical hyperfine parameters of Mbdeoxy (Fig. 4.7a, Fig. 4.9). After irradiation, in order to highlight the presence of CO produced in the samples, thermal cycles were performed. In this way the CO formed during the irradiation can bind myoglobin.

The results show that in the case of **Mbdeoxy$_{wat}$**, during the thermal cycles at T lower than 170K, no CO binding was present. From 170K to 200K only 6% of MbCO is created during the thermal cycles. Moreover from 200K to 280K no more than 10% of MbCO is created. In contrast, in case of **Mbdeoxy$_{gly}$**, about 70% of MbCO is produced during the thermal cycles done from 150K to 200K. From 200K to 280K the MbCO reaches about 75%. The rising of the temperature till 280K showed that there was no more CO available in the solvent. Furthermore, in this case of the Mbdeoxy$_{wat}$ sample no MbCO is formed during the heating cycles at 150K. These evidences mean that the CO molecules, present during the thermal cycles done after the irradiation of Hbmet, Mbdeoxy and Hbdeoxy samples prepared with glycerol, are produced mainly by the glycerol radiolysis and not due to a damaged protein. From the results achieved with Mbdeoxy and Hbmet samples, we can deduce that at T lower than 170K the CO can not enter the heme pocket. These findings, are in agreement with CO flash photolysis results (Fraunfelder et al., 1991; Austin et al., 1975) where it was stressed many times that CO can not escape from or enter into the heme pocket at T below 180K-200K. It is possible to conclude that the greatest part of the CO molecules is produced in the solvent and then it diffuses into the protein until it reaches the heme pocket to bind the iron.

6.3 Following the HbCO and MbCO Formation

In this paragraph, the HbCO and MbCO formation during the heating cycle performed on the irradiated Hbmet, Hbdeoxy and Mbdeoxy$_{gly}$ samples is discussed. In the case of the irradiated Hbmet sample, after overcoming the energy barrier, the protein is going into a stable state such as HbCO or Hbdeoxy. This process needs some comments. In Fig. 4.6 and Fig. 4.7 the relative population of each state as function of the heating time of irradiated Hbmet is reported. In both Hbmet(1) and Hbmet(2) samples, just after irradiation a deoxy-like component is formed, that counts for 10% of the molecules. This is a clear indication for a fast relaxation process, thus there are conformational substates with very low activation energy. They are relaxing already at temperatures below 100K, i.e. during irradiation. Moreover, after irradiation less than 1.5% of HbCO is formed and about 5% of Hbmet, Fe(III) component, is still not reduced. At 140K and 150K practically no relaxation occurs while at 160K the Fe(II)LS relaxes only into the Hbdeoxy component. In addition, no HbCO formation is present at this temperature suggesting that no CO

molecule was produced inside the heme pocket. This is in agreement with the findings just presented in the previous paragraph, that there is no diffusion of CO below T equal to 170K into the heme pocket. At T equal or higher than 170K, the Fe(II) metastable component relaxes only into HbCO. Now the CO molecules created by the irradiated glycerol are able to diffuse into the heme pocket. In other words, when CO molecules are available there is HbCO formation. Two processes are possible when the H_2O is removed from the Fe(II) depending on the CO presence. When CO does not reaches the heme pocket at T lower than 170K or when all the CO molecules are already bound, the Fe(II) low spin relaxes into deoxy state. In the case of the Hbmet(1) sample, this happens at T equal or higher than 190K. Moreover, at T equal to 170K the Hbdeoxy component is decreasing with a combined production of Hbmet, Fe(III). Probably at this temperature some remaining free radicals can oxidize the Fe(II) forming Fe(III).

A sample of Hbdeoxy in glycerol was prepared and irradiated. Afterwards, the thermal cycles have been performed in order to follow the CO binding and to compare the free activation energy of Hbdeoxy with that one of Mbdeoxy. Hbdeoxy is in a T quaternary state and after the binding with the CO, when all the subunits are ligated, it should change to the R quaternary conformation. Mbdeoxy has only a tertiary change from unbound to bound state. In case of Hbdeoxy and Mbdeoxy experiments, at the end of the thermal procedure (280K) a large amount of deoxy molecules have not bound any CO. The rising of the temperature to 280K shows that there is no more CO available in the solvent. It is quite clear that the amount of CO produced is proportional to the irradiation time and to the glycerol amount. All the samples were prepared with 50% glycerol/water (vol/vol) and irradiated roughly for the same time. That means that there is the same amount of glycerol in all the samples since all the sample holders have the same volume. On the contrary, as one can see from the Mössbauer spectra intensity obtained before the irradiation (Fig. 4.9 and Fig. 4.14), the iron concentration is different. In particular, the most concentrated one is the Hbdeoxy sample (Fig. 4.14), while Hbmet samples are the less concentrated. Actually in these last cited samples, the metastable component is relaxing completely into HbCO. In case of Hbdeoxy sample, as it is possible to observe from Figure 4.17, after the heating time at T=180K practically no more HbCO is produced. In fact even if the temperature is raised to 280K (Fig. 4.17) there was no more CO available in the solution.
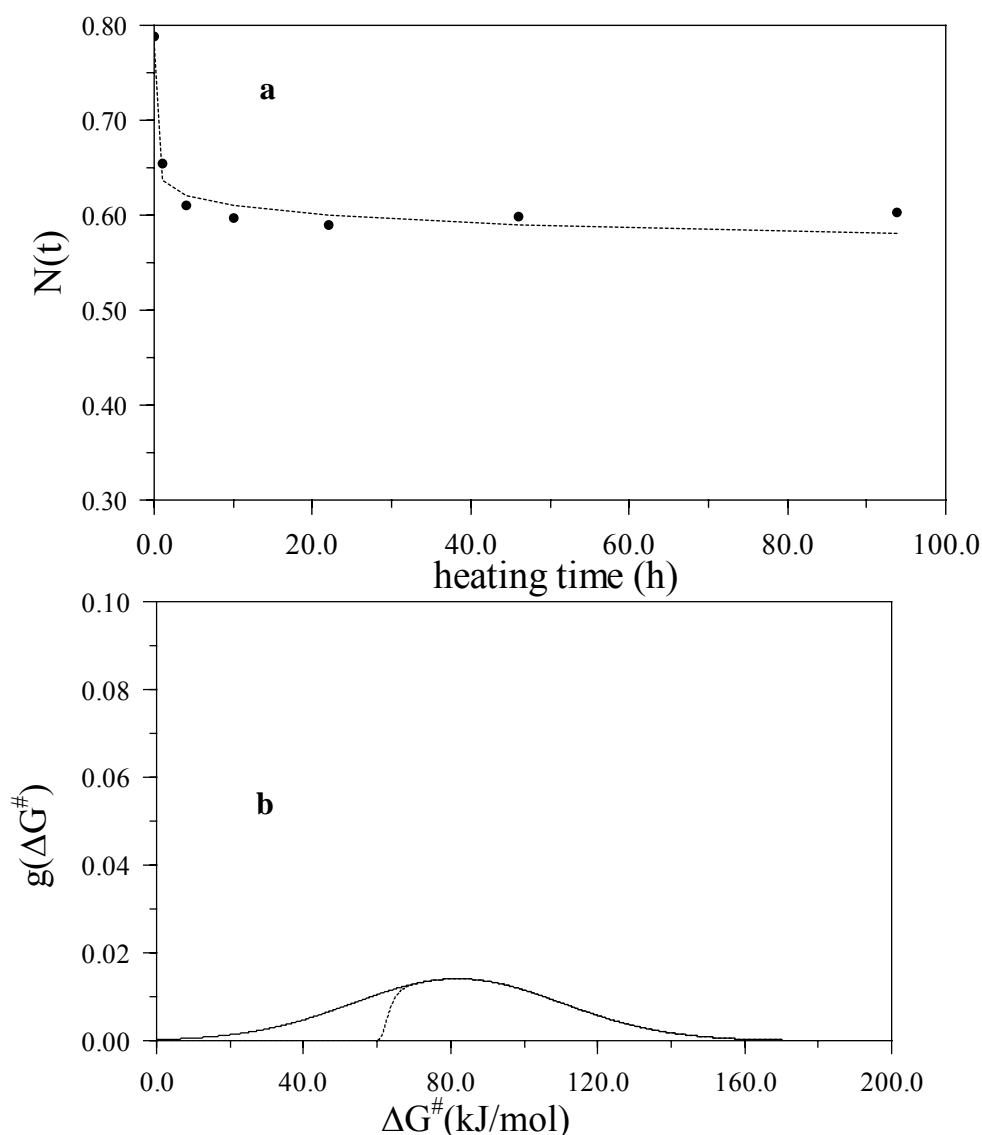
Figure 6.10: a: fit of the Hbdeoxy -Fe(II) HS relaxation to HbCO Fe(II)LS at T = 180K; **b:** the free activation energy barrier distribution used.

Fitting the decrease of the Hbdeoxy component with Eq. 2-42, the resulting free energy distribution is very large. In fact the sigma value is around 28kJ/mol and the Gaussian is centred at $\Delta G^{\#}_0$=82 kJ/mol, as shown in Fig. 6.10. Assuming that this relaxation kinetic is independent from CO concentration, the fit is done again using the same equation but only the first 3 data points (Fig.6.11) are considered. This is done to neglect the fact that N(t) reaches a saturation value that wouldn't be reached if the CO was still present. The omitted points are responsible for the extreme enlargement of the barrier.
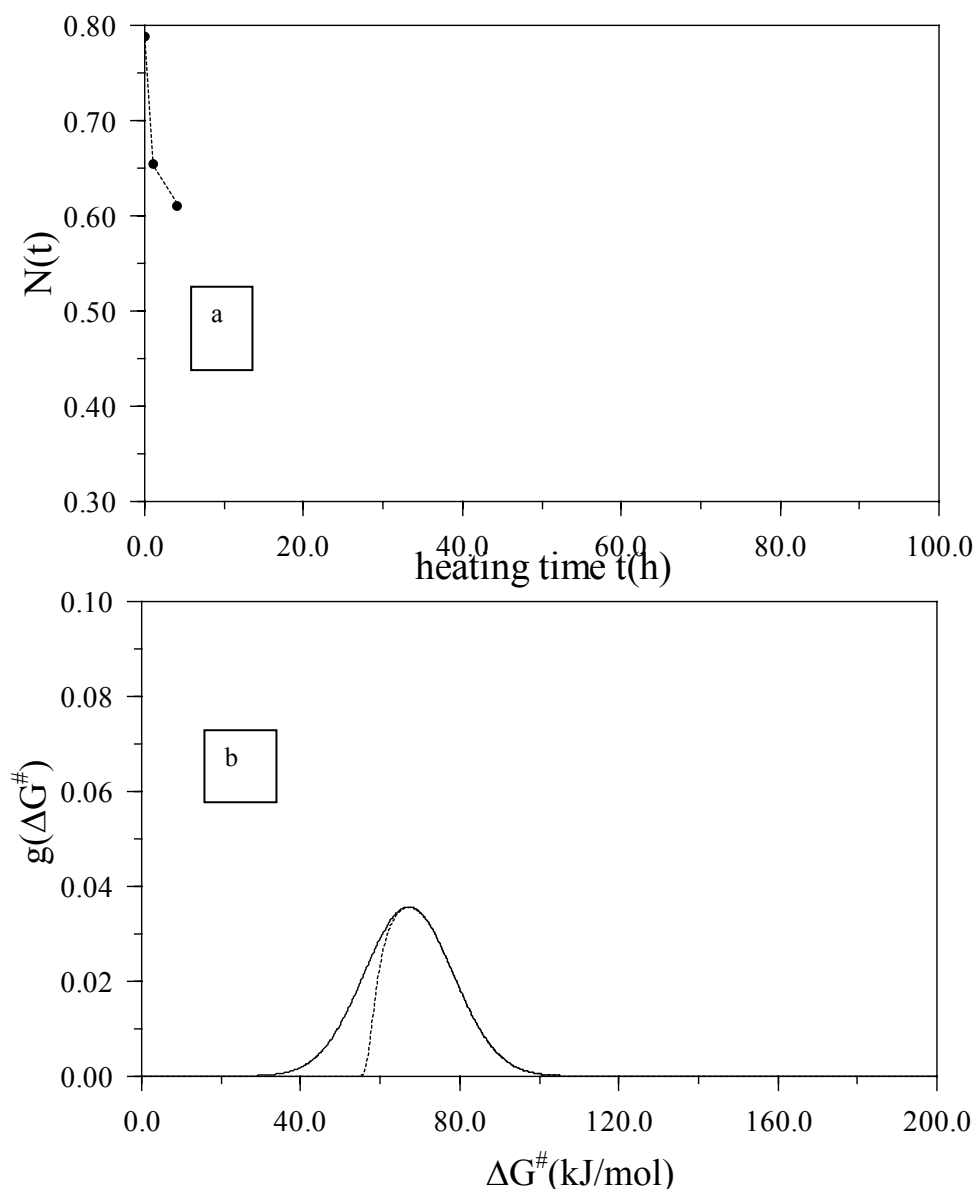
Figure 6.11: a: Fit of the Hbdeoxy – Fe(II)HS relaxation to HbCO Fe(II)LS at T=180K considering only three point; **b:** the free activation energy barrier distribution used.

In this way we obtained a barrier that is centred at $\Delta G_{peak}^{\#} = 67 kJ/mol$ and with a line width about 11kJ/mol. In this experiment only the HbCO is formed: following the Hbdeoxy component diminishing, it is like to look at the activation energy to create HbCO. Similarly to the flash photolysis experiment (Austin et al., 1975), where the change of 436nm band (434 nm – Mb Soret band) is followed to estimate the free binding energy, we look on the decrease of Fe(II)HS component. The irradiated Mbdeoxy sample prepared in the glycerol solution (Fig. 4.13) are analysed in the same way.
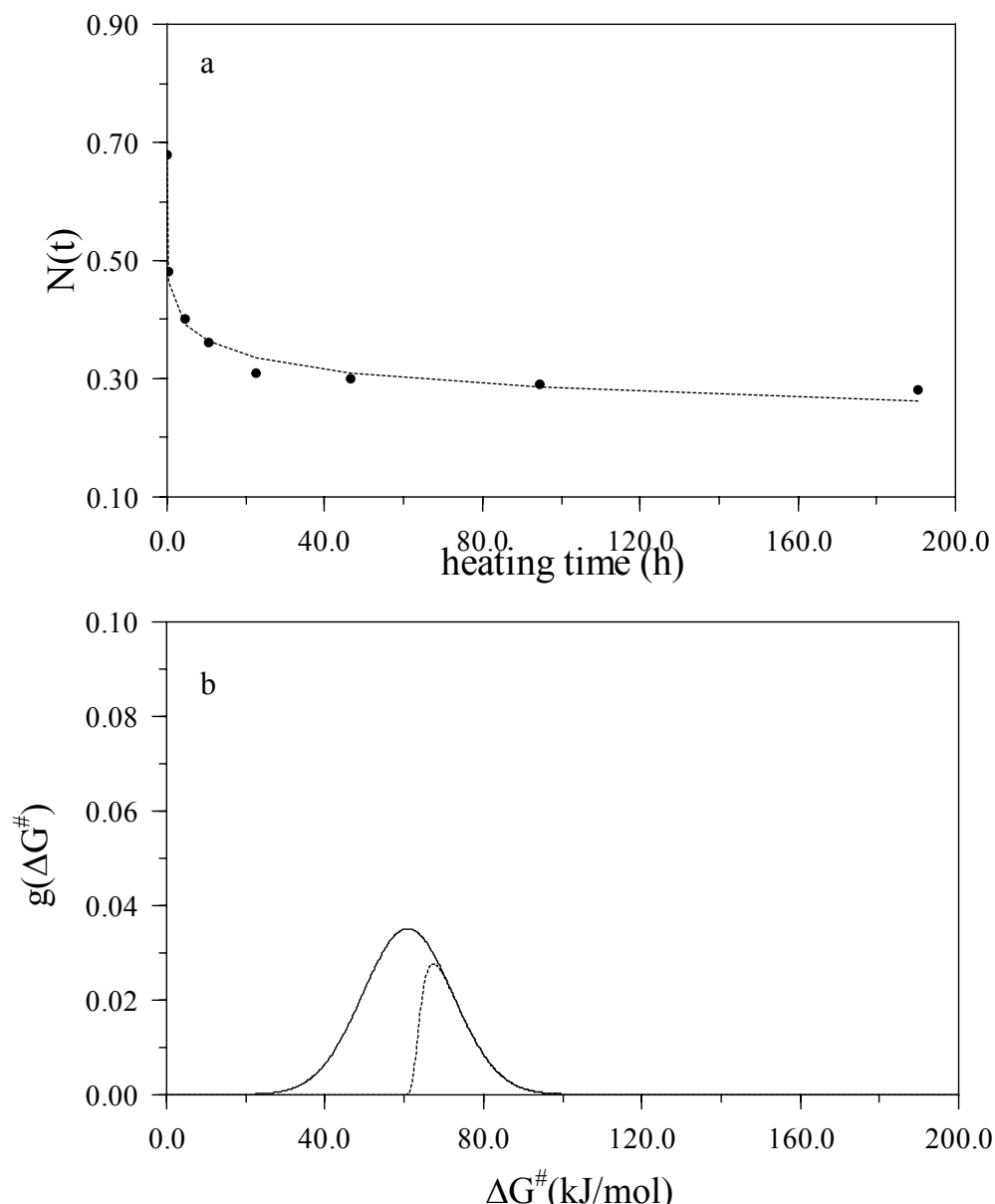
Figure 6.12: a: fit of the Mbdeoxy - Fe(II)HS - relaxation at T=180K; **b:** the free energy barrier distribution used.

In the case of irradiated Mbdeoxy it is not necessary to neglect points, because the N(t) does not reach a saturation level. In particular when the sample was heated from 240K to 280K (Fig. 4.13) some CO molecules were still binding the Mb. The free energy Gaussian distribution used to fit the decrease of the relative area of Mbdeoxy is centred at $\Delta G^{\#}_{peak}$= 60.8kJ/mol and has a σ=11kJ/mol (Fig. 6.12b). Comparing the Hb and Mb data, they seem to be very similar. In case of Hb, the barrier is centred at 7kJ/mol, higher energy. This may be correlated with the different affinity for the ligand that exists between Mb and the Hb. In case of the Hbdeoxy sample at the end of the180K heating cycles, only 20% of Hbdeoxy has bound the CO therefore the molecule is still in a quaternary T state. Thus, less then one subunit in each tetramer has bound to CO. During this

experiment there is no T to R transition and therefore - apart from different affinity constant for the ligand that could explain the different $\Delta G^{\#}_{peak}$ values - the binding kinetics are very similar.

6.4 High and Low Affinity Hbdeoxy

Before going into details of the discussion of High and Low affinity Hbdeoxy samples, some considerations have to be done concerning the particular behaviour of Hbdeoxy hemoglobin in solution, in particular about the line asymmetry effect that was strongly evident at T=5K (Fig. 4.11). An attempt has been done to fit the measurements taken from 5K to 210K with two doublets with equal areas. The quadrupole splitting and the isomer shift values at different temperature in the case of two components are reported in Table 13 (Appendix). This assumption was done with the idea that the two components correspond to α and β subunits. These two components have a quite different quadrupole splitting temperature dependence behaviour. From this information one could deduce a different position of iron with respect to the heme plane according to the theory developed by Eicher et al. (Eicher et al., 1976). The knowledge of the X-ray structure are not enough accurate to deduce this information. The distance of iron from the heme plane can be estimated from X-ray Protein Data Bank – PDB (Seixas et al., 2001) to be roughly the same in α and β subunits: around 0.5 Å with resolution of 1.87 Å.
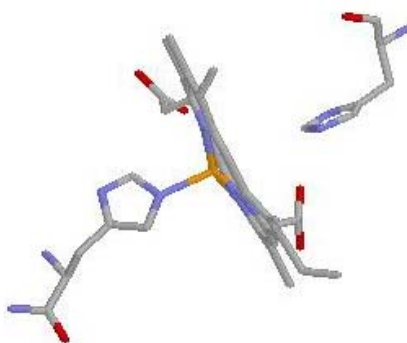
Figure 6.13: Heme crystal structure of α-chain obtained from the data of human Hbdeoxy (Seixas et al., 2001: PDB).

There is no crystallographic evidence of a different distance between the iron and the heme plane in the two subunits. Although a different iron heme distance could be correlated with the difference in oxygen affinity between α and β subunits (Lindstrom and Ho, 1972; Shibayama et al., 1986;

Bettati et al., 1996; Mozzarelli et al., 1997; Bruno et al., 2000) not enough measurements have been done to obtain reliable information. Moreover an experiment was conducted by Trautwein (Trautwein et al., 1976) showing no differences between the quadrupole splitting behaviour of fully ^{57}Fe Hbdeoxy enriched and the quadrupole splitting of Hbdeoxy with only ^{57}Fe α chains enriched. In this respect, differences in α and β subunits remain an open question with some indication for a deeper investigation.

However, as it is shown in Fig 5.9, using one component to fit the spectra of Hbdeoxy in solution, the quadrupole splitting temperature behaviour is very similar to the one of Hbdeoxy samples encapsulated in silica gel. Moreover, the spectrum of HbCO encapsulated in silica gel (Fig. 5.1) has the same hyperfine parameters found in literature. Because there is no change in the hyperfine parameters of encapsulated Hbdeoxy and HbCO, the encapsulation does not denature the protein. Some previous works (Shibaiama et al., 1995; Shibaiama et al., 2001; Bruno et al., 2001; Vappiani et al., 2004) showed the existence of two distinct affinities in the T state of human deoxy-hemoglobin that is encapsulated in wet silica gel in absence or in presence of allosteric effectors. This evidence raises again the question if this different affinity is the result of a different tertiary state already present when all the subunits are unbound or if it is induced by the ligand. In this last hypothesis no differences can be seen if the binding does not happen. According to the first hypothesis, the two unliganded T states should contain different tertiary structures, e.g. *r* or *t*. Fig. 4.16 tries to explain this possibility. Since no change of quaternary structure is present due to the encapsulation in wet silica gel, in this model the different affinities should come from different tertiary states within the T states.
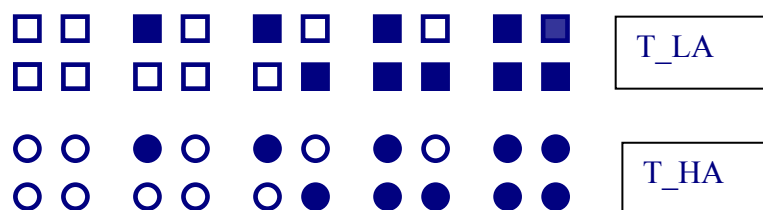
Figure 6.14: Schematic model of possible tertiary conformations in case of one quaternary T state with two different affinities. Squares: *t* tertiary state. Circle: *r* tertiary state. The full symbols represent the liganded subunits while the empty symbols the unliganded subunits.

On the other hand, there is a second possibility: it is the ligand binding that induces the different affinity. This means that when there is no ligand bound, the T quaternary HA and LA states contain the same tertiary states. This hypothesis was supported by the experiment conducted by Viappiani

(Viappiani et al., 2004). In that experiment the rebinding kinetics after photo dissociation of CO molecule in Hbdeoxy sample encapsulated in silica gel in absence and in presence of allosteric effectors were analysed. In particular they could fit the kinetic data obtained from Hbdeoxy HA sample without allosteric effectors, using a linear combination of the curves used to fit the data of Hbdeoxy LA and Hbdeoxy in R state. In that way there was no need to introduce a quaternary unliganded state populated by *r* tertiary states. Fig. 6.15 reports the scheme proposed by Viappiani (Viappiani et al., 2004).
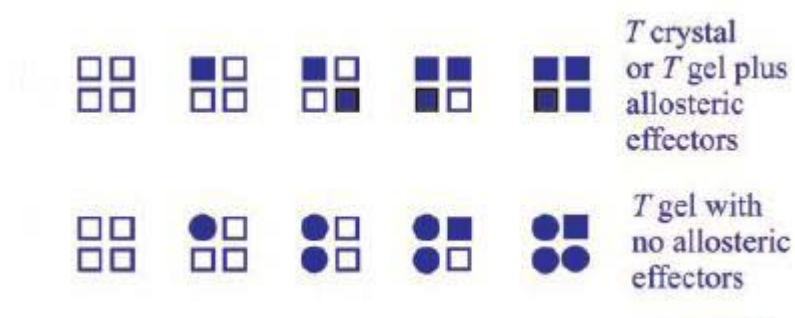
Figure 6.15: Model proposed by Viappiani (Viappiani et al., 2004). The two affinity deoxy states LA and HA are populated by the same tertiary *t* state when they are completely unliganded. <u>Square</u>: *t* teriary state. <u>Circle</u>: *r* tertiary state. The full symbols represent the liganded subunits while the empty symbols the unliganded subunits.

In both models the change in affinity it is not caused by a change in the quaternary structure as it was in the original MWC model. It was already introduced by Henry (Henry et al., 1997) the model based on the existence of the two tertiary states that could be the right approach for the interpretation of the data in presence of allosteric effectors.

Therefore to have an insight in the nearby of the heme, the quadrupole splitting temperature dependence of Hbdeoxy High Affinity (HA) and Hbdeoxy Low Affinity (LA) samples has been fitted with the theory developed by Eicher (Eicher et al., 1974) using the Levenberg-Marquardt algorithm to minimize the sum of the squares of nonlinear function. We use also the same parameter notations. In Fig.5.8 QS data of Hbdeoxy LA and Hbdeoxy HA are reported together with the least square fits. The error associated with QS was estimated to be 0.02 mm/s for each measurement. In this way it is also possible to calculate the error associated with the fit parameters. This calculation was done using the covariance matrix. The data points of the two samples are very similar as one can see from Fig. 6.15; in particular the slope of the curve is practically the same. In the Bade's thesis (Bade, 1975) the temperature dependence of the quadrupole splitting have been simulated varying the parameters ^3E, ^5E, and $^1A_1$, D. Their variation is connected with the shape of

the curves used to fit the quadrupole splitting values. In particular the slope can be influenced by the variation of ^5E term. In the Eq. 2-17 and Eq. 2-18 are reported the relation between the ^3E, ^5E, $^1A_1$, D and the ε_1, ε_2, ε_3 terms. Differences between the data value of HA and LA Hbdeoxy samples are only visible at T lower then 50K. The shape of the fit curve in this temperature range is connected to the variation of ^3E and also $^1A_1$. During the fit procedures, the spin-orbit coupling constant λ and the covalency factor α^2 are kept constant. In particular, for the Hbdeoxy sample the values reported in Eicher (Eicher et al., 1976) are used: $\lambda=69$ cm^{-1} and $\alpha^2=0.88$ for both High and Low Affinity Hbdeoxy samples. In case of HA sample, ε_1 is equal to $496.74(\pm0.04)$cm^{-1}, ε_2 is equal to $9420.1(\pm0.3)$ cm^{-1}, and ε_3 is equal to 16746.1 (±0.2)cm^{-1}, while in the case of LA sample ε_1 is equal to $619.3(\pm0.2)$ cm^{-1}, ε_2 is equal to $10146.9(\pm0.1)$ cm^{-1}, and ε_3 is equal to $16332.89(\pm0.02)$cm^{-1}. From the fitting of QS data, it comes out firstly that the parameters are in agreement with those reported in Eicher (Eicher et al., 1976). The energy ε_2 of the $a_{1g}(d_z{}^2)$ orbital depends on the binding strength with the imidazole nitrogen of the proximal histidine. Consequently, the binding seems to be stronger in the LA with respect to HA sample. Similarly, the ε_3 value is rising when the distance of iron with respect to the heme plane decreases. In this case ε_3 is higher in the HA sample than in the LA one. In this way one could deduce a correlation between the different affinities of the two T states, with the different distance of iron with respect to the heme plane and to the proximal histidine. Due to the small differences in the QS values and because of the quality of the data, it is not possible to conclude that these two sets of measurements are different. A more accurate set of measurements especially in the low temperature regime is necessary. At the present the HA and LA samples behave in the same way supporting the thesis that the change in the affinity is due to the ligand binding and not to a different tertiary structure already present when the hemoglobin has no ligands bound.

Appendix

Table 6: Relative area of each component used to fit the spectra of the irradiated Hbmet(1) during thermal cycles. The first two columns are the heating temperature and heating time respectively, used during the heating cycles. In particular are reported the value of Fe(II)LS metastable component, Hbdeoxy, HbCO, and the not reduced Hbmet.

Heating temperature T(K)	Total heating time (h)	Fe (II) LS %	Hbdeoxy %	HbCO %	Hbmet Fe(III) %
140	0	83.7	10.0	1.3	5.0
140	18.5	82.1	11.4	1.9	4.7
150	38.5	80.2	11.0	4.3	4.4
150	46	82.3	11.5	1.8	4.5
150	55	80.7	11.6	3.3	4.4
160	55.5	79.8	12.7	3.0	4.5
160	62.5	77.9	13.7	3.6	4.9
160	72.5	77.1	15.2	2.8	5.0
160	92.5	77.0	15.0	3.0	5.0
170	93	76.4	14.2	4.3	5.1
170	95	74.2	16.2	4.2	5.4
170	98	72.6	16.1	6.1	5.2
170	103	70.6	15.7	7.9	5.8
170	113	65.3	15.3	12.1	7.3
170	133	58.8	13.5	17.8	10.0
170	173	54.7	10.7	24.2	10.3
180	173.5	52.5	9.8	26.8	11.0
180	174.5	45.0	7.7	34.1	13.2
180	176	40.7	4.9	41.0	13.4
180	179	30.1	3.2	51.7	15.0
180	185	28.4	2.9	53.1	15.7
180	195	27.4	2.8	55.2	14.7
180	219	23.6	2.2	59.4	14.8
180	267	19.6	3.7	60.0	16.8
190	267.5	17.4	3.7	63.4	15.5
190	277.5	14.4	6.0	65.3	14.4
190	297.5	10.5	8.7	66.5	14.3
200	298	10.5	9.5	65.6	14.4
200	299	8.9	9.4	67.2	14.5
200	300.5	8.1	10.3	67.0	14.7
200	303.5	6.1	11.6	67.9	14.5
200	328.5	3.2	14.6	67.7	14.5
200	383.5	3.2	14.6	67.7	14.5

Table 7: Relative area of each component used to fit the spectra of the irradiate Hbmet(2) during thermal cycles. The first two columns are the heating tempearure and heating time respectively, used during the heating cycles. In particular are reported the value of Fe(II)LS metastable component , Hbdeoxy, HbCO, and the not reduced Hbmet HS, Hbmet LS, and hemocroms.

Heating temperature T(K)	Total heating time t(h)	Hbmet Fe(II) LS %	Hbdeoxy %	HbCO %	Hbmet Fe(III) HS %	Hbmet Fe(III) LS %	Fe(II) hemochroms %
180	0.000	64.9	11.7	0.0	5.8	5.8	11.8
180	0.500	56.7	15.6	7.1	5.7	5.7	9.2
180	1.500	50.2	12.2	15.5	5.8	6.6	9.8
180	3,000	45.9	8.9	25.2	5.8	5.8	8.6
180	6.000	40.0	5.9	33.5	5.6	5.6	9.3
180	12.000	33.3	3.5	42.6	5.6	5.7	9.4
180	24.000	27.9	1.8	49.1	5.5	5.5	10.1
180	48.533	21.9	1.8	55.1	5.5	6.5	9.2
190	49.033	20.5	1.8	56.7	5.5	5.5	10.0
190	50.033	19.5	1.8	57.9	5.4	5.4	10.0
190	52. 033	16.3	1.8	61.0	5.4	5.4	10.0
190	56.183	14.8	1.8	62.6	5.4	5.4	10.0
190	64.183	11.9	1.8	65.4	5.5	5.5	10.0

Table 8: Relative area of each component used to fit the spectra of the irradiate Mbdeoxy$_{wa}$ during thermal cycles. The first two columns are the heating temperature and heating time respectively, used during the heating cycles. In particular are reported the values of Mbdeoxy, MbCO, an asymmetric component produced during the irradiation, and a second symmetric one that was forming at T above 220K.

Heating temperature T (K)	Total heating time t (h)	Mbdeoxy %	MbCO %	Asymmetric component %	Symmetric component %
0	0	83.75	0	16.25	0
140	1	86.9	0	13.1	0
150	2	87.7	0	12.3	0
160	3	86.6	3.4	10	0
170	4	86.5	4.6	8.9	0
180	5	85.8	4.5	9.7	0
180	7	86.8	6.4	6.8	0
180	13	86.9	6.1	7	0
190	14	89.7	10.3	0	0
200	15	90.5	9.5	0	0
220	16	90.2	9.8	0	0
240	17	88.6	8.3	0	3.1
260	18	88.2	8	0	3.8
280	19	85.8	7.6	0	6.6

Table 9: Relative area of each component used to fit the spectra of the irradiated Hbdeoxy during thermal cycles. The first two columns are the heating temperature and heating time respectively, used during the heating cycles. In particular are reported the values of Hbdeoxy, of a metastable asymmetric component produced during irradiation, and of HbCO.

Heating temperature T(K)	Total heating time t(h)	Hbdeoxy%	Metastable component %	HbCO %
180	0	65.9	34.1	0
180	0.5	78.9	7.53	13.57
180	1.5	65.43	3.99	30.58
180	4.5	61.11	0	38.89
180	10.5	59.7	0	40.3
180	22.5	58.89	0	41.11
180	46.5	59.84	0	40.16
180	94.33	60.26	0	39.74
190	94.83	60.36	0	39.64
190	95.83	60.6	0	39.4
200	96.33	60.28	0	39.72
200	97.33	60.31	0	39.69
220	98.33	60.41	0	39.59
240	99.33	58.79	0	41.21
240	101.33	59.15	0	40.85
240	104.33	57.92	0	42.08
240	110.33	56.73	0	43.27
240	122.33	56.18	0	43.82
240	146.33	57.21	0	42.79
260	147.33	57.28	0	42.72
260	149.33	57.76	0	42.24
280	150.33	59.22	0	40.78

Table 10: Relative area of each component used to fit the spectra of the irradiated Mbdeoxy sample prepared with glycerol during thermal cycles. The first two columns are the heating temperature and heating time respectively, used during the heating cycles. In particular are reported the values of Mbdeoxy, of MbCO, and of a metastable asymmetric component produced during irradiation.

Heating temperature T(K)	Total heating time t (h)	Mbdeoxy %	MbCO %	I comp %
77	0	62.6	0	37.4
150	0.5	66.4	0	33.6
150	3.5	68.91	0	31.09
180	4	48.32	51.68	0
180	8.183	40.78	59.22	0
180	14	36.57	63.43	0
180	26	31.71	68.29	0
180	50	30.55	69.45	0
180	98	29.36	70.64	0
180	194	28.78	71.22	0
190	194.5	29.01	70.99	0
190	197.5	28.68	71.32	0
200	200.5	29.22	70.77	0
220	203.5	28.9	71.03	0
240	206.5	30.3	69.9	0
260	209.5	28	71.8	0
280	212.5	25.8	74.2	0

Table 11: Values relative to Hbdeoxy High Afinity (HA) sample. In the first column are reported the measurement temperatures. In the following columns are presented: the Quadrupole Splitting (QS), the Isomer Shift (IS) relative to α-iron, the line width (Γ), and the relative area of Hbdeoxy and Fe(II) LS components.

T (K)	Hbdeoxy QS (mm/s)	Hbdeoxy $IS_{\alpha\text{-}Fe}$ (mm/s)	Hbdeoxy Γ(mm/s)	Hbdeoxy %	Fe(II)LS QS (mm/s)	Fe(II)LS $IS_{\alpha Fe}$ (mm/s)	Fe(II)LS Γ(mm/s)	Fe(II)LS %
5.3	2.38	0.896	0.37	65.4	1.03	0.449	0.36	34.6
5.5	2.4	0.909	0.37	77.7	1.03	0.459	0.36	22.3
20	2.39	0.889	0.36	64.0	1.03	0.449	0.33	36.0
39	2.34	0.879	0.36	60.1	1.05	0.439	0.35	39.9
77.4	2.32	0.889	0.36	88.9	1.10	0.419	0.35	11.1
90	2.29	0.889	0.36	89.8	1.02	0.449	0.35	10.2
110	2.24	0.879	0.36	90.4	0.94	0.379	0.35	9.6
130	2.19	0.869	0.36	89.3	0.95	0.399	0.35	10.7
150	2.15	0.859	0.36	88.1	0.99	0.419	0.35	11.9
180	2.05	0.859	0.36	86.2	1.12	0.549	0.35	13.8
200	2.02	0.799	0.31	66.3	0.96	0.439	0.35	33.7

Table 12: Values relative to Hbdeoxy Low Affinity (LA) sample. In the first column are reported the measurement temperatures. In the following columns are presented: the Quadrupole Splitting (QS), the Isomer Shift (IS) relative to α-iron, the line width (Γ), and the relative area of Hbdeoxy and Fe(II) LS components.

T (K)	Hbdeoxy QS (mm/s)	Hbdeoxy $IS_{\alpha\text{-}Fe}$ (mm/s)	Hbdeoxy Γ(mm/s)	Hbdeoxy %	Fe(II)LS QS (mm/s)	Fe(II)LS IS $IS_{\alpha Fe}$ (mm/s)	Fe(II)LS Γ(mm/s)	Fe(II)LS %
6.5	2.42	0.908	0.39	92.8	1.02	0.44	0.38	7.2
20	2.40	0.923	0.33	86.1	0.96	0.45	0.35	13.9
55	2.35	0.912	0.33	84.6	1.02	0.45	0.35	15.4
77	2.33	0.912	0.31	87.9	0.96	0.37	0.35	12.1
90	2.29	0.912	0.34	91.8	1.02	0.38	0.34	8.1
110	2.25	0.902	0.32	88.7	1.13	0.47	0.34	11.3
130	2.18	0.899	0.35	89.3	1.03	0.33	0.36	10.7
150	2.10	0.891	0.34	88.1	1.02	0.37	0.34	11.9
170	2.07	0.878	0.35	88.0	1.01	0.36	0.38	12.0
190	2.06	0.880	0.35	89.5	1.01	0.36	0.34	10.5
210	1.99	0.875	0.38	80.3	1.05	0.35	0.34	19.7

Table 13: Values relative to Hbdeoxy sample fitted with two components (I) and (II), which have roughly the same area: columns sixth and seventh. In the first column are reported the measurement temperatures. In the second and third are reported the QS of component I and II. In the fourth and fifth columns are reported the IS respect α- iron of the component I and II respectively.

T (K)	QS(I) mm/s	QS (II) mm/s	$IS_{\alpha\text{-Fe}}$(I) mm/s	$IS_{\alpha\text{-Fe}}$ (II) mm/s	%I	%II
5	2.53	2.25	0.89	0.92	52.78	47.22
77	2.45	2.18	0.89	0.91	48.53	51.47
98	2.42	2.14	0.88	0.91	45.84	54.16
150	2.24	1.98	0.87	0.87	51.6	48.4
180	2.17	1.88	0.86	0.85	51.66	48.34

Literature

Alberding, N., Chan,S.S., Eisenstein, L., Frauenfelder,H., Good, D., Gunsalus,I.C., Nordlund,T.M., Perutz, M.F., Reynolds, A. H., Sorensen,V., *Binding of Carbon Monoxide to Isolated Hemoglobin Chains*, Biochemistry 17 (1978) 43-51.

Achterhold, K., Keppler, C., Ostermann, A., van Bürck, U., Sturhahn, W., Alp, E. E., Parak, F. *Vibrational dynamics of myoglobin determined by the phonon-assisted Mössbauer effect,* Physical Review E 65 (2002).

Agmon, N., Hopfield, J. J., *CO binding to heme proteins: A model for barrier height distributions and slow conformational changes,* J. Chem. Phys. 79(4) (1983) 2042-2053.

Agmon, N., Hopfield, J. J., *Transient kinetics of chemical reactions with bounded diffusion perpendicular to the reaction coordinate: Intramolecular processes with slow conformational changes,* J. Chem. Phys. 78 (11) (1983) 6947-6959.

Alberding, N., Austin, R. H., Chan, S. S., Eisenstein, L., Frauenfelder, H., Gunsalus, I. C., Nordlund, T. M., *Dynamics of carbon monoxide binding to protoheme*, J. Chem. Phys. 65(11) (1976) 4701-4711.

Ansari, A., Berendzen, J., Bowne, S. F., Frauenfelder, H., Iben, I. E. T., Sauke, T. B., Shyamsunder, E., Young, R. D., *Protein states and proteinquakes,* Proc. Natl. Acad. Sci.USA 82 (1985) 5000-5004.

Ansari, A., Berendzen, J., Braunstein, D., Cowen, B. R., Frauenfelder, H., Hong, M. K., Iben, I. E. T., Johnson, J. B., Ormos, P., Sauke, T. B., Scholl, R., Schulte, A., Steinbach, P. J., Wittitow, J. & Young, R. D., *Rebinding and relaxation in the myoglobin pocket*, Biophys. Chem. 26 (1987) 337-355.

Ansari, A., Jones, C. M., Henry, E. R., Hofrichter, J., Eaton, W. A., *The Role of Solvent Viscosity in the Dynamics of Protein Conformational Changes*, Science 256 (1992) 1796-1798.

Ansari, A., Jones, C. M., Henry, E. R., Hofrichter, J., Eaton, W., A *Conformational Relaxation and Ligand Binding in Myoglobin*, Biochemistry 33 (1994) 5128-5145.

Antonini, E., Brunori, M., *Hemoglobin and Myoglobin in their Reactions with Ligands,* Noth-Holland Publishing Co., Amsterdam, London (1971).

Antonini, E., Rossi-Bernardi, L., Chiancone, E. Hemoglobins, *Methods in Enzymology* 76, Academic Press, New York, London, Toronto, Sydney, San Francisco (1981).

Austin, R. H., Beeson, K. W., Eisenstein, L., Frauenfelder, H., Gunsalus, I. C., *Dynamics of Ligand Binding to Myoglobin*, Biochemistry 14 (1975) 5355-5373.

Beece, D., Eisenstein, L., Frauenfelder, H., Good, D., Marden, M. C., Reinisch, L., Reynolds, A. H., Sorensen, L. B., Yue, K. T., *Solvent Viscosity and Protein Dynamics*, Biochemistry 19 (23) (1980) 5147-5157.

Bellelli, A., Brancaccio, A., Brunori, M., *Hydration and Allosteric Transitions in Hemoglobin*, J. Biol. Chem. 268(7) (1993) 4742-4744.

Benesch., R. E, and Benesch, R., *The effect of organic phosphates from the human erythrocyte on the allosteric properties of hemoglobinerythrocyte on the allosteric properties of hemoglobin,* Biochem. Biophys. Res. Commun. 26(1967) 162-7.

Bettati, S., Kwiatkowski, L. D., Kavanaugh, J. S., Mozzarelli, A., Arnone, A., Rossi, G. L., and Noble, R.W., *Structure and oxygen affinity of crystalline desHis146 human hemoglobin in the T state*, J.Biol.Chem. 272 (1997) 33077–33084.

Bettati, S., Mozzarelli, A., *T state hemoglobin binds oxygen noncooperatively with allosteric effects of protons, inositol hexaphosphate, and chloride,* J. Biol. Chem. 272(51) (1997) 32050-32055.

Bettati, S., Mozzarelli, A., Perutz, M. F., *Allosteric Mechanism of Haemoglobin: Rupture of Salt-bridges Raises the Oxygen Affinity of the T-structure,* J. Mol. Biol. 281 (1998) 581-585.

Bizzarri, A. R., Iakovleva, O. A., Parak, F., *Spin-lattice relaxation in Moessbauer spectra of metmyoglobin: investigation of crystals ,water and water-glycerol solutions*, Chem. Phys. 191 (1995): 185-194.

Bruno, S., Bettati, S., Manfredini, M., Mozzarelli, A., Bolognesi, M., Deriu, D., Rosano, C., Tsuneshige, A., Yonetani, T., and Henry, E. R., *Oxygen binding by α(Fe2+)₂β(Ni2+)₂ hemoglobin crystals,* Protein Sci. 9 (2000) 683–692.

Bruno, S., Bonaccio, M., Bettati, S., Rivetti, C., Viappiani, C., Abbruzzetti, S., Mozzarelli, A., *High and low affinity conformations of T state hemoglobin*, Protein Science 10 (2001) 2401-2407.

Brunori, M., *Hemoglobin is an honorary enzyme,* Trends in Biochem. Sci. 24 (1999) 158-161.

Bulone, D., Palma-Vittorelli, M. B., Palma, M. U., *Enthalpic and entropic contributions of water molecules to the functional T →R transition of human hemoglobin in solution,* International Journal of Quantum Chemistry 42 (1992) 1427-1437.

Chevion, M., Ilan, Y. A., Samuni, A., Navok, T., Czapski, G., *Quaternary Structure of Methemoglobin. Pulse Radiolysis Study of the Binding of Oxygen to the Valence Hybrid*, J. Biom. Chem. 254(14) (1979) 6370-6374.

Chong, S. H., Joti, Y., Kidera, A., Go, N., Ostermann, A., Gassmann, A., Parak, F., *Dynamical transition of myoglobin in a crystal: comparative studies of X-ray crystallography and Mössbauer spectroscopy,* Eurp. Biophys. J. 30 (2001) 319-329.

Colombo, M. F., Rau, D. C., Parsegian, V. A., *Protein Solvation in Allosteric Regulation: A Water Effect on Hemoglobin,* Science 256 (1992) 655-659.

Cordone, L., Galajda, P., Vitrano, E., Gassmann, A., Ostermann, A., Parak, F., *A reduction of protein motions in co-ligated myoglobin embedded in a trehalose glass*, Eur. Biophys. J. 27 (1998) 173-176.

Cupane, A., Leone, M., Militello, V., *Conformational substates and dynamic properties of carbonmonoxy hemoglobin*, Biophys. Chem. 104 (2003) 335-344.

Danon, J., *Lectures on the Mössbauer Effect,* Gordon and Breach Science Publishers New York, 1968.

Doster ,W., Cusack, S. , Petry, W., *Dynamical transition of myoglobin revealed by inelastic neutron scattering*, Nature 337 (1989) 754-756 .

Doster, W., Beece, D., Bowne, S. F., DiIorio, E. E., Eisenstein, L., Frauenfelder, H., Reinisch, L., Shyamsunder, E., Winterhalter, K. H., Yue, K. T., *Control and pH Dependence of Ligand Binding to Heme Proteins*, Biochemistry 21(20) (1982) 4831-4839.

Doster, W., Settles, M., *The dynamical transition in proteins: the role of hydrogen bonds,* Hydration Process in Biology: Theoretical and Experimental Approaches. M.C.- Bellissent Funel, editor. IOS Press, Amsterdam, Vol. 305. (1998)

Eaton, W. A., *Hemoglobin and Allostery is it Understood?, Simplycity and Complexity in Proteins and Nucleic Acids*, Dahlem University press, Berlin 1999.

Eaton, W. A., Henry, E. R., Hofrichter, J., Mozzarelli, A., I*s cooperative oxygen binding by hemoglobin really understood?,* Nature Structural Biology 6(4) (1999) 351-358.

Ehrestein, D., Nienhaus, G. U., *Conformational substates in azurin*, Proc. Natl. Acad. Sci. USA 89 (1992) 9681-9685.

Eicher, H., Bade, D., Parak, F., *Theoretical determination of the electronic structure and the spatial arrangement of ferrous iron in deoxygenated sperm whale myoglobin and human hemoglobin from Mössbauer experiments*, J. Chem. Phys 64(4) (1976) 1446-1455.

Eicher, H., Parak, F., Bade, D., Tejada, J. *Electronic Structure of the Iron in Deoxygenated Myoglobin from Mössbauer Spectroscopy* Journal de Physique C6-12(35) (1974) 363-366.

Eicher, H., Trautwein, A., E*lectronic Structure of Ferrous Iron in Hemoglobin Inferred from Mössbauer Measurements*, J. Chem. Phys. 52(2) (1970) 932-934.

Eicher, H., Trautwein, A., *Electronic Structure and Quadrupole Splittings of Ferrous Iron in Hemoglobin*, J. Chem. Phys. 50 (6) (1969) 2540-2551.

Engler, N., Ostermann, A., Gassmann, A., Lamb, Don C., Prusakov, V. E., Schott, J., Schweitzer-Stenner, R., Parak, F., *Protein Dynamics in an Intermediate State of Myoglobin: Optical Absorption, Resonance Raman Spectroscopy, and X-Ray Structure Analysis*, Biophysical Journal 78 (2000) 2081-2092.

Fenimore, P. W., Fraunfelder, H., McMahon, B. H., Parak, F., *Slaving: Solvent fluctuations dominate protein dynamics and functions*, Proc. Natl. Acad. Sci. USA 99 (2002) 16047-16051.

Ferrand, M., Dianoux, A. J., Petry, W. & Zaccai, G. *Thermal motions and function of bacteriorhodopsin in purple membranes : Effects of temperature and hydration studied by neutron scattering,* Proc. Nat. Ac. Sci (USA) 90 (1993) 9669-9672.

Frauenfelder, H., McMahon, B. H., Fenimore, P. W., M*yoglobin: The hydrogen atom of biology and a paradigm of complexity*, Proc. Natl. Acad. Sci. USA 100(15) (2003) 8615-8617.

Frauenfelder, H., Parak, F., Young, R. D., *Conformational Substates in Proteins*, Ann. Rev. Biophys. Chem. 17 (1988) 451-479.

Frauenfelder, H., Sligar, S. G., Wolynes, P. G., *The Energy Landscapes and Motions of Proteins*, Science 254 (1991) 1598-1603.

Frolov, E. N., Fischer, M., Graffweg, E., Mirishly, M. A., Goldanskii, V. I., Parak, G. G., *Hemoglobin dynamics in rat erythrocytes investigated by Mössbauer spectroscopy*, Eur. Biophys. J. 19 (1991) 253-256.

Goldanskii, V. I., Parak, F., *Some still open questions of relaxational CO-heme rebinding*, Chem. Phys. Lett. 129 (1994) 379-383.

Gonser, U., *Mössbauer Spectroscopy*, Springer Verlag Berlin, 1975,

Greenwood, N. N., Gibb, T. C., *Mössbauer Spectroscopy*, Chapman and Hall Ltd, London (1971).

Hafemeister, D. W., Brook Shera, E., *Calculation of Mossbauer Areas for Thick Absorber* , Nucl. Instr. and Meth. 41 (1966) 133-134.

Hagen, S. J., Hofrichter, J., Eaton, W. A., *Geminate Rebinding and Conformational Dynamics of Myoglobin Embedded in a Glass at Room Temperature*, J. Phys. Chem. 100 (1996) 12008-12021.

Helm, L., Merbach A.E., *Water exchange on metal ions: experiments and simulations*. Coord. Chem. Rev. 187 (1999) , 151-181.

Henry, E. R., Bettati, S., Hofrichter, J., Eaton, W. A., *A tertiary two-state allosteric model for hemoglobin*, Biophys. Chem. 98 (2002) 149-164.

Huang, J., Ridsdale, A., Wang, J., Friedman, J. M., *Kinetic Hole Burning, Hole Filling, and Conformational Relaxation in Heme Proteins: Direct Evidence for the Functional Significance of a Hierarchy of Dynamical Processes*, Biochemistry 36 (1997) 14353-14365.

Huenges, A., Achterhold, K., Parak, F., *Mössbauer Spectroscopy in the Energy and in the Time Domain, a Crucial Tool for the Investigation of Protein Dynamics.*, Hyperfine Interactions 144/145 (2002) 209-222.

Imai, K ., *Allosteric Effect in Hemoglobin*, Cambridge University Press, Cambridge 1982.

Imai, K., *The Monod-Wyman-Changeux allosteric model describes haemoglobin oxygenation with only one adjustable parameter,* J. Mol.Biol. (1983) 167: 741-749.

Ingalls, R., E*lectric-Field Gradient Tensor in Ferrous Compounds*, Phys. Rev. 133(3A)(1964) A787-A795.

Johnson, J. B., Lamb, D. C., Frauenfelder, H., Müller, J. D., McMahon, B., Nienhaus, G. U., Young, R. D., *Lingand Binding to Heme Proteins. VI. Interconversion of Taxonomic substates in Carbonmonoxymyoglobin,* Biophys J. 71(3) (1996) 1563-1573.

Kilmartin, J.,V., Rossi-Bernardi, L., *Interaction of hemoglobin with hydrogen ions, carbon dioxide, and organic phosphates*, Physiol. Rev. 53(4) 1973 Oct 836-90.

Knapp, E., W., Fischer, S.,F., Parak, F., *The influence of protein dynamics on Mossbauer spectra,* J.Chem.Phys. 78 (1983) 4701-4711.

Koshland, D. E., Jr., Nemethy G., Filmer D., *Comparison of experimental binding data and theoretical models in proteins containing subunits*, Biochemistry (1966) 5:365-385.

Kriegl, J. M., Bhattacharyya, A. J., Nienhaus, K., Deng, P., Minkow, O., Burmester, T. Nienhaus, G. U., *Ligand binding and protein dynamics in neuroglobin*, Proc. Natl. Acad. Sci. USA 99 (2002) 7992-7997.

Lalezari, I., Lalezari, P., Poyart, C., Marden, M., Kister, J., Bohn, B., Fermi, G., Perutz M.F., *New effectors of human hemoglobin: structure and function*, Biochemistry 29 (1990)1515-1523.

Lalezari, I., Rahbar, S., Lalezari, P., Fermi, G., Perutz, M.F., *LR16, a compound with potent effects on the oxygen affinity of hemoglobin, on blood cholesterol, and on low density lipoprotein*, Proc. Natl. Acad. Sci. U S A 85: (1988) 6117-6121.

Lamb, D. C., Prusakov, V., Engler, N., Ostermann, A., Schellenberg, P., Parak, F. G., Nienhaus, G.U., *Photodissociation and Rebinding of H_2O to Ferrous Sperm Whale Myoglobin*, J. Am. Chem. Soc. 120 (1998) 2981-2982.

Lang, G., Marshall, W., M*ossbauer effect in some haemoglobin compounds*, J. Mol. Biol. 18(3) (1966) 385-404.

Levy, A., *Low-Temperature Formation of a Distal Histidine Complex in Hemoglobin: A Probe for Heme Pocket Flexibility,* Biochemistry 24 (1985) 6050-6054.

Lindstrom, T. R. and Ho, C., *Functional nonequivalence of α and β hemes*, Proc.Natl.Acad.Sci. 69 (1972) 1707–1710.

Marden, M. C., Bohn, B., Kister, J., Poyart, C., *Effectors of hemoglobin. Separation of allosteric and affinity factors,* Biophys J. 57(3) (1990) 397-403.

Mayo, K. H., Kucheida, D., Parak, F., Chien, C. W., *Structural dynamics of human deoxyhemoglobin and hemochrome investigated by nuclear gamma resonance absorption (Mössbauer) spectroscopy*, Proc. Natl. Acad. Sci. USA 80 (1983) 5294-5296.

Mayo, K. H., Parak, F., Mössbauer, R. L., *Observations of Elastic and Quasi-Elastic Nuclear Gamma Resonance Absorption in Hemoglobin Crystals*, Physics Letters 82A(9) (1981) 468-470.

Minton, A. P. , Imai, K., *The three -state model: aminiman allosteric description of homotropic and heterotropic effects in the binding of ligand to he,oglobin,* Proc. Natl. Acad. Sci. USA 71 (1972) 1418-1421.

Monod, J., Wyman, J., and Changeux, J.-P., *On the nature of allosteric transitions: a plausible model,* J. Mol. Biol 12 (1965) 88-118.

Mozzarelli, A. , Rivetti, C., Rossi, G. L., Henry, E. R., Eaton, W. A., *Crystals of hemoglobin with the T quaternary structure bind oxygen noncooperativelywith no Bohr effect,* Nature 351 (1991) 416-418.

Mozzarelli, A., Rivetti, C., Rossi, G. L., Henry, E. R., Eaton, W. A., *Allosteric effectors do not alter the oxygen affinity of hemoglobin crystals*, Protein Sci. 6 (1997) 484-489.

Mozzarelli, A., Bettati, S., Rivetti, C. Rossi, G. L., Colotti, G., Chiancone, E., *Cooperative Oxygen Binding to Scapharca inaequivalvis Hemoglobin in the Crystal*, J. Biol. Chem. 271(7) (1996) 3627-3632.

Nienhaus, G. U., Mourant, J. R., Frauenfelder, H., *Spectroscopic evidence for conformational relaxation in myoglobin*, Proc. Natl. Acad. Sci. USA 89 (1992) 2902-2906.

Ortalli, I., Pedrazzi, G., Schianchi, G. , *Mössbauer and ESR Evidence of Hemocromes in Neoplastic Pathologies*, Il Nuovo Cimento 10D(7) (1998) 881-885.

Ostermann, A., Waschipky, R., Parak, F. G. and Nienhaus, G. U., *Ligand binding and conformational motions in myoglobin*, Nature (2000) 404: 205–208.

Paoli, M., Liddington, R. C., Tame, J., Wilkinson, A. J., Dodson, G., *Crystal Structure of T State Haemoglobin with Oxygen Bound At All Four Haems*, J. Mol. Biol. 256 (1996) 775-792.

Paoli, M., Nagai, K., *Hemoglobin "Handbook of Metalloprotein"*, Albrecht Messerschmidt, Robert Huber, Thomas Poulos and Karl Wieghardt, Editors John Wiley & Sons, Ltd, Chichester (2001).

Paoli, M., Dodson, G., Liddington, R. C., Wilkinson, A. J., *Tension in Haemoglobin Revealed by Fe-His(F8) Bond Rupture in the Fully Liganded T-State*, J. Mol. Biol. 271 (1997) 161-167.

Papaefthymiou, G. C., Huynh, B. H., Yen, C. S., Groves, J. L., Wu, C. S. ,*Mössbauer studies of Fe2+ in anhydrous hemoglobin and its isolated subunits*, J. Chem. Phys. 62(8) (1975) 2995-3001.

Parak, F., *Physical aspects of proteins dynamics*, Rep. Prog. Phys. 66 (2003) 103-129.

Parak, F., *Protein in action: the physics of structural fluctuation and conformationa changes*. Current Opinion in Structural Biology 13 (2003) 552-557.

Parak, F. G., & Nienhaus, G. U., *Myoglobin, a paradigm in the study of protein dynamic*, Chem. Phys. Chem. 3 (2002) 249-254.

Parak, F., Formanek, H., *Untersuchung des Schwingungsanteils und des Kristallgitterfehleranteils des Temperaturfaktors in Myoglobin durch Vergleich von Mössbauerabsorptionsmessungen mit Röntgenstrukturdaten*, Acta Cryst. A27 (1971) 573-578.

Parak, F., Hartmann, H., Schmidt, M., Corongiu, G., *The hydration of myoglobin molecules*, M.U. Palma MBP-V, F. Parak (Eds.) Conf. Proc. Ital. Phys. Soc. 43 (1993) 5-122.

Parak, F., Hartmann, H., Schmidt, M., Corongiu, G., Clementi, E., *The hydration shell of myoglobin*, Eur. Biophys. J. 21 (1992) 313-320.

Parak, F., Knapp, E. W., Kucheida, D., *Protein dynamics. Mössbauer Spectroscopy on Deoxymyoglobin Crystals*, J. Mol. Biol. 161 (1982) 177-194.

Pauling, L., *The Oxygen Equilibrium of Hemoglobin and Its Structural Interpretation*, PNAS (1935) 21: 186-191.

Perutz, M. F., Rossmann, M. G., Cullis, A. F., Muirhead, H., Will, G., North, A. T. C., *Structure of haemoglobin. A three-dimensional Fourier synthesis at 5.5Å resolution, obtained by X-ray analysis.*, Nature (1960) 185: 416-422.

Perutz, M.F., *Stereochemistry of cooperative effects in haemoglobin*, Nature (1970) 228: 726-739.

Perutz, M. F., Fermi, G., Abraham, D. J., Poyart, C., Bursaux, E. J., *Hemoglobin as receptor of drugs and peptides: X-ray studies of the stereochemistry of binding*, J. Am. Chem. Soc. (1986) 108 1064-1078.

Perutz, M. F., Fermi, G., Luisi, B., Shaanan, B., Liddington, R. C., *Stereochemistry of cooperative mechanisms in hemoglobin*, Acc. Chem. Res.(1987) 20(9) 309-321.

Perutz, M. F., Heidner, E. J., Ladner, J. E., Beetlestone, J. G., Ho, C., Slade, E. F., *Influence of Globin Structure on the State of the Heme. III. Changes in Heme Spectra Accompanying Allosteric Transitions in Methemoglobin and Their Implications for Heme-Heme Interaction*, Biochemistry 13 (1974) 2187-2200.

Perutz, M. F., *Mechanisms of Cooperativity and allosteric regulation in proteins*, Quarterly Review of Biophysics (1989) 22(2) 139-236.

Prusakov, V. E, Steyer, J. and Parak, F. G., *Mossbauer spectroscopy on nonequilibrium states of myoglobin: a study of r-t relaxation*, Biophysical Journal (1995) 68: 2524-2530.

Racah, G., *Theory of Complex Spectra. III*, Phys. Rev. 63[9-10] (1943) 367-382.

Rivetti, C., Mozzarelli, A., Rossi, G. L., Henry, E. R., Eaton, W. A., *Oxygen Binding by Single Crystals of Hemoglobin*, Biochemistry 32 (1993) 2888-2906.

Rupley, J. A., Gratton, E., Careri, G., *Water and globular proteins*, Trends in Biochem. Sci. 8 (1983) 18-22.

Salvay, A. G., Colombo, M. F., Grigera, J. R., *Hydration effects on the structural properties and haem-haem interaction in haemoglobin*, Phys. Chem. Chem. Phys. 5 (2003) 192-197.

Salvay, A. G., Grigera, J. R., Colombo, M. F., *The Role of Hydration on the Mechanism of Allosteric Regulation: In Situ Measurements oc the Oxygen-Link Kinetics of Water Binding to Hemoglobin*, Biophysical Journal 84 (2003) 564-570.

San Biagio, P. L., Martorana, V., Bulone, D., Palma-Vittorelli, M. B., Palma, M. U., *Solvent-Induced Free Energy Landscape and Solute-Solvent Dynamic Coupling in a Multielement Solute*, Biophys. J. 77 (1999) 2470-2478.

Schmidt, M., Parak, F., Corongiu, G., *Density Distributions in the Water Shell of Myoglobin*, Int. Journal of Quantum Chemistry 59 (1996) 263-269.

Shibayama, N. and Saigo, S., *Fixation of the quaternary structures of human adult hemoglobin by encapsulation in transparent porous silica gels.*, J.Mol.Biol. 251(1995): 203–209.

Shibayama, N., Morimoto, H. and Kitagawa, T., *Oxygen equilibrium study and light absorption spectra of Ni(II)-Fe(II) hybrid hemoglobins.*, J. Mol.Biol. 192(1986) : 322–329.

Shibayama, N., Saigo, S., *Direct observation of two distinct affinity conformations in the T state human deoxyhemoglobin*, FEBS Letters 492(1) (2001) 50-53.

Steinbach, P. J., Ansari, A., Berendzen, J., Braunstein, D., Chu, Kelvin, Cowen, B. R., Ehrenstein, D., Frauenfelder, H., Johnson, J. B., Lamb, D. C., Luck, S., Mourant, J. R., Nienhaus, G. U., Ormos, P., Philipp, R., Xie, A., Young, R. D., *Ligand Binding to Heme Proteins: Connection between Dynamics and Function*, Biochemistry 30 (1991) 3988-4001.

Szabo, A., Karplus, M., *A mathematical model for structure-function relations in hemoglobin*, J.Mol.Biol. (1972) 72: 163-197.

Teale, F. W. J., *Cleavage of the heme-protein link by acid methylethylketone*, Biochim. Biophys. Acta. (1959) 535:543.

Trautwein, A., Alpert, Y., Maeda, Y., Marcolin, H. E., *Different properties of ferrus iron in deoxygenated hemoglobin chains*, J.de Physique (1976) C& 12- 37:191-193.

Trautwein, A., Eicher, H., Mayer, A., *Electronic structure, quadrupole splitting, chemical shift, and susceptibility of ferrous iron in anhydrohemoglobin, anhydromyoglobin, and bispyridinehemin*, J. Chem. Phys. 52(5) (1970) 2473-2477.

Viappiani, C., Bettati, S., Bruno, S., Ronda, L., Abruzzetti, S., Mozzarelli, A., and Eaton, W. A., *New insights into allosteric mechanisms from trapping unstable protein conformations in silica gels*, PNAS (2004) 101(40) : 14414–14419.

Winkler, H., *Myoglobin and Related Biomolecular Systems Studied with Mössbauer Spectroscopy and Nuclear Forward Scattering*, Hyperfine Interactions 144/145 (2002) 209-222.

Young, R. D., *Factorization of the association rate coefficient in ligand rebinding to heme proteins*, J. Chem. Phys. 80(1) (1984) 554-560.

Young, R. D., Bowne, S. F., *Conformational substates and barrier height distributions in ligand binding to heme proteins*, J. Chem. Phys. 81(8) (1984) 3730-3737.

Zerner, M., M. Gouterman, and H. Kobayashi, *Porphyrins VIII. Extended Huckel calculations on iron complexes*, Theor. Chim. Acta. 6:383-400.

Thanks

I thank heartily Prof. Dr. F.G. Parak for his support and encouragement during this thesis. He has been always available for discussions and suggestions. The comparison with a different point of view and the way to face a scientific problem accepting criticisms and new ideas have been an important lesson for my future research work. He also found the most favorable conditions to permit a serene carrying out of this research work.

I thank with gratitude Prof. Ida Ortalli, she has been the first one who suggested and believed in this cooperation between two laboratories and groups to realize this research work. She has always supported this work with love and her characteristic passion for science. She has always trusted my work giving me the freedom to organize and to develop it according with my own ideas. She is my Mentore and for this and much more I really thank her.

I thank Dr. V. Prusakov and Dr. S. Bettati for preparing the samples and for the interesting and useful discussions.

I thank Prof. G. Pedrazzi for the discussions and help especially on the statistic aspects.

I thank Dr. Klaus Atcherhold for the discussions, help and friendship.

I thank Matthias Mentler and Andreas Dilg, my first office-mates for introducing me in the lab and Munich life.

I thank Alexandra Huenges, Klaus Gratner, Michael Reiner, Olga Iakovleva, Christian Zach, Walter Gutscher Andreas Weiss, Marius Schmidt my colleagues when I was in Munich for help and cooperation.

I thank particularly Dr. Huenges for his kindness.

I thank Frediani's family, Adriana and Gianni, because they regard me as a daughter. They offered me a welcoming house as if I was at home.

I thank my best Italian friends, Carola, Camilla, Lorenza: they tolerate my long absence.

I thank my aunt Grazia, she is always present with love in my life.

Particular thanks to my parents and my sister, they always support and sustain me during this work with enthusiasm and trust accepting that I was not present any more in their every-day life.

A great thank to my husband, Marco, he supports me also when the life with me appears quite unusual and crazy. He also helped me in the data analysis computing aspect. Above all he encourages me during this work although this work was sacrificing our life.

Lebenslauf

Name:	Croci
Vorname:	Simonetta
Geburtsort:	Correggio
Geburtsdatum:	22/06/1972
Staatsangehörigkeit:	italienisch
Eltern:	Dipl. Ing. Gabriele Croci und Ombretta Losi
Familienstand:	verheiratet, keine Kinder

Bildungsweg:

1978 - 1983	Grundschule, Correggio
1983- 1986	G. Andreoli Hauptschule, Correggio
1986- 1991	A. Moro Realgymnasium, Reggio Emilia, Matura
1991-1998	Physikstudium an der Universität Parma, Diplom Schwerpunkt: Biophysik
1994-1995	Physikstudium an der Universität Leeds, UK- Erasmus Programm.
1998-2000	Studium der Medizinphysik an der Universität Bologna.
Seit 2002	Universitätsforscher an der Universität Parma, Medizinische Facultät.
Seit 2002	Promotion am Lehrstul E17 für molekulare Biophysik bei dem Physik Department der TU München mit Prof.F.G. Parak.
Seit 2003	Universitätslehrer der Physik und der Medizinphysik für den Akademiker in den gesundheitlichen Berufen - Medizinische Facultät der Universität Parma.
Seit 2003	Universitätslehrer der Biophysik, der Angewandten Biophysik, der Medizinischen Physik, für die medizinische Spezialisierung in Kardiologie an dem Medizin Insitut der Universität Parma.
Seit 2003	Universitätslehrer des Strahlenschutzes, für die medizinische Spezialisierung im Strahlentherapie an dem Medizin Insitut der Universität Parma.